EFFECT OF MICROSTRUCTURE OF CLOSED CELL FOAM ON STRENGTH AND EFFECTIVE STIFFNESS

A Dissertation

by

JI WOONG SUE

Submitted to the Office of Graduate Studies of
Texas A&M University
in partial fulfillment of the requirements for the degree of

DOCTOR OF PHILOSOPHY

December 2006

Major Subject: Materials Science and Engineering

EFFECT OF MICROSTRUCTURE OF CLOSED CELL FOAM ON STRENGTH AND EFFECTIVE STIFFNESS

A Dissertation

by

JI WOONG SUE

Submitted to the Office of Graduate Studies of
Texas A&M University
in partial fulfillment of the requirements for the degree of

DOCTOR OF PHILOSOPHY

Approved by:

Chair of Committee,	John D. Whitcomb
Committee Members,	Dimitris C. Lagoudas
	J. N. Reddy
	Terry S. Creasy
Chair of Intercollegiate Faculty,	Joseph N. Ross, Jr

December 2006

Major Subject: Materials Science and Engineering

ABSTRACT

Effect of Microstructure of Closed Cell Foam on Strength and Effective Stiffness.

(December 2006)

Ji Woong Sue, B.S.; M.S., Hanyang University, Korea

Chair of Advisory Committee: Dr. John D. Whitcomb

This research is concerned with the modeling and failure analysis of closed cell foam with various scales of microstructure that is disordered due to defects. This foam material is used for the forward bipod closeout on the space shuttle external tank. Three dimensional finite element simulations of closed cell foams with various microstructures are performed to study the influence of the geometric character of the microstructure (eg. defect size and distribution) on the stiffness and failure behavior of the foam. First, regularly arrayed cells are modeled for a reference to compare with the disordered microstructure. For studying the effect of cellular microstructure, a discrete model is developed where in every edge and face of each cell are modeled. Two types of defects, point defects (void) and area defects (knot), are indicated from the examination of BX250 and BX265 polyurethane foams. However, this research is focused on the point defect.

Analyzing a material with such complex microstructure is especially challenging in terms of computation power as well as required modeling techniques. A finite element model consisting of only beam and shell elements was developed. Certain

complications that arise from using beam and shell elements were resolved using novel techniques. Stiffness predictions from the model agreed with data from the literature for a wide range of relative densities. Parametric studies were performed to examine the effect of different properties, such as relative densities and edge fraction, on the effective stiffness, Von Mises stress, and buckling stress. The thickness of the face plays an important role in the behavior of the foam material. Linear buckling and postbuckling analyses were performed to understand the effect of local buckling on the effective properties of the foam and stress concentrations.

A distorted multicell model was developed to analyze the effect of point defects on the foam behavior. In particular, two geometric parameters, the defect size and the defect density (or the distance between two defects) were varied to find their effect on the stress concentrations and the effective stiffness of the foam. It is seen that the discrete model that accounts for the foam microstructure reveals much more about the foam behavior than a homogenous model.

DEDICATION

To God, my parents, my wife, Eunyoung, and my daughter, yeonwoo.

ACKNOWLEDGEMENTS

I would first like to thank my Lord and Savior, Jesus Christ, through whom all things are sustained and held together. May He receive all the honor and glory due Him.

I would also like to express my appreciation to Dr. John D. Whitcomb for his guidance, encouragement and help throughout my graduate study.

I am grateful to my parents for their love and encouragement. I also thank my wife, Eunyoung, for her endless support and my daughter, yeonwoo, for her smile.

Special thanks to my colleague, Julian, who encouraged me and helped me in many ways. I would also like to thank my other colleagues and friends. Their advice, help and friendship are greatly appreciated.

I also wish to thank the staff of the Department of Material Science and Engineering for their kindness and help provided during my studies at Texas A&M University.

TABLE OF CONTENTS

CHAPTER Page

LIST OF FIGURES

FIGURE Page

FIGURE Page

FIGURE Page

LIST OF TABLES

NOMENCLATURE

$\bar{n}$	vertices connection number
t_f	face thickness
t_e	edge thickness
ϕ	fraction of material for edge
ρ^*	density of the cellular material
ρ_s	density of the solid material
ρ^*/ρ_s	relative density
l	edge length
C_4	coefficient of relative density relation
E	Young's modulus (Pa)
E_s	Young's modulus of solid material
u_x	displacement of x direction
u_y	displacement of y direction
u_z	displacement of z direction
u_i	displacement of i direction
rot_x	rotation about x axis
rot_y	rotation about y axis
rot_z	rotation about z axis
x_α	coordinate

x_β coordinate

x_i coordinate

$d_{\alpha.}$ periodic vector

$d_{\beta.}$ periodic vector

$\sigma_{V.M.}$ Von Mieses stress

σ_y stress in y direction

$\underline{r}$ relative position vector

$\underline{r}$’ distortion vector

R radius of distort domain

$\underline{x}$ position vector

$\underline{x}$’ distorted position vector

$\underline{c}$ position vector of distortion center

a coefficient of plane equation

b coefficient of plane equation

c coefficient of plane equation

r_i radius of region in current region

a_f sum of area of face in current region

l_e sum of length of edge in current region

N_v number of vertices in current region

V_r volume of current region

Size ratio* defect diameter/undistorted foam cell diameter

factor coefficient of distortion function

CHAPTER I

INTRODUCTION

Closed cell foam covers the shuttle external fuel tank to provide insulation for the cryogenic fuel in the tank. Insulating the tank also prevents the exterior surface of the tank from becoming so cold that ice forms on the surface. This is critical since the ice could become projectiles during launch. The foam is not a structural material, but it must be strong enough to remain attached to the tank. This is not a trivial requirement since the foam is subjected to extreme temperature change, vibration, and aerodynamic loads during the launch phase. Foam is inherently a complex material. It is even more complex for some foam types such as BX250 and BX265 polyurethane foams which are used for the manual close-out spray. These foams are prone to have many defects (large pores), which create a complicated microstructure (Figure 1.1). Two types of defects are recognized in the micrographs of BX250 foam in Figure 1.2 [1]. The first type is large voids, which are classified as point defects. There is a wide range of sizes for these defects as well as the distance between them. One of the major causes of foam failure when used on the cryogenic fuel tank is the internal pressure in the point defects [1-4].

This dissertation follows the style of *Journal of Fluids Engineering*.

The second type of defects is called knots and is classified as surface defects. Knots are the layers of smaller than normal cells that form at the interface between sequential spray passes.

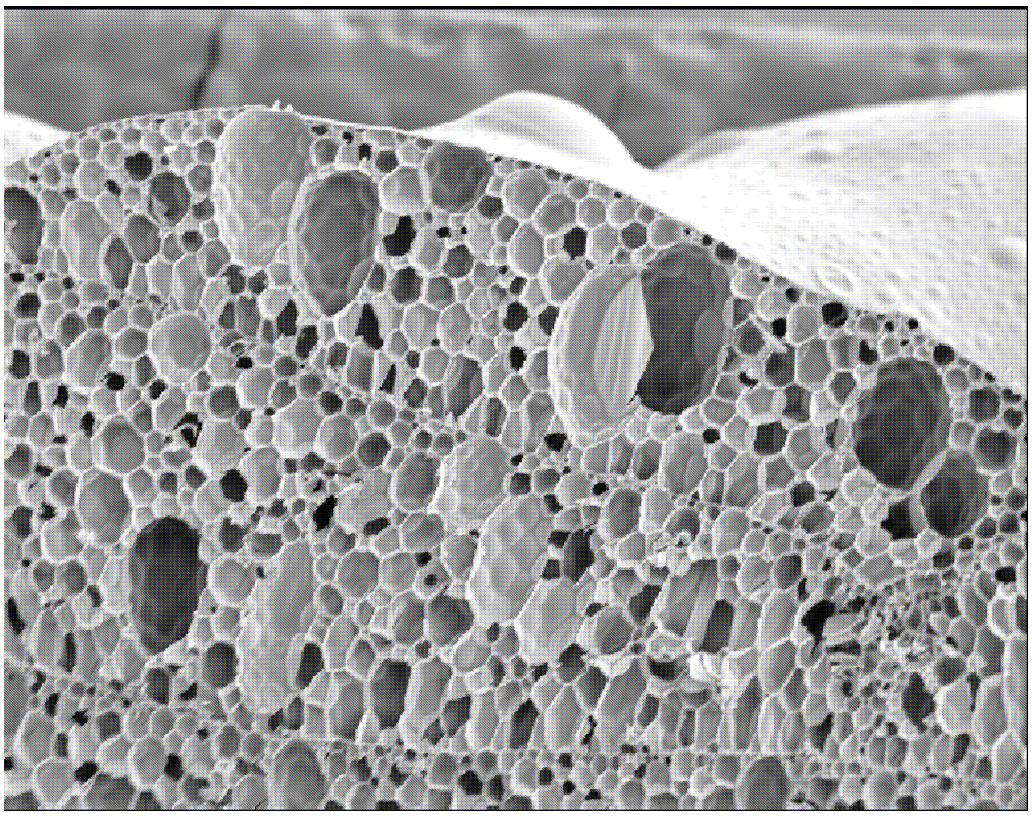

Figure 1.1 Scanning electron microscopy photomicrograph (30X) [2]

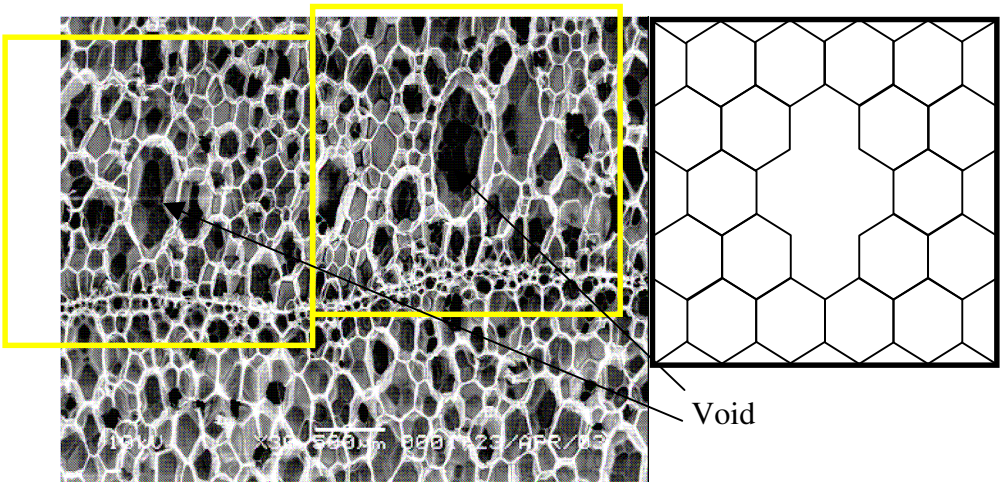

(a) Point defect (void)

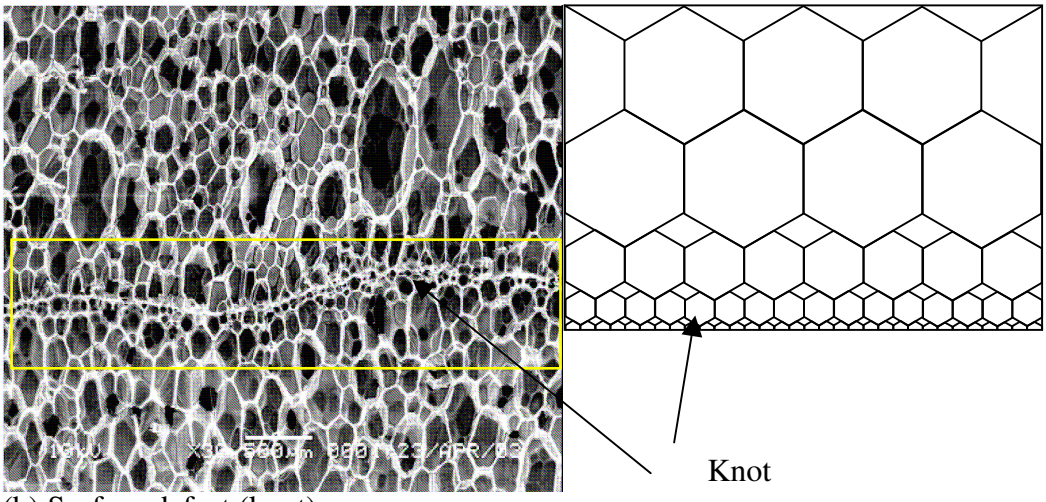

(b) Surface defect (knot)

Figure 1.2 Two types of defects [5]

The complete analysis of this type of material must be multiscale because of the need to account for microstructure at very different scales. The "defect pores" can be much larger (or much smaller) than the normal pores. It is not practical to conquer this problem with large computers and three dimensional finite element models. There are too many geometric details. Accordingly, one would develop a hierarchy of models with different levels of geometric detail (Figure 1.3). In regions sufficiently far from the failure initiation sites, which are expected to be near defects, the foam can be replaced by an effective homogeneous solid material. For large strains, this material could be nonlinear because of buckling of the foam cell faces and material nonlinearity. Closer to the failure site, the model would need more information about the geometry of the foam cells. Detailed description of the failure site requires three-dimensional analysis using solid elements.

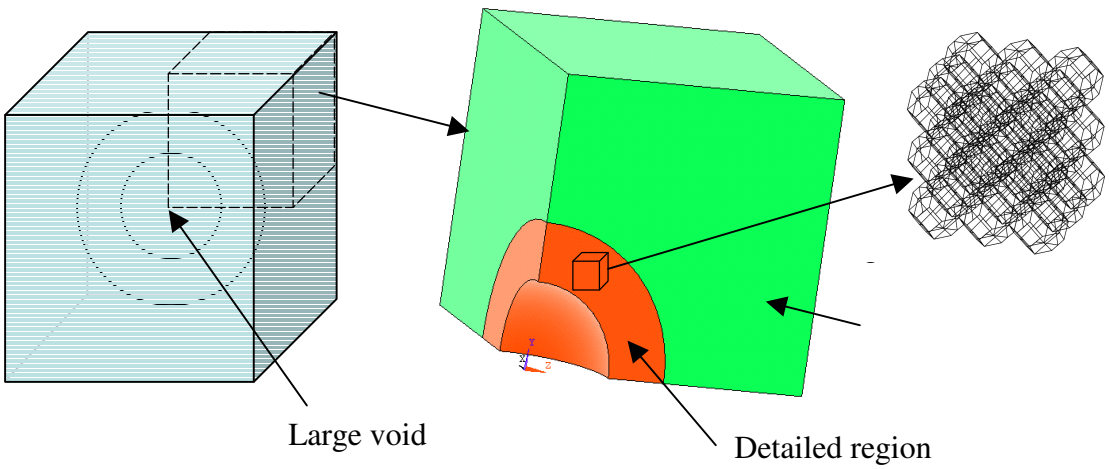

Figure 1.3 Schematic of multi scale model

The non-uniform microstructure of the foam materials affects the stiffness, strength and failure behavior of the foam material [6-9]. Therefore, in order to fully understand the behavior of realistic foam material, one has to consider non-uniform arrays of foam microstructure that incorporates defects. This research will be focused on developing appropriate models for each level of approximation and integration of the various approximations to create a model for predicting failure of closed cell foams. The first step is to identify and develop techniques to model the "unit cell" for the foam microstructure. This can serve as building blocks that can be used to discretely model the critical regions of a large scale model. They could also be used to obtain effective properties for the material. This could be then used for modeling homogenized regions in a multi scale model that are far away from the critical regions. The generation of the unit cell model is discussed in Chapter III. It is necessary to understand the behavior of a uniform array of unit cells before attempting multiscale analysis. Moreover, the behavior will serve as a reference when analyzing non-uniform arrays of foam unit cells. For example, the behavior of a non-uniform array of unit cells should be compared to that of a uniform array with the same nominal relative density. The critical buckling stresses obtained from the analysis of the uniform array of unit cells could be used to help understand failure initiation in larger multi-scale models. Postbuckling behavior of the unit cell can be used to determine if the effective material properties for the homogenized region need to account for geometric nonlinearity. The local stress concentrations and its locations could change after the onset of buckling. This could have an effect on the modeling of damage. The main goal of this research is to describe

the models used to analyze uniform foam microstructure and discuss results of a limited parametric study. In particular, we look at the effect of microstructure on the stiffness and strength of the foam. This includes the strengths based on the onset of buckling under different loading conditions by conducting linear buckling analysis. Due to the complex microstructure of the foam material, simple onset of buckling of a particular face or edge does not imply that the material has failed. For this reason, we also need to conduct post-buckling analysis.

Chapter IV discusses the modeling of the foam microstructure at a larger scale. A distorted multicell model is developed that can incorporate point defects (or large voids) in the foam microstructure. A regular array of unit cells is distorted to form the defect in the microstructure. Different functions were tested in the distortion procedure to see which function would be able to generate the most realistic microstructure of the foam with a large void. It was found that from the functions that were investigated, the cosine function was best suited for the job. The procedure to generate the model is explained in more detail in this chapter. Parametric analyses are conducted to determine the effect of defect size and defect density on the strength and effective stiffness of the foam in the linear regime.

CHAPTER II

BACKGROUND

2. 1 Polymer foam materials

Foams are three-dimensional cellular materials made from an interconnected network of the edges and faces of cells. There are different types of foams including metallic foams. In particular, this work deals with polymer foam materials used for insulating the space shuttle. This section of the chapter gives a brief background on polymer foam materials and starts by mentioning the different classifications of foam materials. Then the different types of synthetic polymer foams and their applications are discussed. The process for manufacturing polyurethanes and their material properties are mentioned. The method used to manufacture the rigid polyurethane form is discussed also.

2. 1. 1 Natural and synthetic foam

Foams can be classified two different ways. Humans use various foam materials such as cork, wood, balsa, and sponge (Figure 2.1); and these called natural foam. Recently, people have made synthetic foam materials for a variety of products ranging from disposable coffee cups to thermal insulation foam for the space shuttle. These synthetic foams can be made out of almost any material: metal, plastic, ceramic and glass as shown in Figure 2.2. The choice of material for foam depends on the application.

Most of the foams currently used are polymer based. There have been growing interest in metal foam and carbon foam. This research will focus on rigid polyurethane foam with solid material properties that have a typical Young's modulus of 1.6 GPa and a Poisson's ratio of 0.3 [10].

Another foam classification is microstructure based. If the solid material resides in the cell edges the cells have open faces; this foam is called open-cell foam. If the cell faces also have solid matter so that each cell is sealed from its neighbors, it is a closed-cell foam. Some foam is partly open-cell and partly closed-cell. This research considers synthetic closed cell foam.

Open and closed cell foams have different behaviors and for this reason different applications as well. The material on the faces makes the closed-cell foam stiffer. Since each cell of the closed-cell foam is isolated from the others, the closed cell foam provides thermal insulation. The BX250 and BX265 are both closed cell foam; they give good thermal insulation. Therefore, they are applied on the space shuttle. The solid faces in the closed cell foam complicate the foam's mechanical behavior.

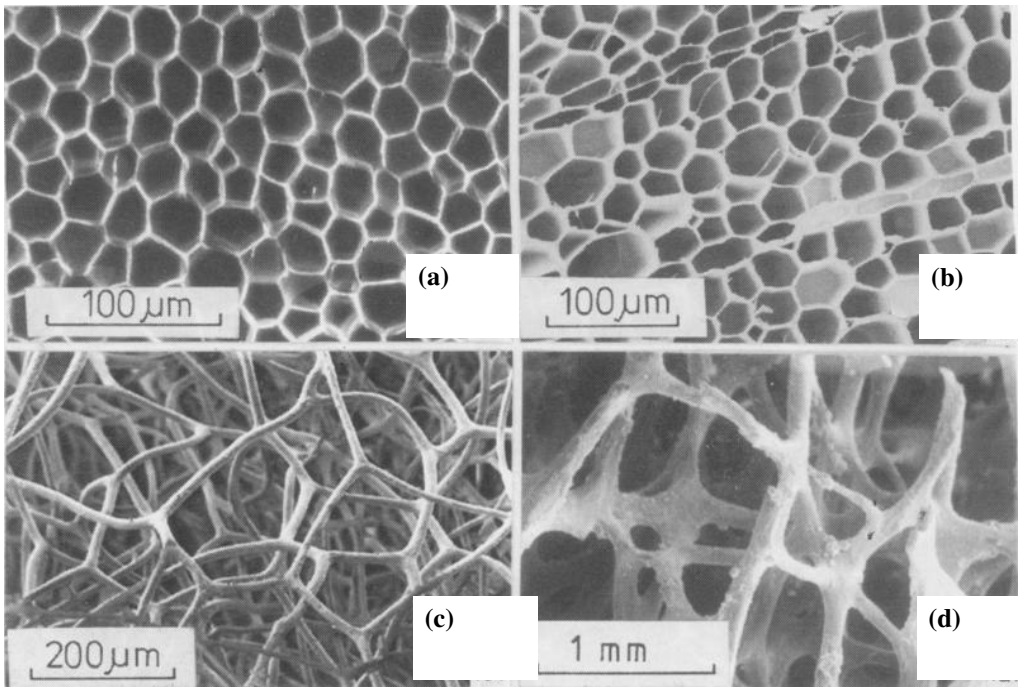

a) Cork b) Balsa c) Sponge d) Cancellous bone

Figure 2.1 Various natural foams [10]

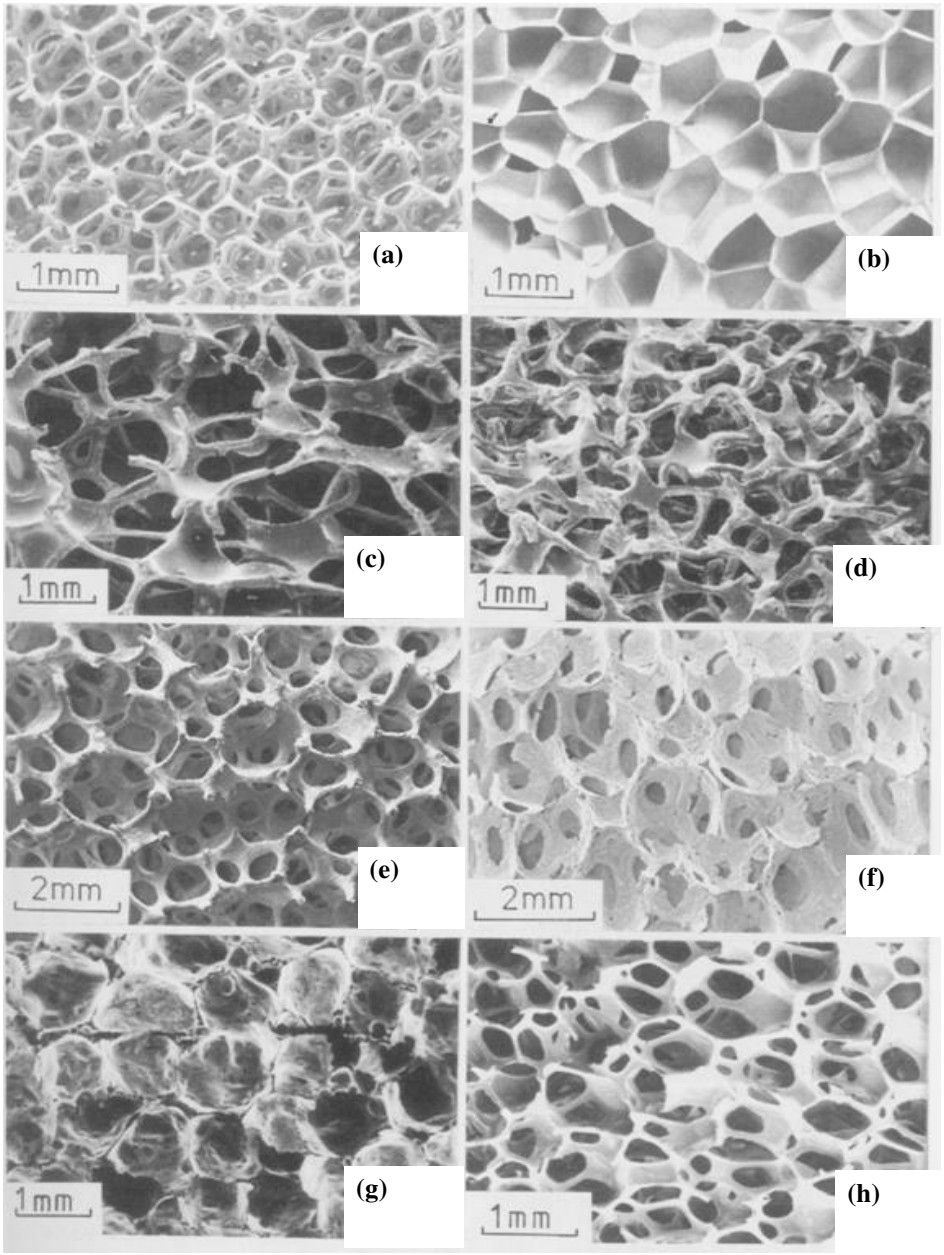

a) Polyurethane b) Polyethylene c) Nickel d) Copper e) Zirconia f) Mullite g) Glass h) Polyether

Figure 2.2 Various synthetic foams [10]

2. 1. 2 Types of synthetic foam

Different types of solids require different foaming techniques. Polymers are foamed by a process that uses these steps: introduce gas bubbles into a liquid monomer or a molten polymer, allow the bubbles to grow and stabilize, and finally, solidify the foam by cross-linking the monomer or by cooling the melt. The gas is introduced either by mechanical stirring or by mixing a blowing agent into the polymer. When a blowing agent is used the process is called blowing foam. The next section will discuss manufacturing of synthetic foam in detail.

Synthetic foams have a large range of applications for mechanical, thermal, and acoustic purposes. Figure 2.3 shows some of these applications. Four major foam material applications are thermal insulation, packing material, structural core, and buoyancy [10]. The largest single application for polymeric and glass foams is thermal insulation. For space-craft, foam materials are used in the thermal protection system. The second major use of synthetic foams is in packaging that must absorb the energy of impacts during shipping. Foam is employed well as a structural core in sandwich panels [10]. Sandwich panels in modern aircraft use glass or carbon-fiber composite skins separated by rigid polymer foams to give a panel enormous specific bending stiffness and strength. Closed-cell foams are used extensively as supports for floating structures and as floatation in boats. Foams are much more damage-tolerant than flotation bags or air chambers. Finally, foam materials have other uses such as filters at many different levels and water-repellant membranes.

a) Thermal Insulation

b) Packing

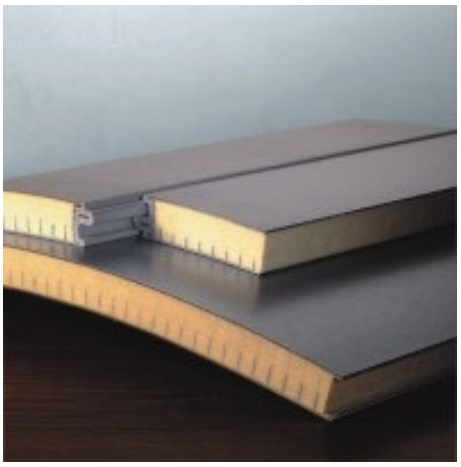

c) Structural Use

d) Filter, Water Repellent Membranes

e) Buoyancy

Figure 2.3 Application of foam materials [10]

The BX250 and BX265 polyurethane foams studied in this research were the thermal insulation on the space shuttle Columbia. They have a low relative density to obtain good thermal properties; however, they should have enough strength to maintain structural integrity to prevent significant shedding of debris, which can cause devastating consequences for the spacecraft.

2. 1. 3 Foamable polymer

The material used to make BX250 and BX265 foam is polyurethane. In this chapter, the chemical structure and characteristic of polyurethane itself are introduced. Then, the manufacturing technique to make rigid polyurethane foam is shown.

Polyurethanes have a urethane linkage on their backbones. Figure 2.4 shows these urethane links. Figure 2.5 shows a simple polyurethane, but polyurethane can be any polymer containing the urethane linkage in its backbone chain. Sophisticated polyurethanes are possible. Polyurethanes are produced by mixing hydroxy compounds with either polyisocyanates or phosgene and ammonia. Polyurethanes are versatile polymers. They have use as elastomers, molding resins, foams, and coatings. Their hardness spans the range from hard are rigid solids to soft elastomeric solids. Finally, polyurethanes can be either a thermoset or a thermoplastic.

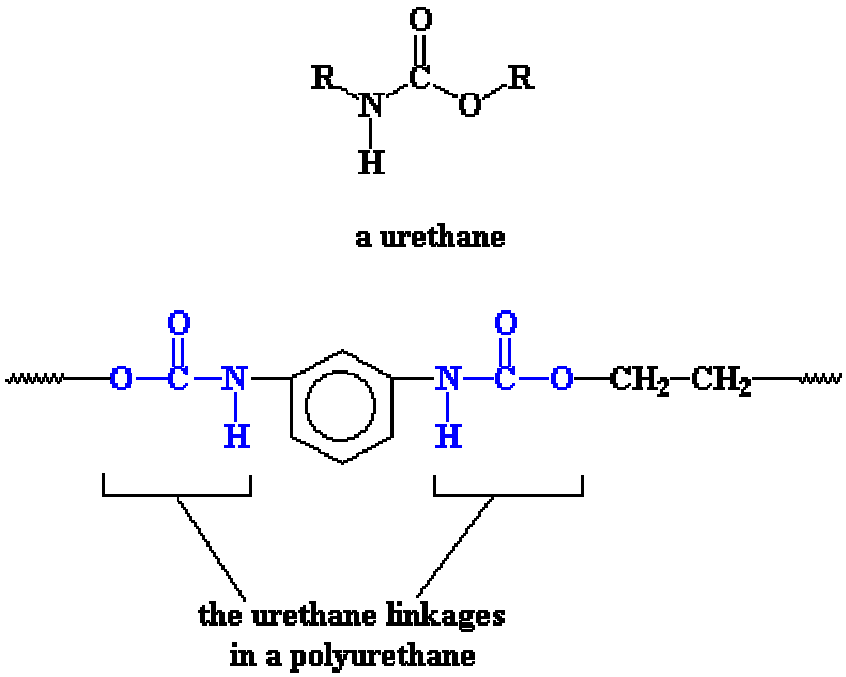

Figure 2.4 Chemical structure of typical polyurethane

Figure 2.5 shows the more complicated chemical structure of typical polyurethanes. Polyurethanes are phase-separated block copolymers in which one polymer segment is stiff and rigid and the other is soft and elastomeric. The stiff segments hold the material together at room temperature, but at processing temperatures the stiff segments can flow and be processed. The stiff segments govern the heat resistance of the polyurethane. Formulators can vary the properties of polyurethanes by changing the type or amount of the three basic building blocks of polyurethane chemistry, which are diisocyanate, short-chain diol, and long-chain diol. Polyurethanes can be flexible or rigid depending on the type of cross-linking that exists between the molecules. The type of catalysts used determines the mechanical properties of polyurethane, since the cross-linking is very dependent on the catalyst.

For example, tertiary amines, or ganometallics (primarily tin compounds) and carboxylic acid salts are used to catalyse the reaction of isocyanates with water (blowing) and polyols (polymer gelation). The catalyst controls the relative reaction rates of the isocyanate with polyol and water [11].

Amine catalysts are generally the preferred blowing catalysts since they tend to catalyse the isocyanate-water reaction better than the isocyanate-polyol reaction. However, amines do catalyse both reactions, with the relative rates of each reaction being dependant on the specific amine catalyst used. Some common amine catalysts are listed in Table 2.1 [11].

As depicted in the Table 2.1 the group of catalysts for the synthesis of rigid polyurethanes shows much higher reactivity which can readily react with the carbon of

the isocyanate group and produce a urethane group. However, the ternary amine catalysts, generally, for curing of the flexible polyurethanes show lower number of reactive sites than those of catalysts for the rigid polyurethanes. As is well known, the strength of polymeric materials is related to density and is reflected in the inter- and intramolecular forces that hold the polymer chains together under applied stress. Thus the catalyst group for rigid polyurethane, which produces much higher reactivity before curing and even smaller free-volume after crosslinkings, results in superior mechanical and physical properties, such as tensile and compressive strengths.

Other than crosslinking factors, generally, MDI (methylene-*bis*-dyphenyl diisocyanate)-based polyurethanes are stiffer and harder than TDI (Toluene diisocyanate)-based systems [12]. For a given isocyanate, stiffness and compressive strength vary together. The backbone on which a polyurethane is built consists of a number of covalent bond types; the urethane bond is the least common. Each bond has a cohesive energy that defines how much energy is required to tear it a part physically. This characteristic clearly has an effect on the strength of the polyurethanes. The Table 2.2 [12] compares the cohesive energies of the most of the important chemical bonds in a polyurethane. Both the chosen catalysts and the properties of base materials affect the final mechanical and physical properties of polyurethane. Selective mechanical properties are listed and compared in the Table 2.3 [12].

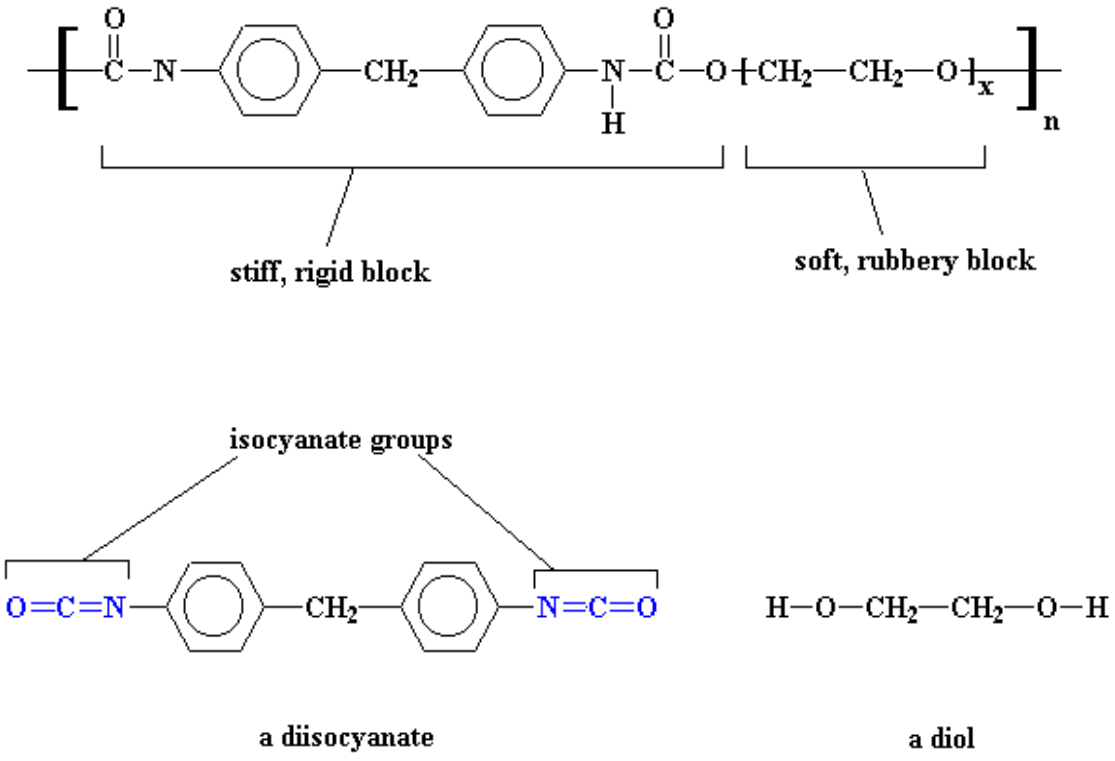

Figure 2.5 Structure and row materials of polyurethane

Table 2.1 Tertiary amine catalysts and their characteristics [11]

Characteristics	Catalyst	Formulae
Rigid	N,N-dimethylethanolamine (DMEA)	$(CH_3)_2NCH_2CH_2OH$
	N,N-dimethylcyclohexylamine (DMCHA)	$C_6H_{11}N(CH_3)_2$
	N,N,N',N',N',pentamethyl diethylenetriamine (PMDETA)	$(CH_3)_2NCH_2CH_2N(CH_3)CH_2CH_2N(CH_3)_2$
	1-(bis(3-dimethylamino)-propyl)amino-2-propanol	$(CH_3)_2N(CH_2)_3N(CH_2CHOHCH_3)(CH_2)_3N(CH_3)_2$
Flexible	2-(2-dimethylaminoethoxy)-ethanol (DMAEE)	$(CH_3)_2NCH_2CH_2OCH_2CH_2OH$
	N,N-dinethylbenzylamine	$C_6H_5CH_2N(CH_3)_2$
	N,N'-diethylpiperazine	$CH_3CH_2N(CH_2CH_2)_2NCH_3CH_2$

Table 2.2 Molar Cohesive Energy of Organic Groups [12]

Group	Cohesive Energy (kcal/mol)
—CH— (methylene)	0.68
—O— (ether)	1.00
—COO— (ester)	2.90
—C6H4— (aromatic)	3.90
—CONH— (amide)	8.50
—OCONH— (Urethane)	8.74

Table 2.3 Effects of hard segments on mechanical properties of polyurethanes [12]

	15% Hard segments (Flexible)	40% Hard segments (Rigid)
Tensile strength (psi)	2000	6500
% Elongation	500	200
Tear strength (N/m)	480	187

Polyurethane foams can be flexible, semirigid, or hard and rigid materials. The foam density can range from as low as 16.02Kg/m^3 (1lb/$ft^{3)}$ or lower to as high as 961.2Kg/m^3 (60lb/ft^3). Polyurethane foams, in general, are produced by the reaction of a diisocyanate and a polyol or a mixture of polyols that are hydroxy terminated. Such materials are polyesters or polyethers.

The reaction between the isocyanate and the polyol produces the urethane resin. A further reaction between a slight excess of isocyanate and water, added to the polyol, can then produce carbon dioxide gas to form the cellular structure of the foam. A low-boiling, inert liquid fluorocarbon is mixed in with the polyol. When the polymerization reaction takes place, the exotherm is sufficient to cause the fluorocarbon to volatilize and act as blowing agent. It should also be noted that a typical urethane formulation, in addition to the isocryanate, polyol, and blowing agent, will also have incorporated, usually in the polyol, a catalyst and a surface-active agent. The catalyst, in most cases an organotin compound, is used to accelerate the reaction so gelation will take place before the gas is dispersed. The surface-active agent, called a surfactant, is usually a silicone liquid and is used to obtain finely dispersed cells.

2. 2 Models of foam materials

2. 2. 1 Model structures

A main concern of foam analysis is the shape of the model unit cell. It is difficult to define a representative unit cell for foam because foam has many irregularities such as different cell shapes, distributed cell sizes, cell face curvature, and solid distribution. However, idealizations make the problem tractable. In 1873, Plateaus suggested using the space filling rhombic dodecahedron to describe foam; but, this is not very realistic because of that model's large surface area per unit volume. Kelvin in 1887 introduced the tetrakaidecahedron cell, which has 14 faces [13]. Kelvin's cell is broadly applied to this day. Figure 2.6 shows the rhombic dodecahedron of Plateaus and the tetrakaidecahedron of Kelvin.

In 1994 Weare and Phelan found the most efficient cell shape to minimize surface area per unit volume using computer techniques [14] (Figure 2.7 (a)). This model has six 14-side polyhedrons and two 12-side polyhedrons. However, the surface to volume ratio is only 0.3% better than Kelvin's model. In addition, this model is too complicated to use; it is not an attractive option. When real foam is made, surface tension and other manufacturing effects play an important role in determining the cell shape. Specially, cell types such as open or close cell tend are influenced by surface tension. Moreover, solid distribution like the fraction of solid in the cell edges depends largely on surface tension. If the manufacturing process bonds together previously expanded spheres or granules, spherical cell shapes can be included into the unit cell model (Figure. 2.7(b)). Most unit cells with sphere is made from metal foam.

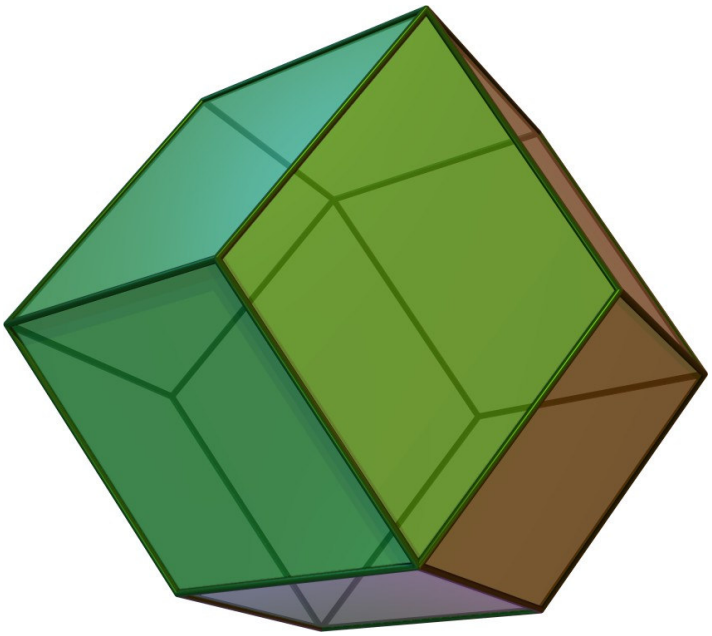

(a) Rhombic dodecahedron

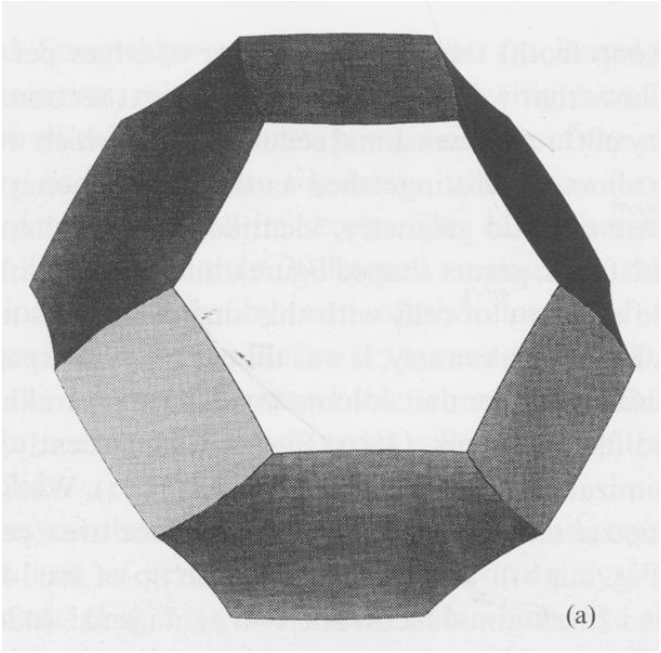

(b) Tetrakaidecahedron

Figure 2.6 Rhombic dodecahedron and tetrakaidecahedron [10]

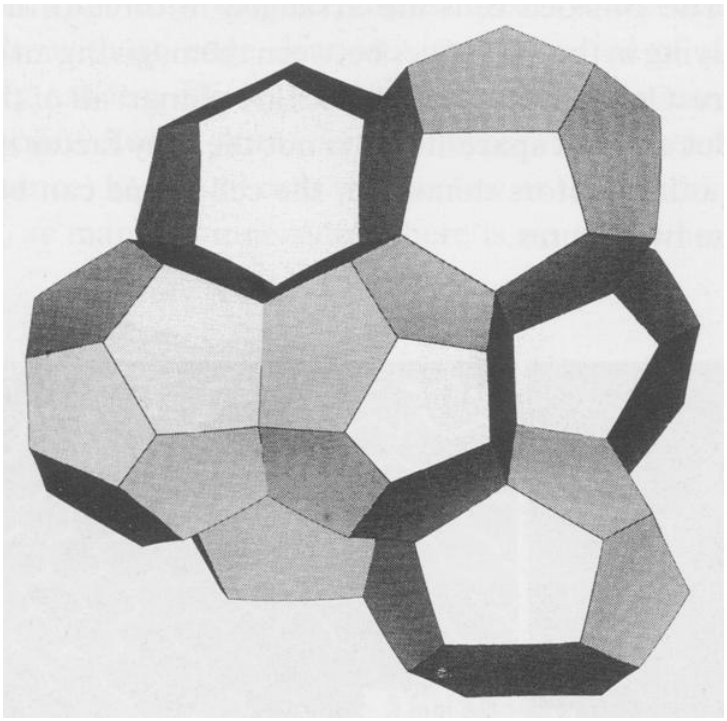

(a) Model from Weare and Phelan

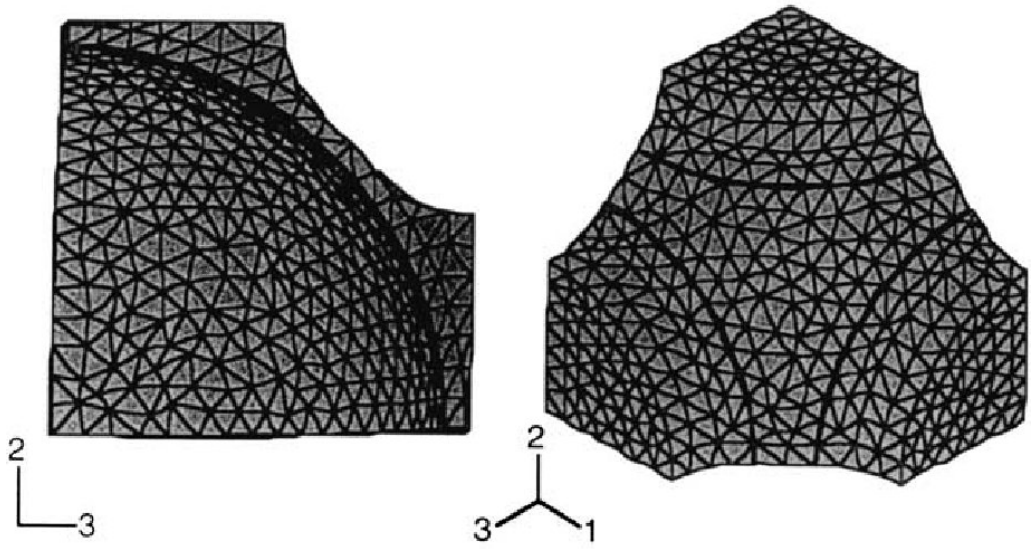

(b) Spherical model

Figure 2.7 Model from Weare and Phelan and unit cell model with sphere

A more direct approach to embody irregularity is the Voronoi tessellation model (Fig 4.) used by Robert and Garboczi's [3] (Figure 2.8). In a voronoi tessellation, a cell is defined by the space that is closer to a specific seed point than to any other. Mathematically, the voronoi tessellation is obtained by allowing spherical bubbles to grow with uniform velocity from each seed point. Wherever the bubbles touch, growth halts at the contact surface, but growth continues elsewhere. In this respect the tessellation is similar to the actual process of liquid foam formation.

The amount of structure or disorder in the voronoi tessellation depends on the spatial distribution of the seed points. Seed points in a poisson distribution, randomized lattice arrangements or seeds deployed by random sequential adsorption (RSA) algorithm [15, 16] may result in unstructured, random voronoi tessellations. The seed distribution influences the cell morphology, the spatial disposition of the cells, and the cell size distribution.

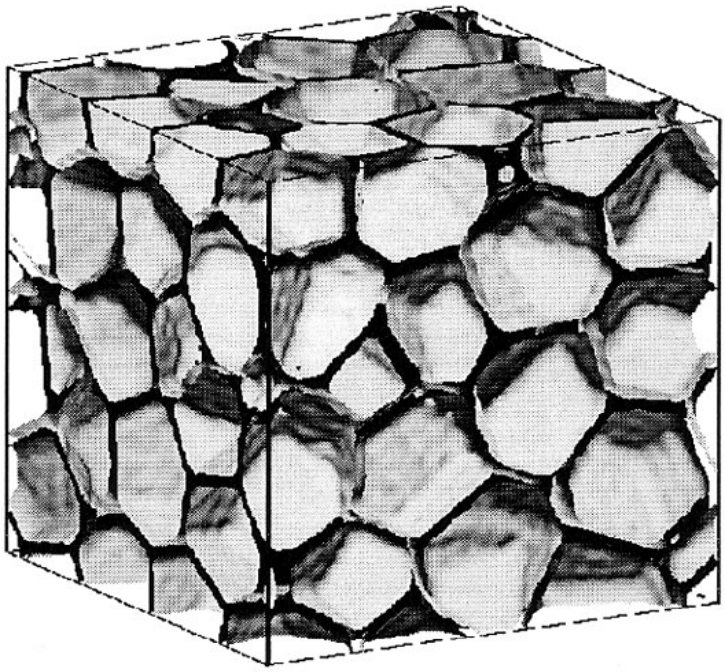

Figure 2.8 Typical voronoi tessellation model [3]

However, they did not consider solid distribution. The study about the solid distribution is well presented in Simone and Gibson's paper [2]. The curvature of the cell wall significantly affects the effective properties of foam cell. Simone and Gibson's paper [1] considers this geometrical effect. In this study, to consider the irregularity, novel techniques are used to generate irregularly distributed cells. The reason that voronoi tessellation model is not adopted is that it is very difficult to control directly the irregularity.

Recently, new techniques have been introduced to depict real foam shape. Mathew and Allen 2004 [13] used X-ray tomography and image processing to identify the actual foam architecture, including mean geometric parameters such as strut length, area of cell and interior angle (Figure 2.9(a)). Youssef and Maire 2004[14] used the same technique to make a 3D solid model, and they calculated effective properties using this 3D model by FEA method (Figure 2.9(b)).

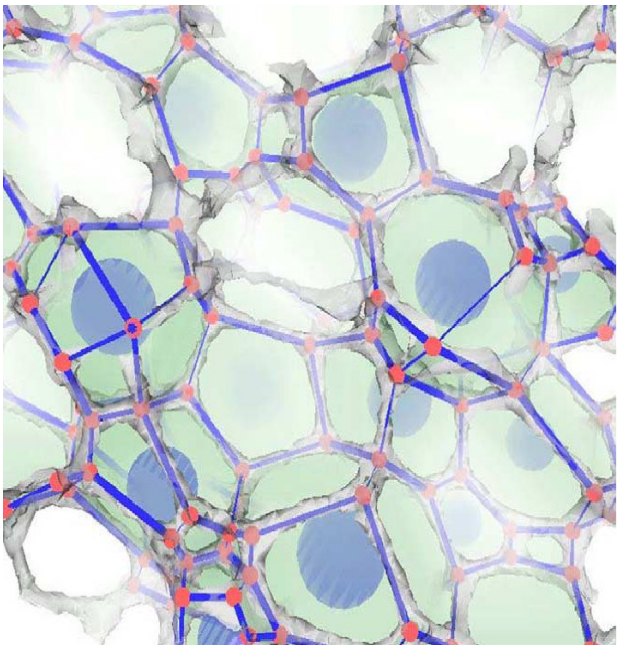

(a) 3D image from X-ray tomography

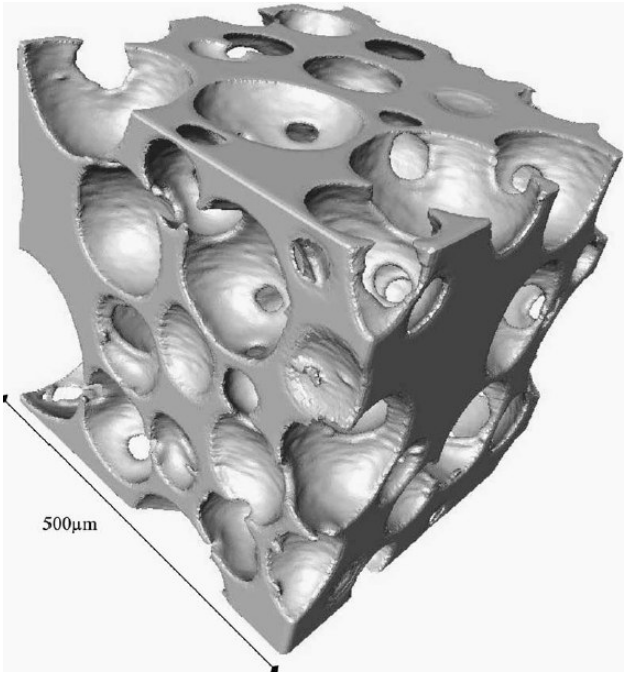

(b) 3D solid model from image processing technique

Figure 2.9 3D images from X-ray tomography and 3D solid model from image processing technique

While being a close digital reproduction of the structure of a real foam, these models are unique for each individual foam sample and may not necessarily be representatives. Generally, digitized models are not periodic, which may hamper the application of boundary conditions in FEM.

The mechanical properties of the modeled foam may depend on the digitizing process numerical errors to the FE analysis which could be avoided by a including a high level of detail in the digitizing but then it may not always be possible to create a finite element model from the data as the model may be very large [14].

In this study, the tetrakaidekahedral model with flat faces is adopted as the representative volume element for closed cell foam for regions where the foam is assumed to be regular.

The dimensions for the tetrakaidekahedral model considered in this study are given in Table 2.4 and are obtained from Ref. [10]. The edge fraction (φ) is defined as ratio of the edge volume in the cell to the total material volume in the cell.

Table 2.4 Dimensions of tetrakaidekahedron unit cell

	Set 1
t_e(cell edge thickness)	0.03mm
t_f (cell face thickness)	0.003mm
L(cell edge length)	0.22mm
φ (edge fraction)	0.7
ρ^*	32 Kg/m^3
ρ_s	1.05 Mg/m^3
ρ^*/ρ_s (relative density)	0.0305

2. 2. 2 Properties of model structures

The effective properties of foam materials depend on the material from which they are made, their relative density, and their internal geometrical structure. It is important to relate the elastic properties of foam materials to their density and complex microstructure, in order to understand how such properties can be optimized for a given application. At low densities, experimental results indicate that the Young's modulus (E) of the foam materials is related to their density (ρ) through Equation 2.1 [10]:

$$\frac{E}{E_S} = C\left(\frac{\rho}{\rho_S}\right)^n \qquad 2.1$$

where E_s and ρ_s are the Young's modulus and density of the solid materials. The constants C and n depend on the microstructure of the foam. The value of n generally lies in the range n=1~4 [5, 17-18]. For closed-cell foams, experimental studies indicate that $1< n <2$. The complex dependence of C and n on microstructure is not well understood, and this remains a crucial problem in the ability to predict and optimize the elastic properties of foam materials. At the local scale, important variables include the cell character (e.g. open or closed), the geometrical arrangement of the cells (e.g. angle of intersection), and the shape of the cell walls (e.g. curvature). At the larger scale, the geometrical arrangement of the cells is also crucial. The values of both C and n will depend on whether the material is periodic or disordered. Analysis of simple models shows that three basic mechanisms of deformation are important for closed cell foam [10]. If the cell walls are much thinner than the cell edges, the deformation is governed by edge bending. In this case, E varies according to n=2, and can be described by results

for open cellular solids [10]. If cell-wall bending is the mechanism of deformation, Gibson and Ashby [17] have shown that n=3. However, experimental and analytical results [5, 10, 19-21] show that *n* actually lies between 1 and 2, indicating that cell-wall stretching ($n = 1$) is actually the dominant behavior. The tetrakaidecahedral foam model has been the subject of many recent studies [18, 22–25]. This tetrakaidecahedral model of the foam has a relatively low anisotropy [22] (*E* varies by less than 10% with direction of loading), and is thought to be a good model of isotropic cellular solids. A Typical anisotropic tetrakaidekahedral model for open cell is shown Figure 2.10. In all cases, *E* was found to increase linearly with density ($n = 1$) [10]. However, real materials exhibit a larger dependence of *E* on density ($n>1$), indicating that periodic models do not capture salient features of foam microstructure. It is possible that the disorder is responsible, and it is important to study its influence on the properties of foam materials.

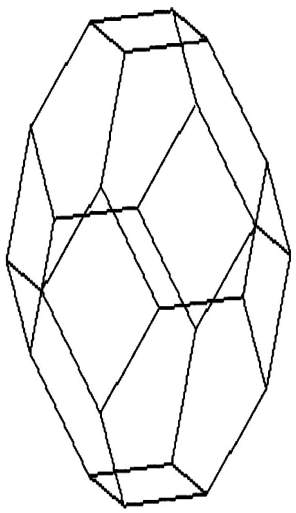

Figure 2.10 Anisotropic tetrakaidekahedron unit cell

There have been several recent studies of the effect of disorder in cellular solids. For two-dimensional models, variation in cell-shape leads to a variation of 4–9% in elastic properties [9], while deletion of 5% of cell struts decreased the modulus by 35% [9]. Similar effects of "imperfections" were seen in spring lattices, which have some similarities to foams [26]. In three-dimensions, Grenestedt [27] showed that disorder decreased the Young's modulus of the tetrakaidecahedral foam (with 16 cells) by 10%. Grenestedt [27] has also estimated the effect of "wavy imperfections" on the stiffness of a cube with closed cell walls. If the wave-amplitude was five times the cell-wall thickness, the stiffness decreased by 40% compared to the case of flat faces. In figure 2.11, a unit model with a wavy imperfection is shown. From the previous discussion, it is clear that more complex, three-dimensional disorder models are necessary to improve predictions for the behavior of foam materials. There are two main problems in studying disorder models. First, a sufficiently accurate model of the microstructure must be developed. And second, the properties of the model must be accurately evaluated.

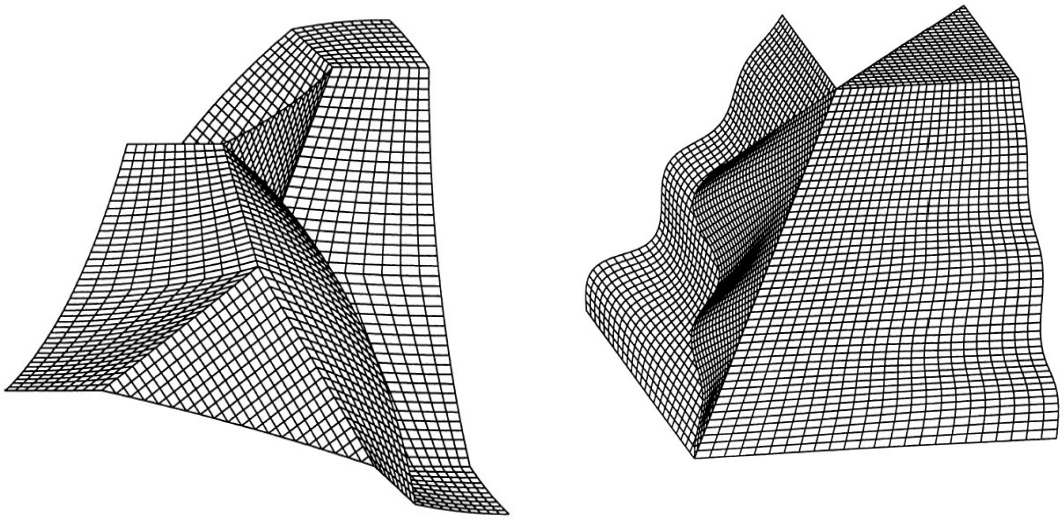

Figure 2.11 Unit cell model with cell face curvature and corrugation [28]

Numerous publications can be found on the failure behavior of polymer foams covering deformation behavior, failure modes, constitutive modeling and other related issues. Most of this research has been performed experimentally. Brittle foams under uniaxial loading fail when the stress in the bent cell strut reaches the modulus of rupture of the solid cell wall material. In compression, the cells crush progressively in a brittle manner [29-34] while in tension the material fractures suddenly by fast crack propagation [32-38].

Foam can be classified into three categories: elastomeric foam, elastic-plastic foam, and elastic-brittle foam. Most rigid polymer foams are elastic-plastic foam. Figure 2.12 shows a typical stress-strain diagram for elastic-plastic foam. Foam shows different character according to the loading. When compression is applied, the deformation behavior can be divided into three areas. In the small strain range, open cell foam will act as a linear material, and bending of the cell struts is very important. In the case of closed cell foam, the cell wall can bear a small portion of load as stretching. Subsequently, plastic yielding starts. After cell walls or struts contact each other, foam stiffness increases. This regime is called densification. When tension is applied, a different behavior is exhibited. Although the linear elastic behavior is similar, after plastic yield, because of cell alignment, foam shows stiffer behavior.

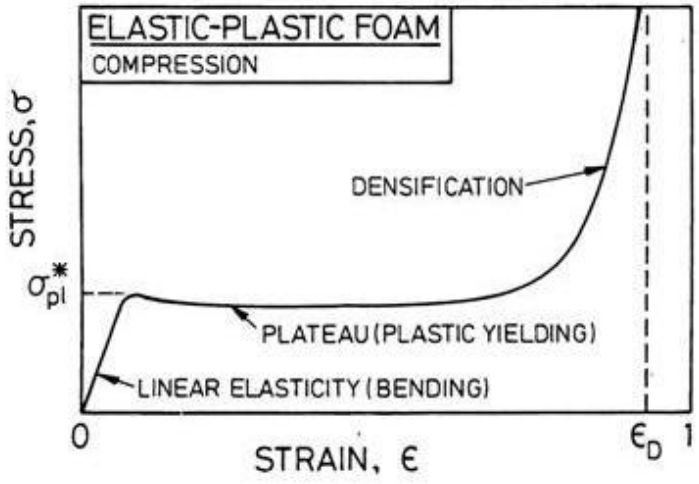

(a) Compressive strain –stress curve

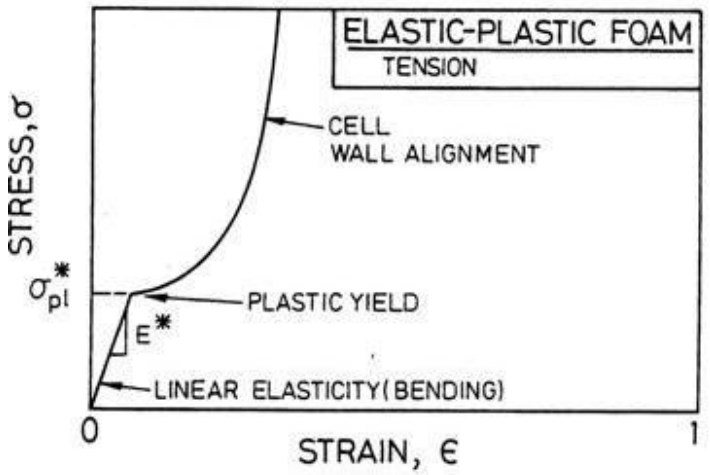

(b) Tensile strain-stress curve

Figure 2.12 Schematic stress-strain curve for foam [10]

The failure of foams under multiaxial stress states was first measured by Shaw and Sata [39], who tested polystyrene foams, and by Patel and Finnie [29] and Zaslawsky [15], working with rigid polyurethane foams. Their results indicated that under biaxial compression both foams yield according to a maximum principal stress criterion. This is an unusual result since fully dense plastic solids yield according to the von Mises criterion which involves all three principal stresses. In biaxial tension, the rigid polyurethane failed by fast brittle fracture following the expected maximum principal tensile stress criterion. Recently, elastic buckling and plastic yield failure envelopes for foams under a general state of stress have been developed [16, 40]. The results indicate that, in general, failure depends on all three principal stresses. In biaxial compression, however, the yield envelope is roughly elliptical and can be approximated by a maximum principal stress criterion in two quadrants. However, these experimental approaches are unable to study the effect of microstructure of the foam on the failure.

Recently, computational and theoretical analysis has been performed to calculate the fracture toughness [41]. Most of the research work has been focused on open cell foams. However, in this research, the closed cell foam is studied.

2. 2. 3 Present work

As mentioned earlier, the tetrakaidekahedral model is the unit cell model for all the analyses in this research. Most of FE models mentioned in the literature are three-dimensional solid elements. However, beam elements are used for modeling open cell foams. In this work, shell and beam elements are used to model closed cell foam. A

review of the literature did not show any work using this kind of method to model the defects in the foam material. Here, instead of just random effect (voronoi tessellation), we control the defect and examine the effect of defects on foam behavior. In the next chapter a novel beam and shell model for tetrakaidekaheron is introduced. The effect of geometric characteristics (relative density and edge fraction) on the stiffness and strength are also discussed.

CHAPTER III

UNIT CELL MODEL

3. 1 Introduction

This chapter explains the generation of the a novel unit cell model for the foam microstructure using beam and shell elements. The regular array unit cell model should be developed for two reasons. One is so that a reference can be obtained which can be compared with the disordered array model. The second reason is that a full 3D analysis is very expensive. Three dimensional solid elements have been utilized by other researches to model regular array unit cell [28, 25]. However, too many elements are consumed to make the multi cell model by three dimensional solid elements. Therefore, a more different model which is composed of beam and shell element is developed. The next section discusses the geometry of the foam unit cell and the development of the beam and shell model. The dimensions, material properties and boundary conditions used in the model are also discussed. This section discusses the result from the analysis of the unit cell model. This includes the parametric studies as well the results from linear and post-buckling analysis.

3. 2. Beam and shell model

Three dimensional solid elements have been utilized by other researchers to model a regular array unit cell [17, 28, 42]. However, too many elements are consumed

to make a multi cell model using three dimensional solid elements. Therefore, a simpler model composed of beam and shell elements was developed. The edges were modeled with beam elements, and the faces were modeled with shell elements. For simplicity, the beam element has a circular cross section.

Figure 3.1 (a) shows a mesh for a typical tetrakaidecahedral unit cell. However, two problems exist with this geometry when beam and shell elements are used. When the representative volume element (RVE) is assumed to be as shown in Figure 3.1 (a), the edges and faces are divided through the thickness at the boundaries. This split through the thickness of faces and edges causes the shift of the neutral axis in the beam and shell elements. There exist several options to solve this problem such as the use of fairly complicated multi point constraints. However, the simplest solution is to choose a different RVE such that the boundaries do not split faces or edges. The cuboid model (Figure 3.1 (b)) is obtained by slicing a cuboid out of a regular array of tetrakaidecahedra. This cuboid contains the volume of four tetrakaidecahedra and its dimensions are $4l$ x $4l$ x $2\sqrt{2}l$. The total length of the edges and area of the faces in cuboid model is twice the corresponding number in the single tetrakaidecahedron model. Therefore, the number of elements increases to twice that of the single tetrakaidecahedron model. The second problem involved in beam and shell models deals with establishing the interface between adjoining beam and shell elements. The easiest way to connect the beam and shell elements is for them to share the same corresponding nodes. Unfortunately, this creates overlapping material, since the beam element nodes are located along the central axis of the beam. To eliminate this problem, the beam and

shell elements were joined with rigid links, as illustrated in Figure 3.2. The beam and face were joined at the boundary of the beam element rather than the interior of the beam. This was accomplished by using links that join the surface nodes to the beam nodes. These links account for both translations and rotations. Since it is considerably more difficult to add these links than it would be to allow the overlap, a few cases were analyzed both ways. As shown later, allowing the overlap causes large errors.

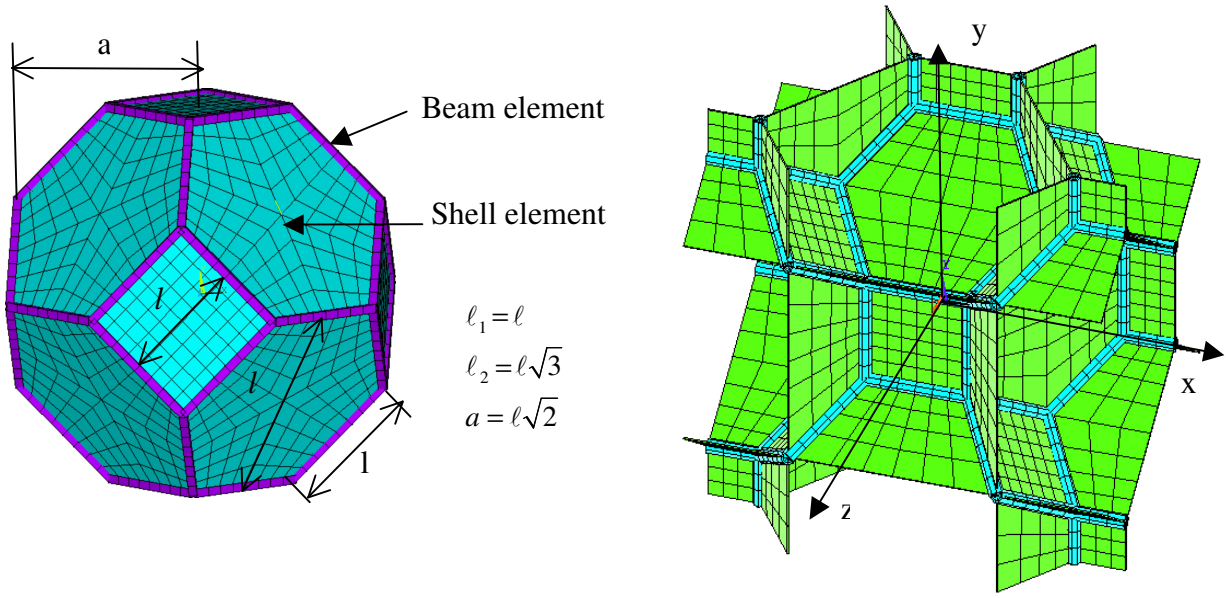

a) Single tetrakaidecahedron model b) Cuboid model

Figure 3.1 Beam and shell model

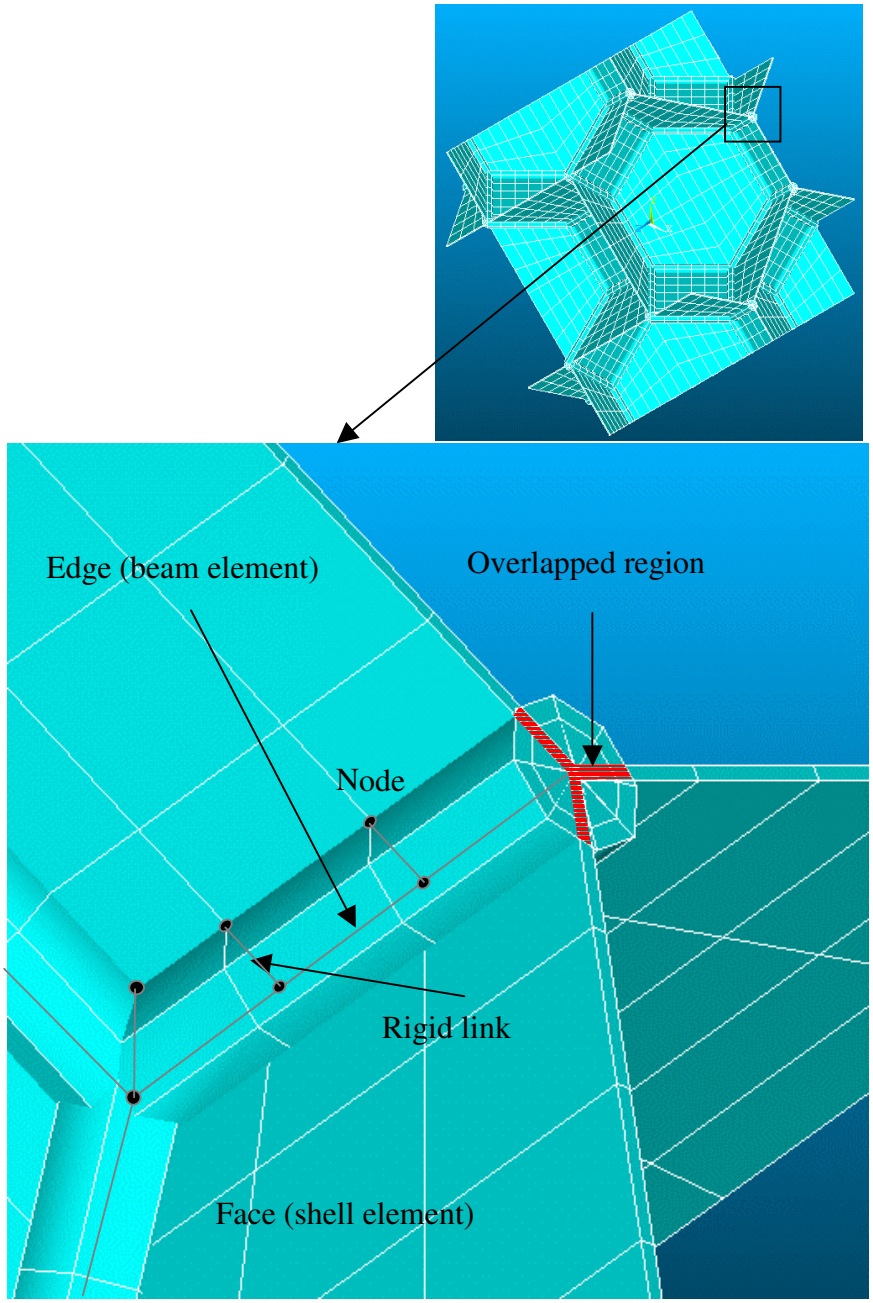

Figure 3.2 Rigid link model

Rigid links can be implemented in two different ways in ANSYS. The first one is a linear rigid link which is a multipoint constraint applied using the command "CERIG" in ANSYS. To define a rigid link, the two nodes that are being linked together using this element need to be specified. Specifying the nodes for such a huge model is not a trivial task and scripts were developed to automate this task. The six degrees of freedom from each node are then related to those from the other node. Equation 3.1 shows the relationship between two nodes for a linear rigid link.

$$\begin{bmatrix} u \\ v \\ w \\ Rot_x \\ Rot_y \\ Rot_z \end{bmatrix}^1 = \begin{bmatrix} 1 & 0 & 0 & 0 & z & -y \\ 0 & 1 & 0 & -z & 0 & x \\ 0 & 0 & 1 & y & -x & 0 \\ 0 & 0 & 0 & 1 & 0 & 0 \\ 0 & 0 & 0 & 0 & 1 & 0 \\ 0 & 0 & 0 & 0 & 0 & 1 \end{bmatrix} \begin{bmatrix} u \\ v \\ w \\ Rot_x \\ Rot_y \\ Rot_z \end{bmatrix}^2 \qquad 3.1$$

In this multipoint constraint, the rigid link is assumed to have small rotations. Therefore, this link is not suitable for a large deformation analysis like post buckling analysis, but it is valid for linear elastic and linear buckling analysis. The nonlinear rigid link is designed to take into account large deformations. This is designated as the "MPC184" element in ANSYS. However, this link method is not supported for linear buckling analysis. Therefore, both types of constraints are needed. All the results discussed in this paper (except for the limited evaluation of the overlap model) are obtained by using the rigid-link cuboid model (Figure 3.1 (b)) containing 3746 elements. This level of refinement was chosen based on convergence studies. Hereafter, the rigid link cuboid model will be simply called the rigid link model.

3. 2. 1 Dimensions and material properties

Some of the dimensions and material properties used for modeling the foam microstructure were obtained from Ref. 6. The cell edge length (l) is taken to be 0.22mm and the reference edge fraction (Ø) is taken to be 0.7. The solid foam material was assumed to be an isotropic rigid polyurethane with the Young's modulus=1.6 GPa and Poisson's ratio=0.3. In order to model the foam unit cell using beam and shell elements, we need to calculate the dimensions of the edges and faces. Using the cell edge length and edge fraction, the other dimensions need to be calculated based on the assumption that the beam has a circular cross section. The equations for the cell edge thickness and cell face thickness are derived as follows. The regular tetrakaidecahedron geometry consists of square and hexagonal faces and their volumes are given by:

Square Face Volume: $12(l - t_e)^2 t_f$

Hexagonal Face Volume: $16(l - \frac{t_e}{\sqrt{3}})^2 t_f$

The cell edges are idealized to be beams with circular cross-section and the beam's end-surfaces are normal to the beam's central axis. Due to this assumption, there is an overlap of material at the vertices where these edges meet. This overlap also depends on the number of edges meeting at the vertex. An approximate correction term was derived to account for this overlap of material (Appendix A). The main formulas are summarized below.

Edge Volume with Correction Term: $12\pi l(t_e)^2 - 6\pi(t_e)^3$

The volume of the entire RVE (cuboid model) is given by $\frac{64}{\sqrt{2}}l^3$

Based on these assumptions, the relative density of the foam can be expressed as

$$\frac{\rho^*}{\rho_s} = \frac{\text{volume of solid material}}{\text{volume of foam RVE}} = \frac{12(l-t_e)^2 t_f + 16(l-\frac{t_e}{\sqrt{3}})^2 t_f + 12\pi l(t_e)^2 - 6\pi(t_e)^3}{\frac{64}{\sqrt{2}}l^3} \quad 3.2$$

The edge fraction of the foam can also be expressed as

$$\phi = \frac{\text{edge volume}}{\text{material volume}} = \frac{12\pi l(t_e)^2 - 6\pi(t_e)^3}{12(l-t_e)^2 t_f + 16(l-\frac{t_e}{\sqrt{3}})^2 t_f + 12\pi l(t_e)^2 - 6\pi(t_e)^3} \quad 3.3$$

Equations 3.2 and 3.3 can be combined to eliminate the cell face thickness:

$$6\pi(t_e)^3 - 12\pi l(t_e)^2 + \phi\frac{\rho^*}{\rho_s}\frac{64}{\sqrt{2}}l^3 = 0 \quad 3.4$$

Equation 3.4 is solved to obtain t_e. Finally, this value of t_e is substituted into Equation 3.3, which is then solved to obtain the following formula for t_f.

$$t_f = \frac{(1-\phi)(12\pi l(t_e)^2 - 6\pi(t_e)^3)}{\phi(12(l-t_e)^2 + 16(l-\frac{t_e}{\sqrt{3}})^2)} \quad 3.5$$

Two sets of parametric studies were conducted – one involved varying the edge fraction and the other involved varying the relative density.

3. 2. 2 Finite element analysis

Effective properties for the foam were calculated by conducting linear analysis of the periodic rigid link model using ANSYS. Shell 63 elements with six degrees of freedom (u_x, u_y, u_z, rot_x, rot_y, rot_z) were used for the faces, and Beam 188 elements with circular cross-section and six degree of freedoms (u_x, u_y, u_z, rot_x, rot_y, rot_z) were used for the edges. Periodic boundary conditions can be derived from Equation 3.6.

$$\begin{aligned} u_i\left(x_\alpha + d_\alpha\right) &= u_i\left(x_\alpha\right) + \left\langle \frac{\partial u_i}{\partial x_\beta} \right\rangle d_\beta \\ rot_i\left(x_\alpha + d_\alpha\right) &= rot_i\left(x_\alpha\right) \end{aligned} \qquad 3.6$$

where u_i are the displacements, rot_i are rotations, d_β is the vector of periodicity, and $\left\langle \frac{\partial u_i}{\partial x_\beta} \right\rangle$ are the volume averaged displacement gradients. The term $\left\langle \frac{\partial u_i}{\partial x_\beta} \right\rangle d_\beta$ describes the rigid body motion. When Equation 3.6 is applied to the rigid link model in Figure 3.1 (b), multi-point constraints are obtained that relate the displacements on conjugate planes in Figure 3.3. For the linear buckling analysis, the Block Lanczos method was used for eigenvalue and eigenvector extraction in ANSYS [43]. For the post-buckling analysis, the arc-length method [43] in ANSYS was used. The arc-length method is particularly suitable for non-linear static equilibrium solutions of unstable problems such as post buckling analysis where there are bifurcations in the response path.

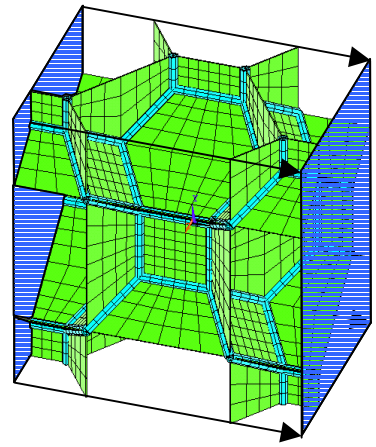

* Face: $x = \pm 2l,\ d_\alpha = 4l\,\underset{\sim}{i}$

$$u_i(2l, y, z) = u_i(-2l, y, z) + 4l < \frac{\partial u_i}{\partial x_1} >$$

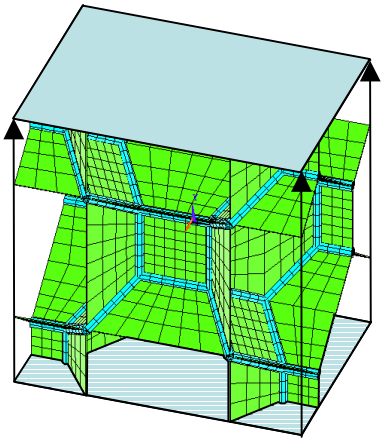

* Face: y $= \pm 2l,\ d_\alpha = 4l\,\underset{\sim}{j}$

$$u_i(x, 2l, z) = u_i(x, -2l, z) + 4l < \frac{\partial u_i}{\partial x_2} >$$

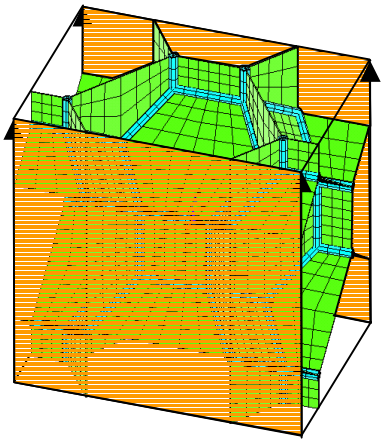

* Face: z $= \pm l/\sqrt{2},\ d_\alpha = \sqrt{2}l\,\underset{\sim}{k}$

$$u_i(x, y, l/\sqrt{2}) = u_i(x, y, -l/\sqrt{2}) + \sqrt{2}l < \frac{\partial u_i}{\partial x_3} >$$

Figure 3.3 Conjugate planes for the periodic boundary conditions for the unit cell model

3. 3 Results and discussion

This section is divided into four sections. First, it will be shown that the rigid link model is required, since allowing overlap in the model causes too much error. The next section presents the results from the parametric studies of linear elastic analyses of the foam material. The effect of different parameters such as relative density and edge fraction on stiffness and maximum Von Mises stress were determined. The variation of effective stiffness with respect to relative density was calculated and compared with data from the literature. The third section discusses the results from the linear buckling analysis for different loading conditions. The last section presents the results of the post-buckling analysis, which provides an idea of the behavior of the foam after the onset of initial buckling.

3. 3. 1 Comparison of rigid link model with overlapped model

The critical linear buckling stresses for compression, tension and shear loading cases were calculated for the cuboid model with and without rigid links (i.e. with and without overlap). Table 3.1 shows that allowing overlap in the model causes an error of 16.35 to 36.91%. The effective stiffness of the foam material in the y-direction (Figure 3.1 (b)) was also determined for both models and it was found that E_{yy} for the rigid link model was almost 21% larger than that of the overlapped model. These results show clearly that allowing overlap introduces large errors into the predictions.

Table 3.1 Linear buckling stresses for different loading cases

In-plane Loading(*10^4Pa)	Overlapped Model	Rigid Link Model	% Difference
Compression Loading (y)	5.3589	6.5244	17.85
Tension Loading (y)	13.2816	21.055	36.91
Shear Loading (xy)	0.8563	1.0237	16.35

3. 3. 2 Effective stiffness and strength

The effective stiffness of the foam material was calculated by conducting a linear analysis on a periodic rigid link model. The effective stiffness was calculated for a range of relative densities while keeping the edge fraction constant at 0.7. The results were compared with two different sets of data from the literature. The first set of data was obtained by considering an empirical equation derived from a cubic cell model which is then curve-fitted to experimental data. This data is labeled 'Cellular Solids' in Figure 3.4 and is obtained from Ref. 6. The empirical equation is of the form

$$\frac{E^*}{E_s} = C_1\phi^2\left(\frac{\rho^*}{\rho_s}\right)^2 + C_1^{'}(1-\phi)\left(\frac{\rho^*}{\rho_s}\right) \qquad 3.7$$

For an edge fraction of 0.7, curve-fitting gives $C_1 \approx 1$ and $C'_1 \approx 1$. Equation 3.7 is valid for relative density less then 0.2 [10]. Additional reference data is from Simone and Gibson [22], who modeled the foam microstructure using three-dimensional solid elements with a plateau border at the edges, where the plateau border is the scalloped-triangular channel where three faces meet. For relative densities less then 0.2 and for an edge fraction of 0.7, they described the variation of the stiffness with the relative density by Equation 3.8:

$$\frac{E^*}{E_s} = 0.3188\left(\frac{\rho^*}{\rho_s}\right)^2 + 0.3163\left(\frac{\rho^*}{\rho_s}\right) \qquad 3.8$$

Figure 3.4 shows that the results from the rigid link model agree well with both sets of data from the literature for a relative density less than 0.1. The rigid link model starts to

deviate from the other models beyond a relative density of 0.07. The foam materials that we are interested in analyzing in this work are BX250 and BX265, which were used on the space shuttle. By inspecting micrographs [2], we estimated that these foams have a relative density of less than 0.02.

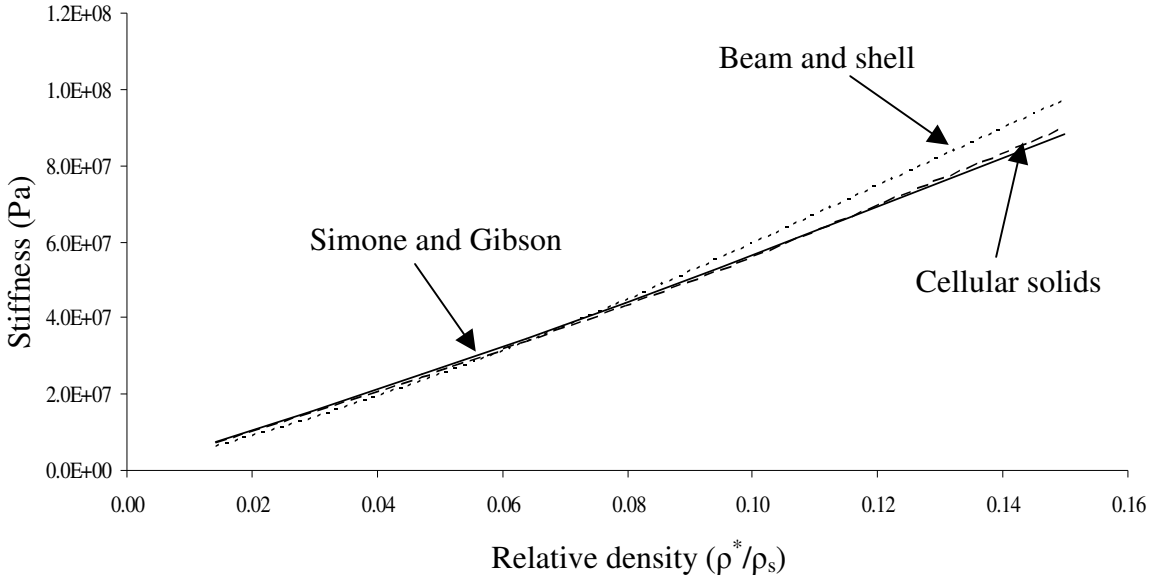

Figure 3.4 Stiffness versus relative density (Ø=0.7, *l*=0.22mm)

The effect of solid distribution on the foam stiffness was studied. "Solid distribution" refers to how much of the material is in the edges and how much is in the faces. This is indicated by the edge fraction. Figure 3.5 shows the effect of edge fraction on the effective stiffness for two different relative density cases. We see that for both the 0.05 and 0.1 relative density cases, the curves follow the same general trend, which

is an almost monotonic decrease with increase in edge fraction. This indicates that the face plays an important role in providing stiffness to the foam material. We also see that for both cases, for very low edge fraction (0.05 – 0.1), we see a very slight increase in the stiffness with increase in edge fraction. As expected, the curve for the higher relative density lies above the one for the lower. Note that the cell edge length is kept constant in all the models.

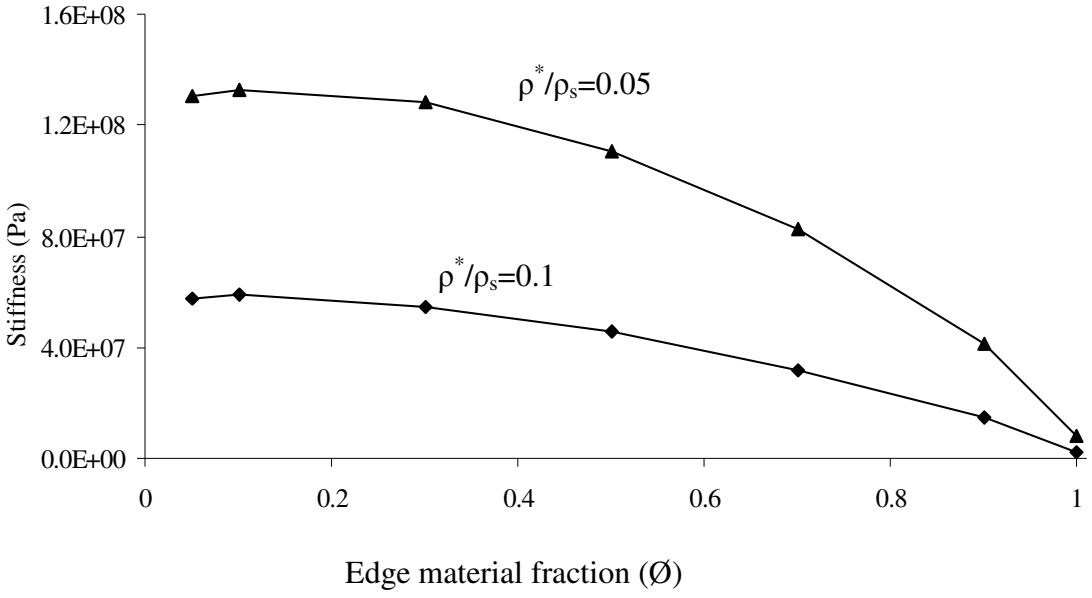

Figure 3.5 Edge fraction versus stiffness

Figure 3.6 shows a normalized plot of the data in Figure 3.5 in order to give a fair comparison of the trend irrespective of the relative density. The stiffnesses are normalized with respect to the first corresponding data point in Figure 3.5 (for edge fraction =0.05). We see that the relative behavior for both cases is almost the same.

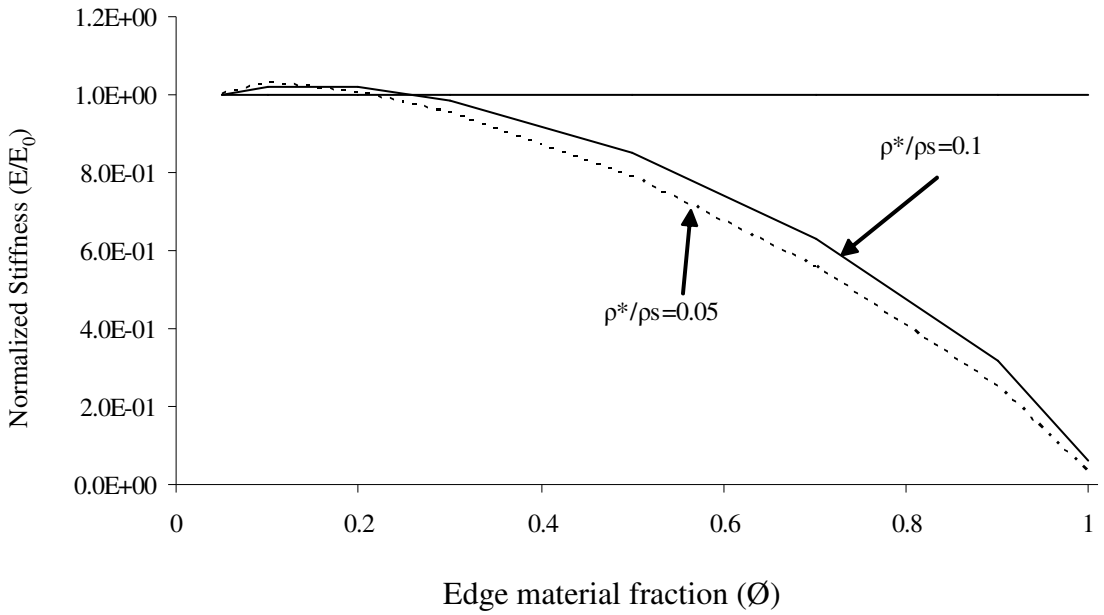

Figure 3.6 Normalized stiffness versus edge material

Figure 3.7 shows the region on the foam cell where the maximum Von Mises stress occurs. The foam cell has an edge fraction of 0.7 and relative density of 0.1 and is under tension in the y-direction. The maximum Von Mises stress occurs on the

transverse hexagonal faces close to the top and bottom vertices. Therefore, at the onset of failure, we expect the faces to rupture first under this kind of loading. Figure 3.8 shows the effect of relative density on the maximum Von Mises stress for a fixed edge fraction of 0.7. The nominal stress is kept constant for each case (2.075GPa). As the relative density increases, the maximum Von Mises stress occurs at the same region shown in Figure 3.8. It can be seen that the maximum Von Mises stress decreases significantly with an increase in relative density for low relative densities (up to 0.04) and then gradually decreases.

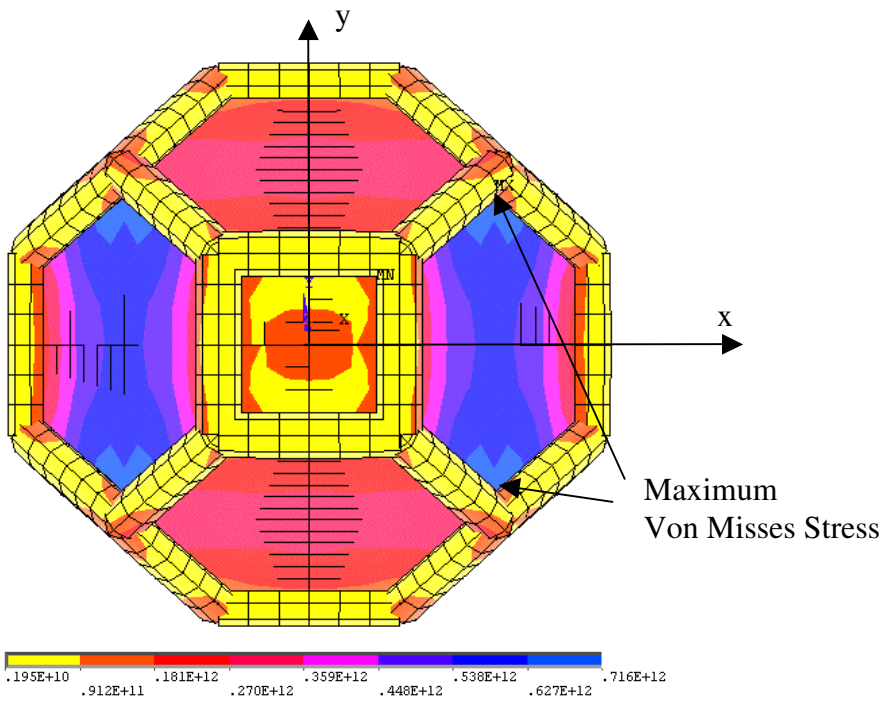

Figure 3.7 Contour plot of Von Misses stress (Ø=0.7)

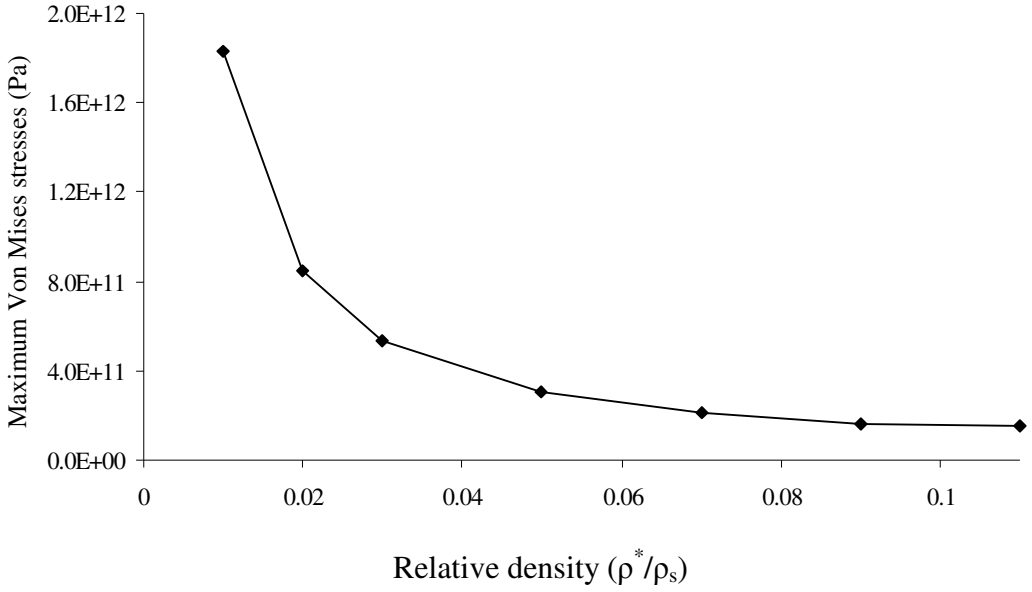

Figure 3.8 Von Mises stress versus relative density

Although there is a significant variation in the maximum Von Mises stress, the stress concentration with respect to the nominal Von Mises stress in the faces was found to be almost constant (2 – 2.5) with varying relative density (Figure 3.9). The Von Mises stress concentration with respect to nominal Von Mises stresses in the whole material is found to be practically constant at 8 for low relative density and gradually increases to 10 as the relative density goes up to 0.1. This is attributed to the fact that the edge fraction is held constant for all the cases and therefore the distribution of material between the edge and faces does not change.

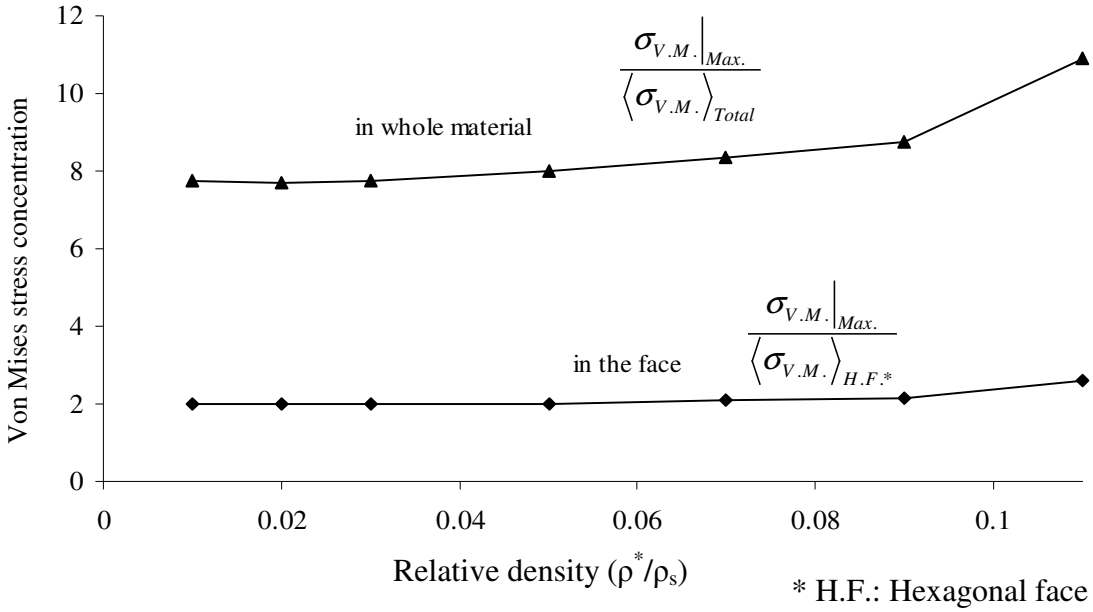

Figure 3.9 Von Mises stresses concentration versus relative density

Next, the effect of the edge fraction on the maximum Von Mises stress is considered. The relative density was held constant. Again, the maximum Von Mises stress occurs at the same location as shown in Figure 3.7. Figure 3.10 shows the effect for two relative density cases: 0.05 and 0.1. It can be seen that for both cases, the maximum von Mises stress remains almost constant up to 0.7 edge fraction. When the edge fraction is increased beyond 0.7, a much steeper increase is seen in the case with the lower relative density. As the edge fraction increases, the faces become thinner and therefore, under the same nominal stress level, it is expected that the face will have much larger von Mises stresses. Note that the data points corresponding to edge fraction = 1.0 refers to the configuration where there are no faces, or in other words, open cell foam.

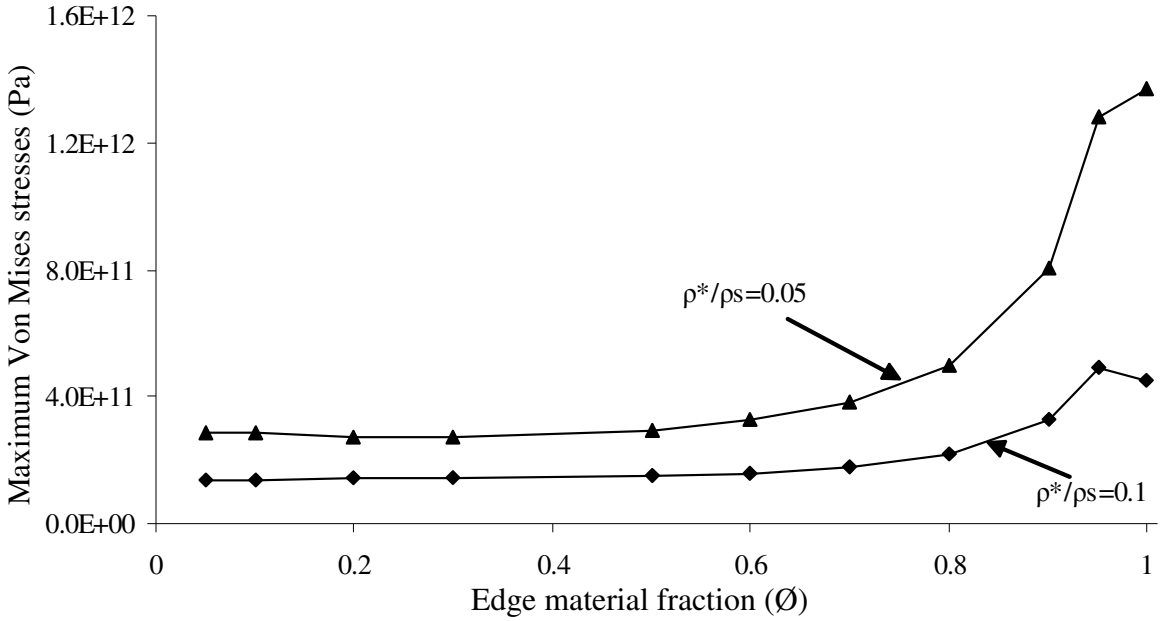

Figure 3.10 Von Misses stresses versus edge material fraction

Therefore the location of the maximum Von Mises stress is no longer on the face but on the edge.

3. 3. 3 Linear buckling analysis

This section discusses the results of the linear buckling analysis on the foam unit cell. Because of the geometric complexity, any loading cases like tension or shear (not just compression alone) can cause face buckling. Two sets of loading conditions were considered. One is along the y-axis (Type A) while the other is along the 45 degrees off-axis direction (Type B) as shown in figure 3.11. For each loading set, we consider the three cases – compression, tension and shear. In all the cases, it is seen that the faces buckle first and not the edges. Table 3.2 gives the lowest critical stress for each

loading case considered. Although it is the faces that buckle first, it is not the same face that buckles for each loading case. Figure 3.12 shows the first mode shape of buckling for the tension, compression and shear loading cases under the Type A loading. It is seen that the buckling occurs at different sets of faces. For the tension case, it can be seen that the buckling occurs on the smaller square face and accordingly we see that the lowest critical stress for the corresponding loading is larger than that for compression or shear.

Table 3.2 Lowest buckling stress for different loading.

	Compression	Tension	Shear
Loading type A	6.52	21.05	1.02
Loading type B	6.42	35.09	0.52

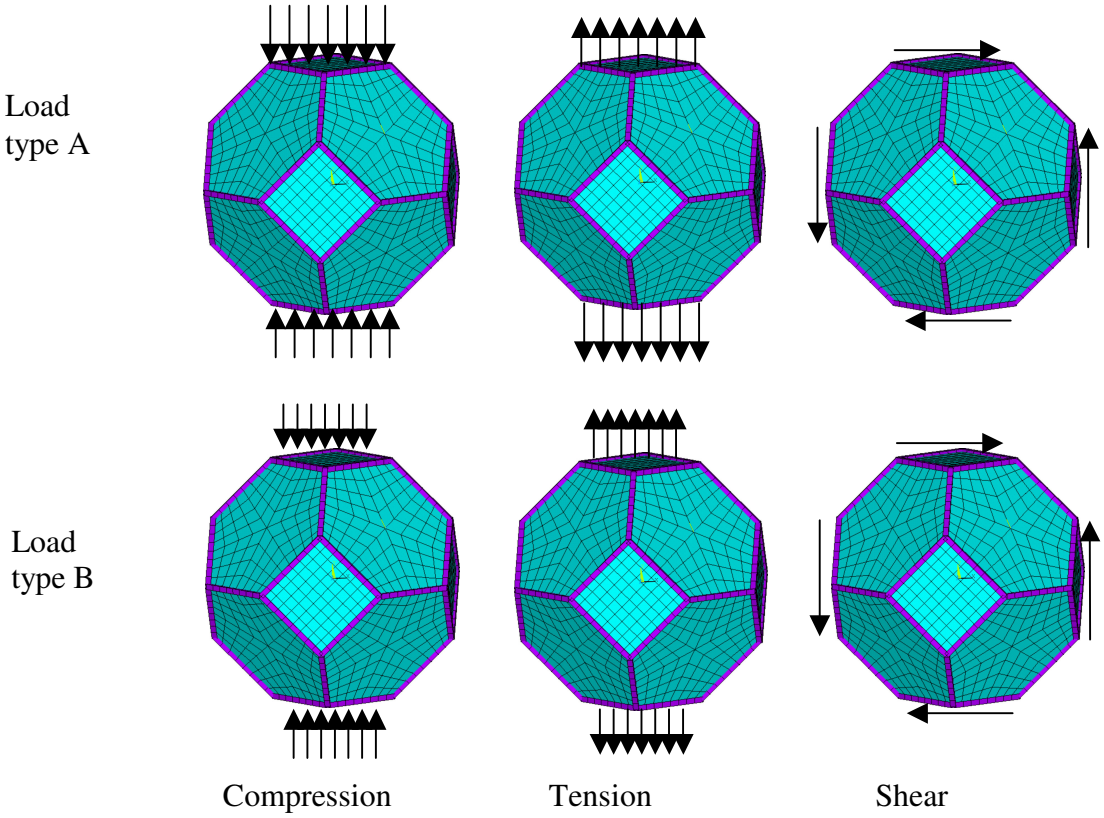

Figure 3.11 Loading direction type

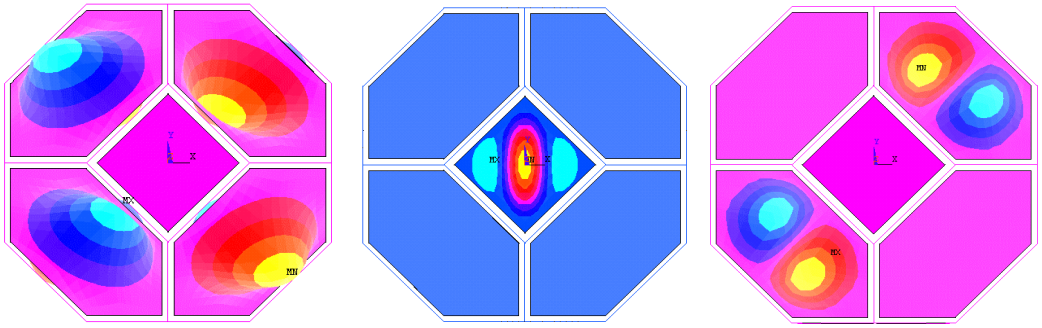

Figure 3.12 First mode shape for different loading cases in loading type A

Next the effect of solid distribution (edge fraction) on the buckling stress is considered. The buckling stress depends on the buckling strength of the faces since it is always the face that buckles first. As the edge fraction increases, the face area and the face thickness decrease as given by equations (3) and (4). A decrease in the face area would cause the buckling stress to increase whereas a decrease in the face thickness would cause the buckling stress to decrease. Therefore, we have two competing effects on the buckling stress due to the change in edge fraction. Figure 3.13 shows the effect of edge fraction on the buckling stress for a fixed relative density of 0.05. It can be seen that the buckling stress decreases as the edge fraction increases. As expected, the thickness of the face seems to be a dominant factor in the buckling stress of the foam.

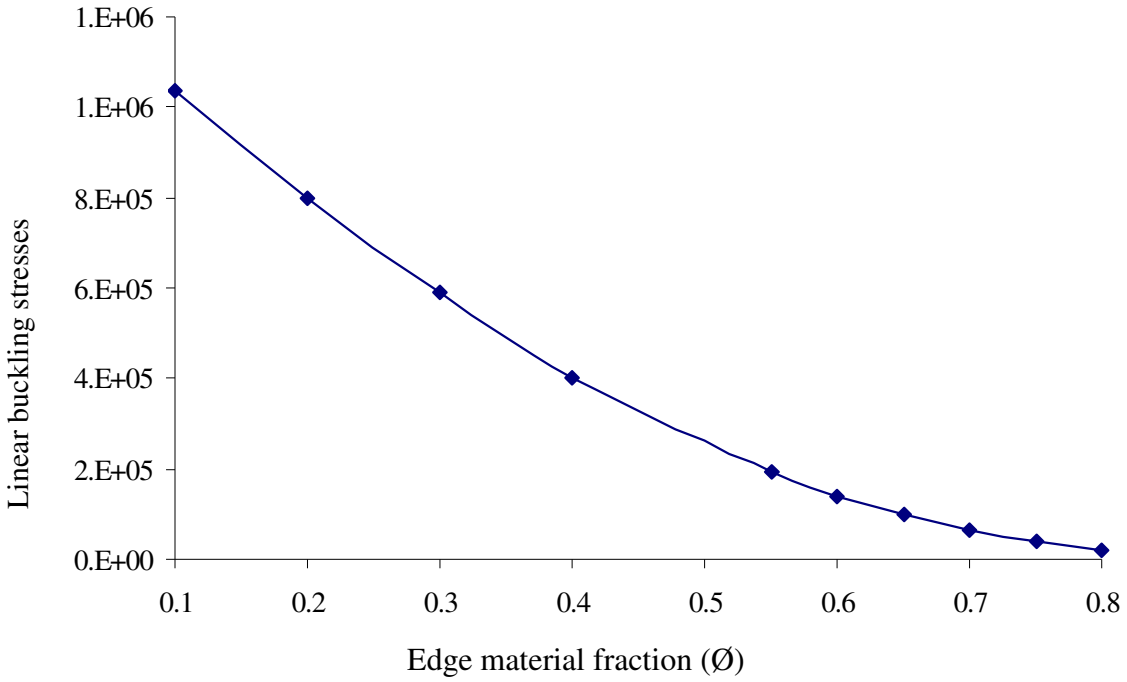

Figure 3.13 Linear buckling stress of unit cell vs. fraction of edge

3. 3. 4 Postbuckling analysis

Postbuckling analyses showed that the overall stiffness is not significantly affected by the face buckling. However, if one removes the face from the model, the stiffness is greatly reduced, even in the linear regime. Post buckling analysis is performed for the unit cell under compression loading. Typical results are shown in Fig. 3.14. The analysis shows a mild nonlinearity rather than an abrupt change in behavior when buckling occurs. The buckling strain from the linear buckling analysis is plotted in Fig. 3.14. The face buckling in the first mode occurs very early, which is far from the collapse strain. (which is beyond the range of the plot). Comparison of the maximum Von Mises stresses between the linear and postbuckling response at a 2.5% strain gives a difference of only 14.8%. This suggests that we can obtain effective homogenized properties for the foam based on linear analysis and still obtain fairly good predictions. More cases must be considered before accepting this hypothesis.

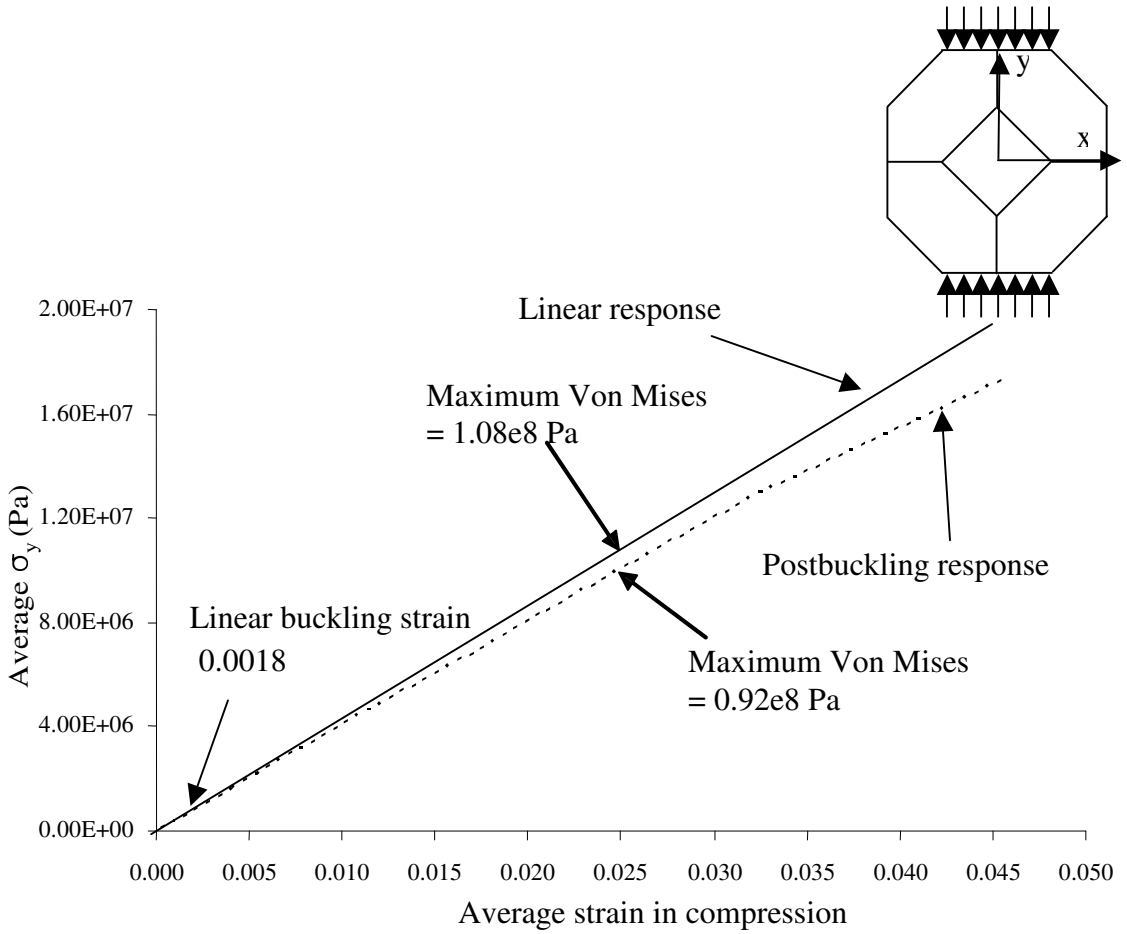

Figure 3.14 Postbuckling response (edge fraction = 0.7)

CHAPTER IV

NON-PERIODIC MULTI CELL MODEL

4. 1 Introduction

The previous section dealt with the analysis of foam microstructure using a single unit cell. Such an analysis cannot be used to model defects, which are of a larger scale than the unit cell. This chapter discusses the analysis of foam using a non-periodic multi cell model incorporating point defects. Typical non-periodic analyses make use of voronoi tessellation. Voronoi tessellation is effective in generating a random microstructure [44-47]. The objective in this research is not to achieve 'randomness' but to be able to model point defects in the foam microstructure, and this is harder to do using voronoi tessellation. In this work, the defects are modeled using two other methods which are described in section 2. One is the 'missing cell' model while the other method which is more realistic is called the 'function distorted' model. Section 2, 3 and 4 discusses the procedure to generate the fucntion distorted model. Building the function distorted multicell model is not a trivial task. One reason is simply because of the large number of geometric entities such as points, lines and surfaces required to define the microstructure for the mesh generation. Other complications involve the use of rigid link elements. Moreover, there should be a way to control the relative density and edge fraction. Another complication is that when the regular array is distorted, the faces need to be kept flat. Scripts were developed to make the generation of this model much easier

for the analyst. Using this model, the effect of the defect size and defect density on the foam microstructure is studied. In particular their effect on the effective stiffness and stress concentrations in terms of Von Mises stresses is examined. These results are discussed in section 5.

4. 2 Generation of distorted multicell model

Two types of defects are illustrated in Figure 1.2 … point defects and line defects. In this work, only the effect of point defects is studied. A large void can be assumed as point defect. Two different methods (missing cell model and function distorted model) are developed to generate this large void.

The “missing cells” model is obtained by using a numerical zero for the stiffness of the cell at the position of the void. Figure 4.1 shows a typical 2D model with defect using missing cells. This model can be very easily generated, but the overall shape of disordered cell is quite unrealistic one and the relative density and edge fraction can not be controlled.

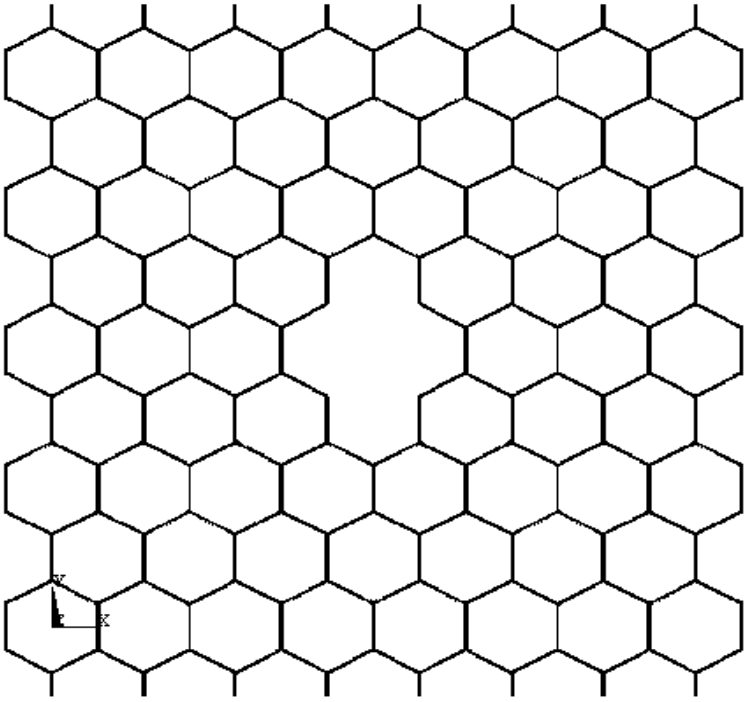

Figure 4.1 Missing cell model in 2D

The second method called the function distortion model is a more realistic model. In this model, an ordered multicell model can be deformed or distorted by specific functions. Several functions were tested to generate large voids as point defects in a 2D array model. Figure 4.2, 4.3 and 4.4 show some of the functions used and the corresponding models. Figure 4.2 shows a couple of cases where unidirectional distortion was obtained using polynomials. Figure 4.3 illustrated three examples of two directional distortions using a sine function. To generate a void, radial distortion seemed the best option. It was seen that among the functions that were tried out, radial distortion using the sine or cosine function was best able to generate a microstructure resembling a void. As seen in the Figure 4.3, the cosine function can generate the shape best resembling a point defect by apt choice of the function parameters, Wn and factor.

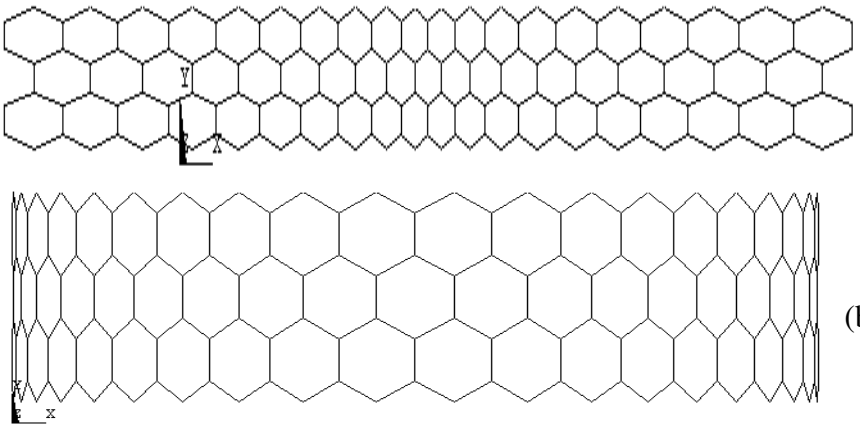

Figure 4.2 One directional distortions

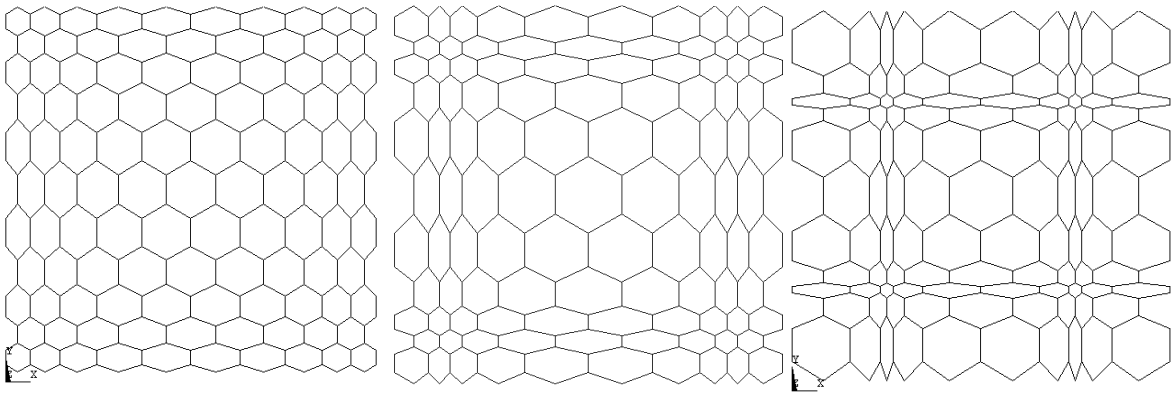

(a) x=L (b) x=3L/2 (c) x =2L

$$u = factor \times \sin\left(\frac{n \times \pi \times x}{L}\right)$$

Figure 4.3 Two directional distortions by sine function

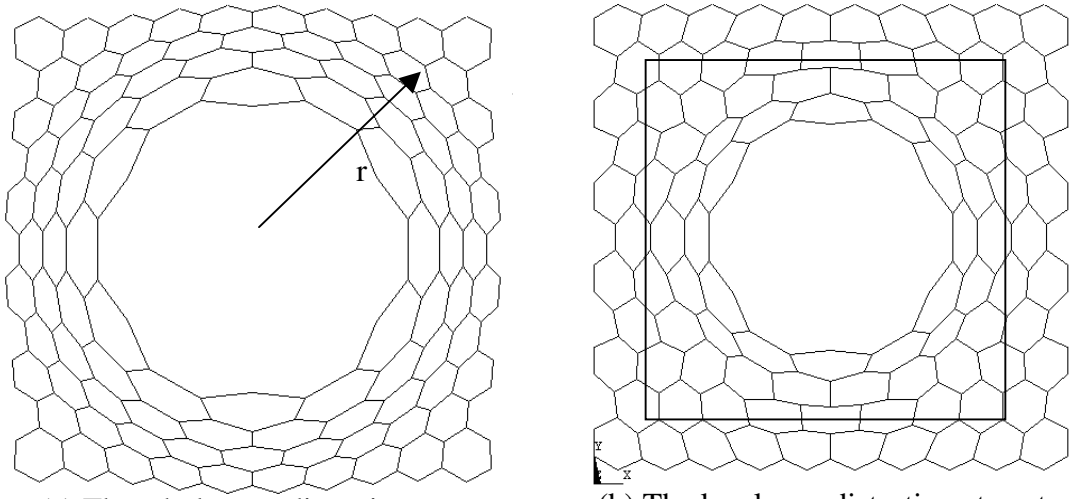

(a) The whole area distortion (b) The local area distortion at center

$$|r'| = factor \times \cos\left(\frac{wn \times \pi r}{2R}\right)$$

Figure 4.4 Radial direction distortions by cosine function

When distortion is applied by this function, there exists one crucial problem which is that curved faces can be generated. These curved faces not only affect the behavior of foam material but also makes mesh generation difficult. Also, these curved faces make the relative density uncontrollable. In this research, the main geometric parameters considered are defect size and the defect density (or in other words, the distance between defects). The effect of these parameters cannot be clearly analyzed when you have other effects in play. It is seen that the effect of curvature of the face on the foam behavior is significant. Since the goal is to study the effect of geometric parameters such as defect size and defect density, it is necessary to maintian flat faces in the foam microstructure model.

Figure 4.5 shows the flowchart for the algorithm to generate the 3D distorted multicell model. The algorithm explains the steps in the process up to the point of meshing the model. The meshing procedure will be described in the next section. The first step in generating a distorted array model is making an ordered multicell model. After a single unit cell (which is described in chapter I) is generated, it is duplicated to get the desired number of cells. From this ordered array model, the data of the geometric constituents in each face such as points and edges surrounding each face is generated. The geometry information is used later for generating the flat faces, introducing the rigid links and in the meshing process. The geometry is distorted using a script written in APDL in ANSYS (APENDIX B).

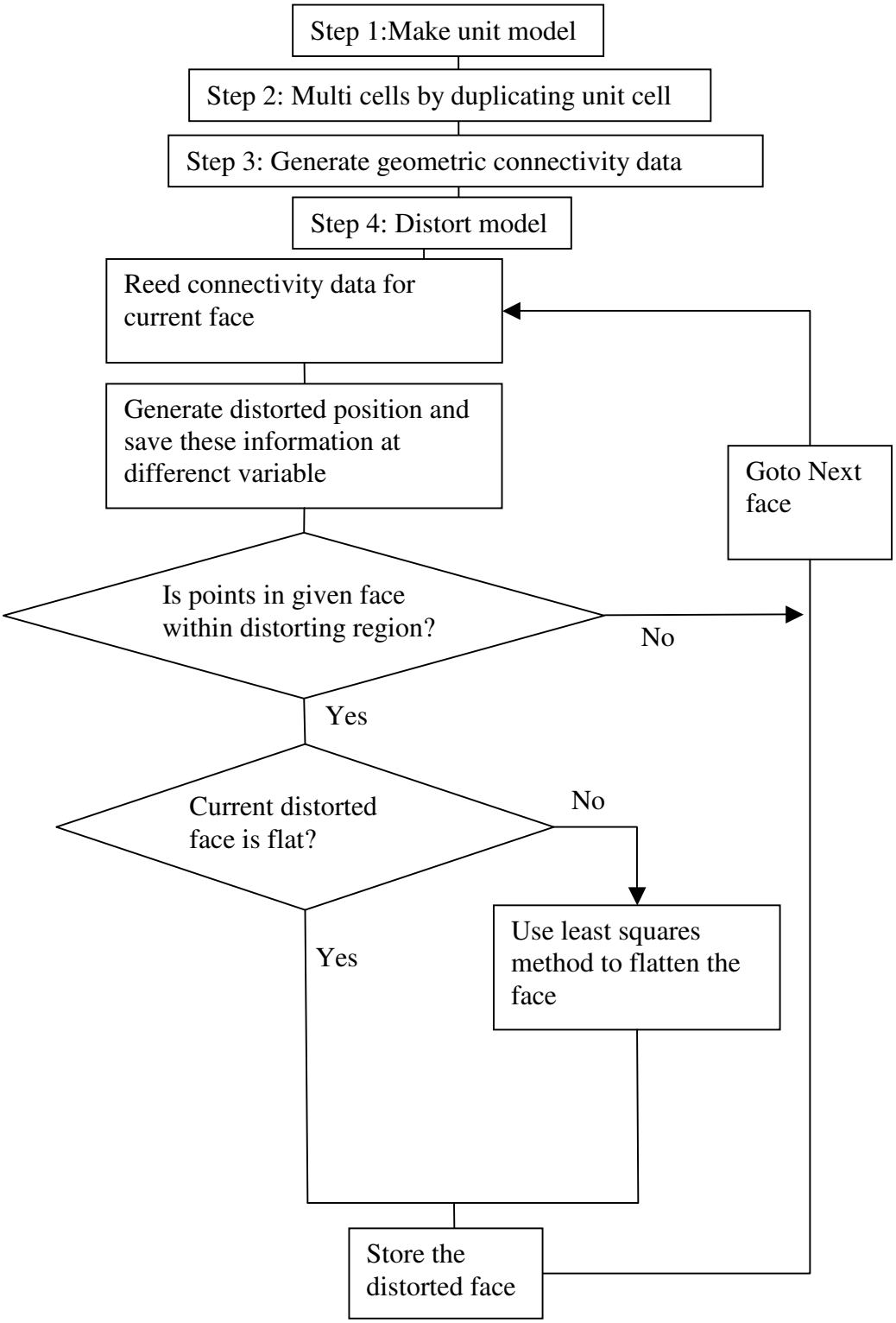

Figure 4.5 Procedure to make distorted multi cell model

Figure 4.6 shows a schematic for the distortion procedure. A distortion center is defined about which the geometry is distorted. This distortion center is located at the center of a unit cell. Equation 4.1 gives the final position v ector of the distorted point. Using this procedure, all the points in the geometry are moved to achieve the distorted configuration.

$$(\underline{x}' - \underline{c}) = (\underline{x} - \underline{c}) - r(\underline{x} - \underline{c}) \qquad 4.1$$

where $\underline{x}$' is the distort position vector,

$\underline{c}$ is the position vector of the distiortion center,

$\underline{x}$ is the position vector about the grobal coordinate,

r is distortion amount given by

$$r = (factor) \times \cos\left(\frac{\pi |(\underline{x} - \underline{c})|}{2R}\right) \qquad 4.2$$

factor is magnitude of distortion function, and R is domain radius.

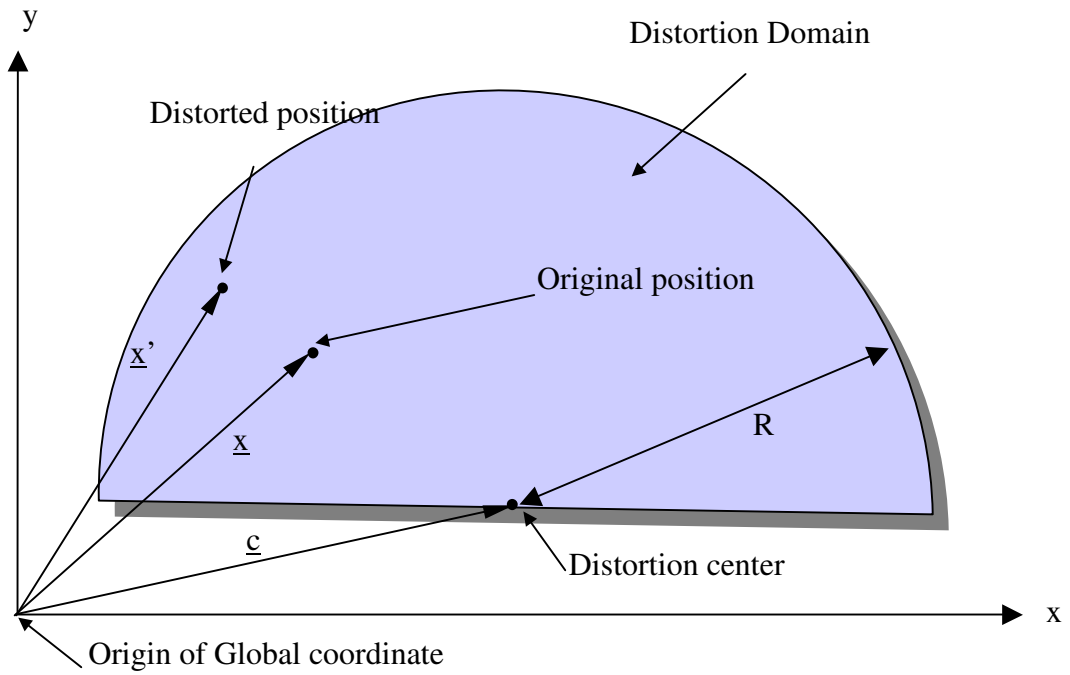

Figure 4.6 Schematic for the distortion procedure

The edges are first deformed using the geometric data for edges and cosine function with given parameter such as wn and factor. The geometric data for each face is loaded and each face within the distortion region is deformed. Whenever a face is deformed, its curvature is checked, and the curved faces are flattened by the least squares algorithm, which is described next.

A curved face is detected by calculating the equation of the plane passing through any three vertices on the edges surrounding a face and checking if the other vertices satisfy the equation for the plane. If the face is curved, a new plane is generated

using a least squares fit of all the vertices on the edges surrounding the face. Equation 4.3 gives the equation for the new plane. The error function is given by equation 4.4 where xi, yi and zi are the coordinates of the vertices. The three unknowns in the equation are then calculated by differentiating the error function with respect to the unknowns and solving the set of three linear equations (Equation 4.5). The new face is then generated by fitting the vertices of the face onto this new plane.

$$Plane\ Equation: a\,x + b\,y + c\,z = 1 \tag{4.3}$$

$$Error\ function: \sum (ax_i + by_i + cz_i - 1)^2 \tag{4.4}$$

$$\begin{bmatrix} \sum x_i^2 & \sum y_i\,x_i & \sum z_i\,x_i \\ \sum x_i\,y_i & \sum y_i^2 & \sum z_i\,y_i \\ \sum x_i\,z_i & \sum y_i\,z_i & \sum z_i^2 \end{bmatrix} \begin{bmatrix} a \\ b \\ c \end{bmatrix} = \begin{bmatrix} \sum x_i \\ \sum y_i \\ \sum z_i \end{bmatrix} \tag{4.5}$$

4. 3 Meshing distorted multicell model

The mesh generation feature of ANSYS was used to generate the models described in this work. Beam elements and shell elements are used to model the foam microstructure. As with any mesh generator, the user has to specify the geometry of the domain and the corresponding type of elements that need to be created for that domain. One of the most basic geometric components used to define the regions are lines. The lines can be used to define a two dimensional region in 3D space which depicts the faces. These faces are modeled using shell elements. Lines are also used to define the edges of

the unit cells in the array. These edges are modeled using beam elements. The size of these distorted array models can become very large with some of the models in this work having as many as 80 unit cells. This means that the corresponding geometry is defined using a large number of lines. To mesh an edge as a beam, lines should be classified and grouped. The lines denoting edges are meshed using beam elements (beam 188) in ANSYS. The Shell element type (shell 63) is used to mesh the faces. There is another important concern when meshing edges and faces. Relative density and edge fraction are the most important parameters which affect the behavior of foam material. Therefore, we need to control these parameters. After the array model is distorted, it is very difficult to maintain initial relative and edge fraction. A technique was developed here to exactly generate the distorted array model which has the required relative density and edge fraction. Figure 4.7 illustrates the flowchart for the algorithm used to mesh the geometry.

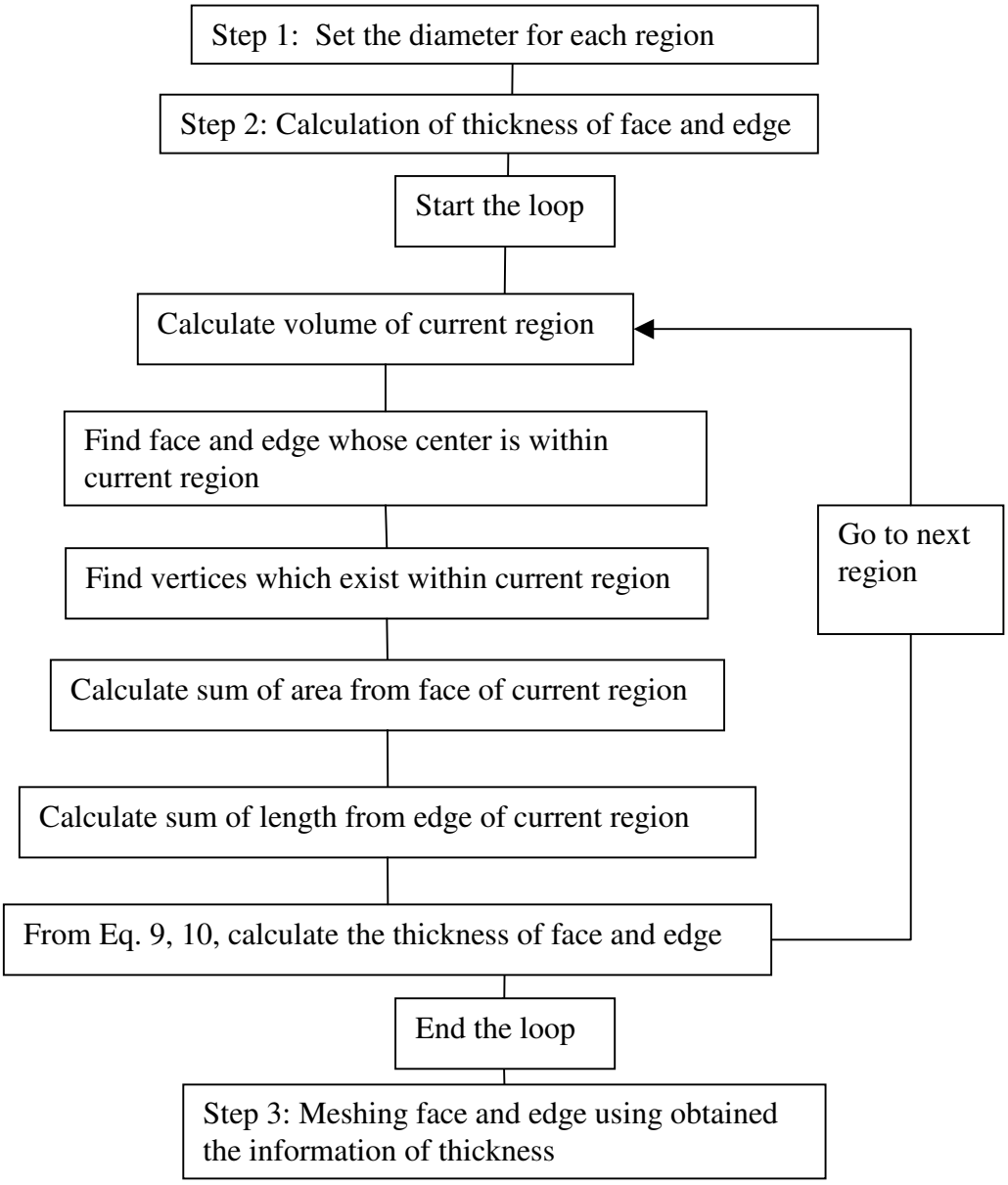

Figure 4.7 Procedure to mesh each region

After distortion, the multi cell model is divided into a number of regions as shown in Figure 4.8. In this work, we deal with two types of cases where we have either two regions or four regions excluding the undistorted region. Figure 4.8 shows the schematic of a model that has four regions excluding the undistorted region.

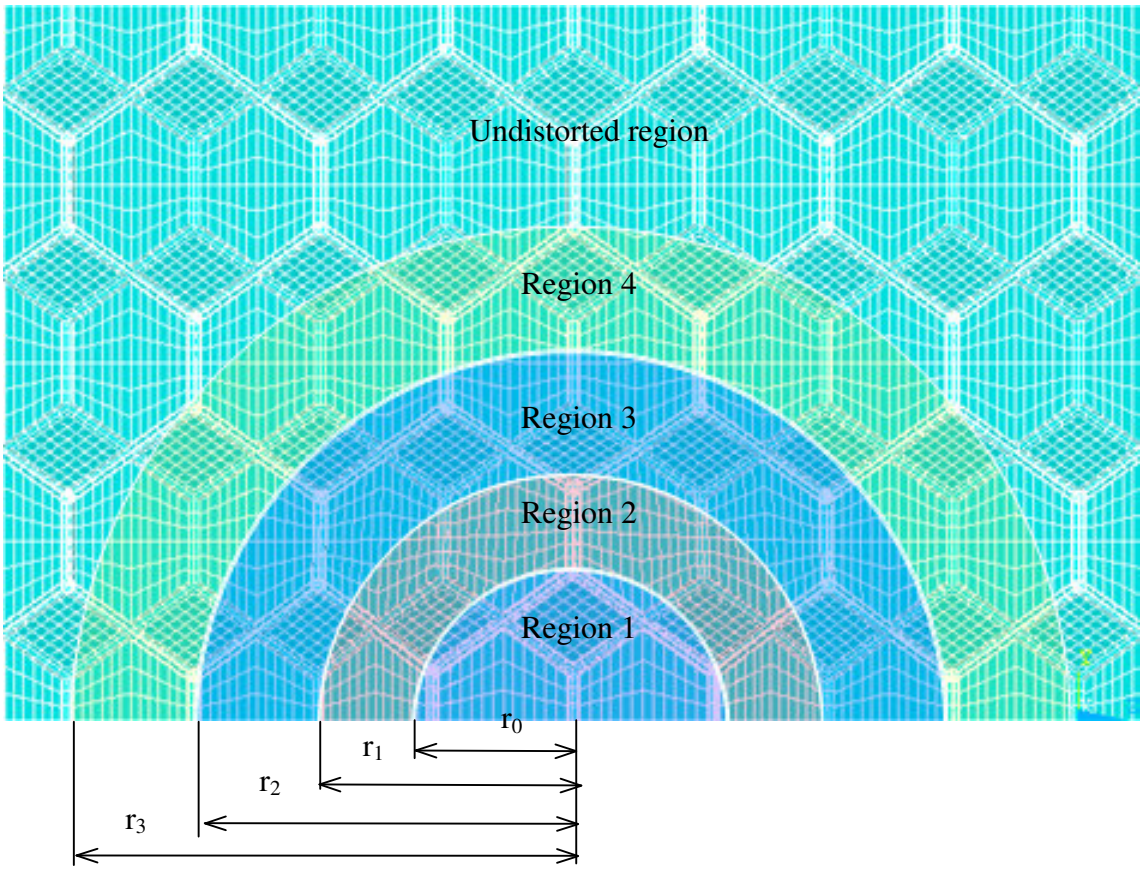

Figure 4.8 Distortion regions and radius

Once the diameters for the spherical regions have been set, the next step is to calculate the thickness of the face and edge in order to mesh the region accordingly. In order to do this, the volume of the region is first cacluated. The list of all the faces and edges that fall under this region is generated. A face or edge is considered to fall under a region if its centroid falls under that region. The sum of the face areas and the edge lengths are calculated. The vertices that fall within this region are also determined in order to account for the overlap volume. Using this information, the thickness of the faces and edges can be calculated. Equation 4.6 is used to obtain an expression for the material volume.

$$material\ volume = a_f \times t_f + l_e \times \frac{\pi}{4}(t_e)^2 - N_v \times (\frac{\pi}{8}(t_e)^2 t_f) \qquad 4.6$$

where a_f is area of face in the current region,

l_e is the length of edge in the current region,

and N_v is number of vertices in the current region.

Equation 4.7 and 4.8 are then simultaneously solved to obtain the face thickness and edge thickness which are given by Equation 4.9 and 4.10.

$$\frac{\rho^*}{\rho_s} = \frac{material\ volume}{V_R} = \frac{a_f \times t_f + l_e \times \frac{\pi}{4}(t_e)^2 - N_v \times (\frac{\pi}{8}(t_e)^2 t_f)}{V_R} \qquad 4.7$$

where V_R is the volume of region.

$$\phi = \frac{edge\ volume}{material\ volume} = \frac{l_e \times \frac{\pi}{4}(t_e)^2 - N_v \times (\frac{\pi}{8}(t_e)^2 t_f)}{a_f \times t_f + l_e \times \frac{\pi}{4}(t_e)^2 - N_v \times (\frac{\pi}{8}(t_e)^2 t_f)} \qquad 4.8$$

$$t_f = \frac{(1-\phi)\times V_R\left(\frac{\rho^*}{\rho_s}\right)}{a_f} \qquad 4.9$$

$$t_e = \sqrt{\frac{\phi(a_f t_f)}{(1-\phi)\left(l_e \times \frac{\pi}{4} - N_v \times (\frac{\pi}{8} t_f)\right)}} \qquad 4.10$$

Once this information is obtained for each region in the model, the geometry can be meshed with the appropriate elements.

Figure 4.9 shows a typical mesh obtained using the procedure outline above. The elements are color-coded to differentiate the regions in the model. The script of ANSYS to generate this distorted multi cell model is attached in APENDIX B.

4. 4 Configuration and boundary conditions

Symmetry boundary conditions are applied on two surfaces (x=0, y=0) to reduce the size of the model. However, symmetry condition can not be applied on the surface perpendicular to z axis because the cutting surface would pass through the edges causing the same problem explained earlier in chapter I. Therefore, we are able to achieve a reduction of 75% in model size using the symmetry conditions. The outer boundaries of the model are subjected to periodic boundary conditions. Figure 4.10 shows a typical model and boundary conditions.

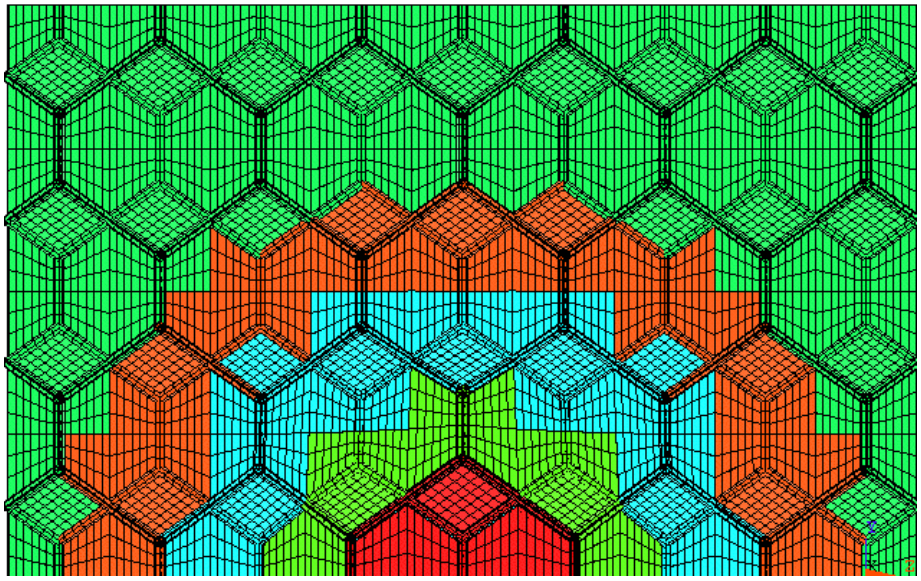

(a) Side view

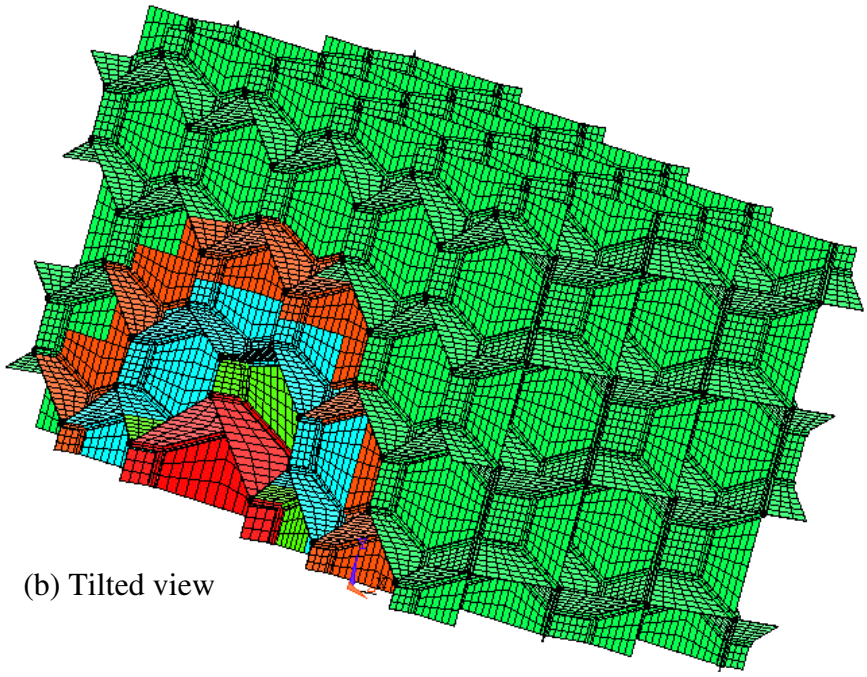

(b) Tilted view

Figure 4.9 Distorted array model with regions

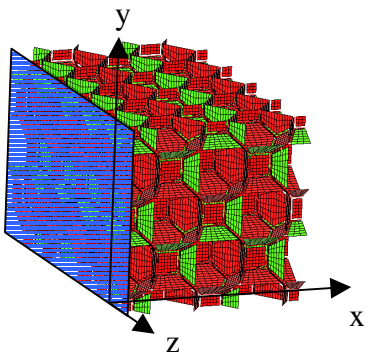

* Face; $x = 0$, symmerty condition

$$u_x = 0,\ rot_z = 0,\ rot_y = 0$$

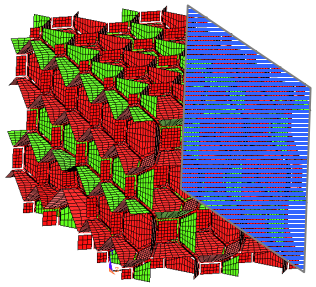

* Face; $x = 4l \times n$

$$u_x(4l \times n, y, z) = 4l \times n \ < \frac{\partial u_x}{\partial x} >$$

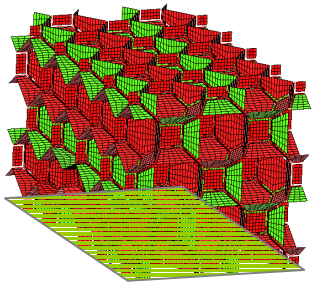

* Face; $y = 0$, symmerty condition

$$u_y = 0,\ rot_x = 0,\ rot_z = 0$$

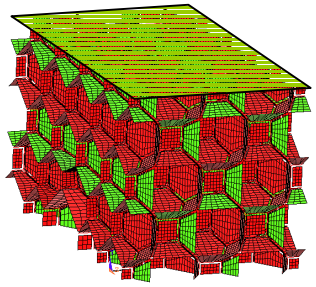

* Face; $y = 4l \times m$

$$u_y(x, 4l \times m, z) = 4l \times m \ < \frac{\partial u_y}{\partial y} >$$

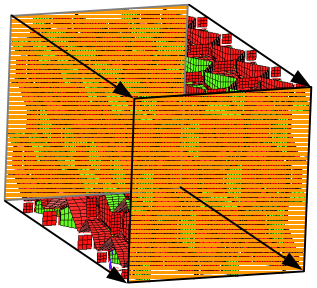

* Face; $z = 2b, -4b \times k + 2b,\ d_\alpha = 4b \times k\ \underset{\sim}{k}$

$$u_i(x, y, 2b) = u_i(x, y, -4b \times k + 2b) + 4b \times k \ < \frac{\partial u_i}{\partial z} >$$

Figure 4.10 Conjugate planes for the periodic B.C. and symmetry B. C. for the multi cell model

4. 5 Results and discussion

Parametric studies using the distorted multicell model are conducted by varying two geometric parameters – the defect size and the defect density. The effect of these parameters on the strength and effective stiffness are examined. Section 1 first discusses the relationship between the parameters of distortion function such as factor and the defect size. Then the effect of defect size on the strength and effective stiffness of the foam structure is discussed in section 2. The strength of the foam in the linear regime is assumed to be indicated by the maximum Von Mises stress. Section 3 discusses the effect of the defect density (spacing between defects) on the strength and the effective stiffness of the foam.

4. 5. 1 Effect of distortion function parameters on foam microstructure

As mentioned in section 2 of this chapter, the cosine function was chosen as the distortion function. The distortion domain radius, R, is fixed and the parameter *wn* is taken as one for this study. Therefore the defect size is controlled by the only remaining parameter, *factor*. In order to give an idea of the size of the defect, we define Size Ratio as the ratio of defect size over the undistorted foam cell size (Figure. 4.11).

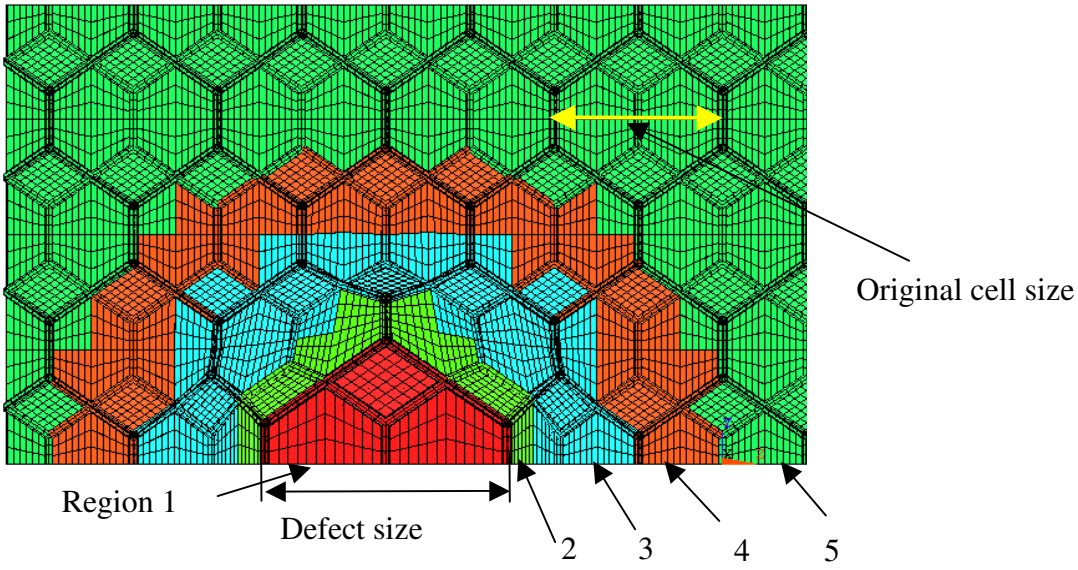

Figure 4.11 Distortion region and defect and undistorted cell diameter

Figure 4.12 shows that the effect of *factor* on the Size Ratio is linear. In this parametric study, the parameter, *factor* is varied from 0.00005 to 0.0004. We can see that the defect size at the higher extreme of *factor*=0.0004 is roughly 3.5 times the original undistorted cell size. Figure 4.11 shows a typical model with a *factor* of 0.0001. It can be seen that the defect size is roughly 1.5 times the undistorted unit cell size. One point to be noted is that after the distortion, the defect itself remains as a regular tetrakaidekahedron whereas the cells surrounding the defect are no longer regular.

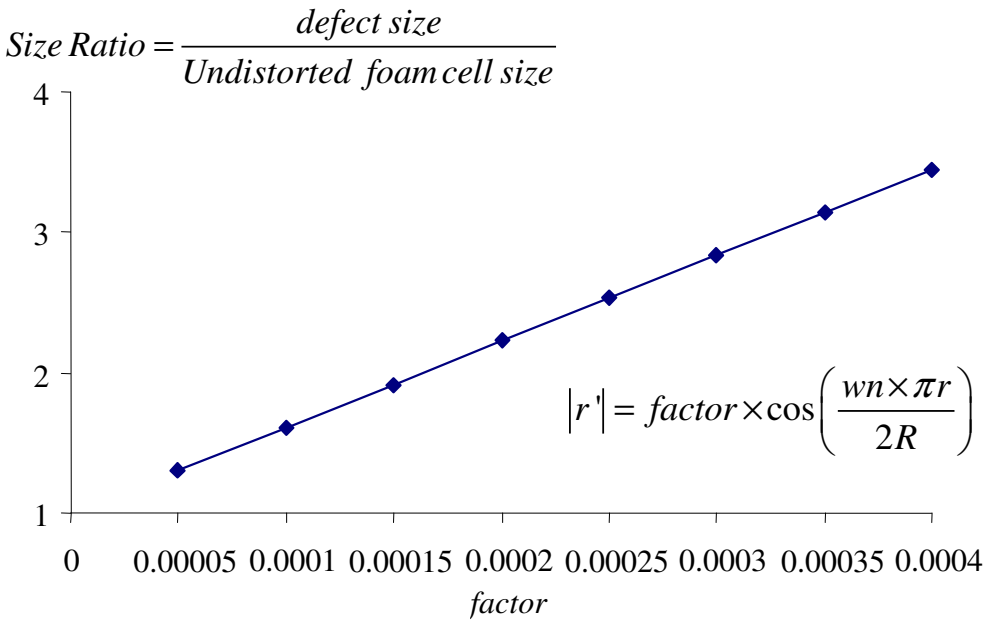

Figure 4.12 Size Ratio versus *factor*

The face thickness is determined by maintaining the relative density and edge fraction in each region to be the same. The region diameters are decided based on the position of the distorted cells around the void (which is considered as the first region). Therefore, the first layer of cells around the void defines the second region and so on. Four such regions are defined and the fifth region is the remaining undistorted region in the model. The cosine function used cause the most distortion in the second region and therefore it turns out to be the narrowest region in the model. Therefore in order to maintain the same relative density and edge fraction in all regions, the edge and face thickness in region two is invariably larger than that in the other regions. Figure 4.13 shows the variation in face thickness for the different regions for a number of cases with different *factor* values. The relative density for all the cases shown in Figure 4.13 is maintained at 0.029166 and the edge fraction is kept at 0.7. Figure 4.14 shows the effect of variation in the *factor* parameter on the edge thickness. As expected, it is seen that as you proceed away from the void the face thickness and edge thickness tend to approach the corresponding values for the undistorted unit cell.

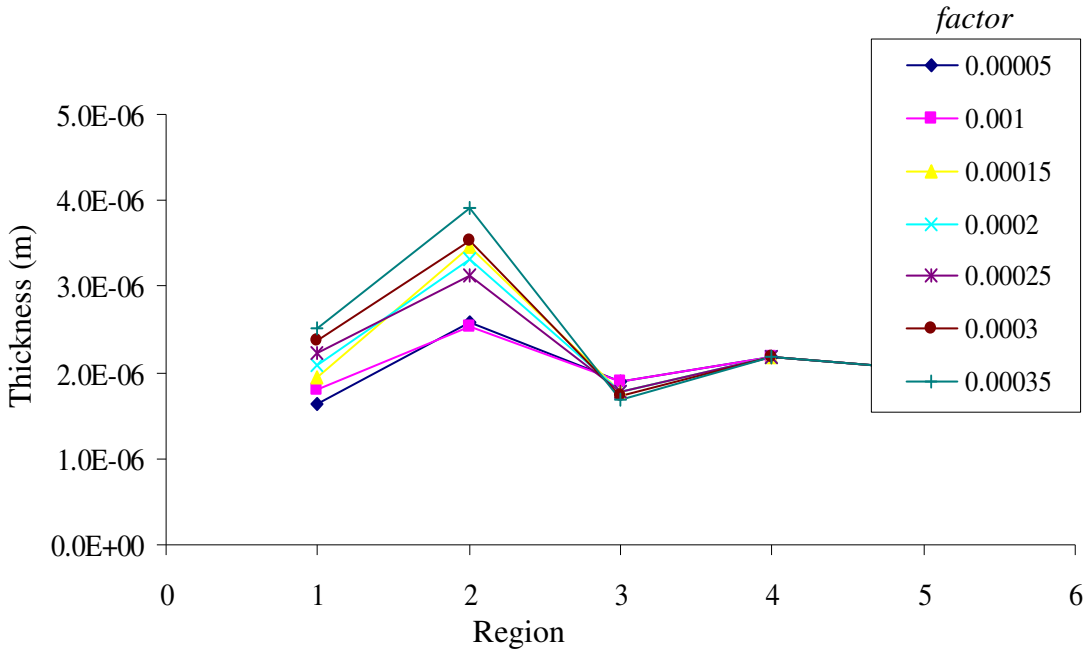

Figure 4.13 Face thicknesses along the region

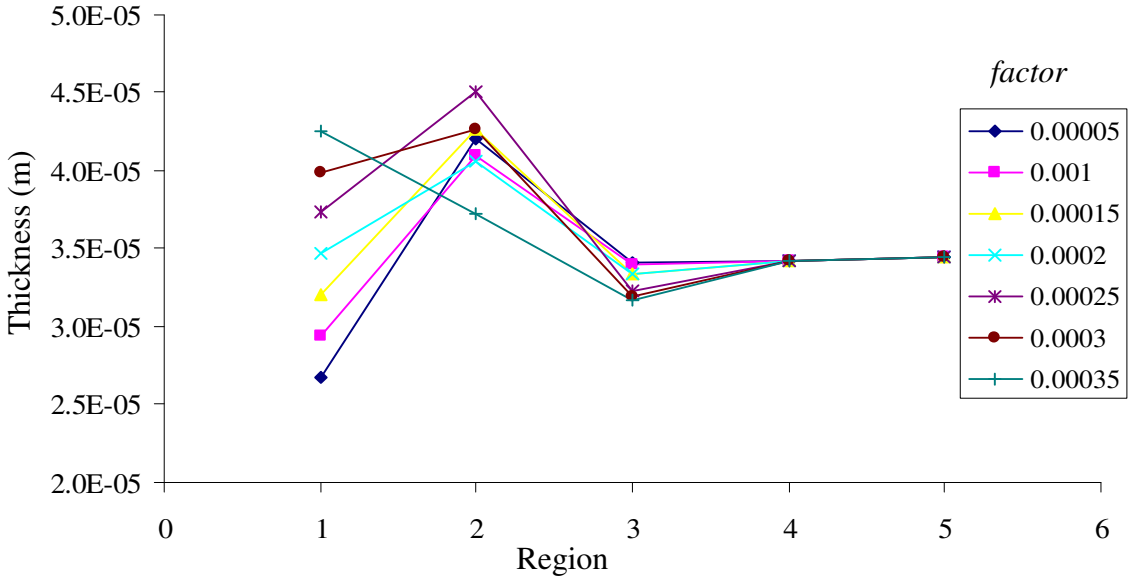

Figure 4.14 Edge thicknesses along the region

4. 5. 2 Effect of defect size on the Strength and Effective Stiffness of the foam

It has been analytically [10] and experimentally [10] observed that the effective stiffness of closed cell foam material is dominated by the relative density and edge fraction. Figure 4.15 shows the effect of the *factor* parameter on the effective stiffness of the foam material. A *factor* parameter of 0.0 denotes uniform multicell model. It is seen that as *factor* increases, meaning that the size of the void increases, the effective stiffness decreases very little. For the largest *factor* parameter case analyzed, where the defect size is roughly 3.5 times the size of a regular undistorted unit cell, the effective stiffness has dropped only 1.4% from that of a regular unit cell. This is in line with the analytical and experimental observations since the relative density is kept constant although the *factor* parameter is varied.

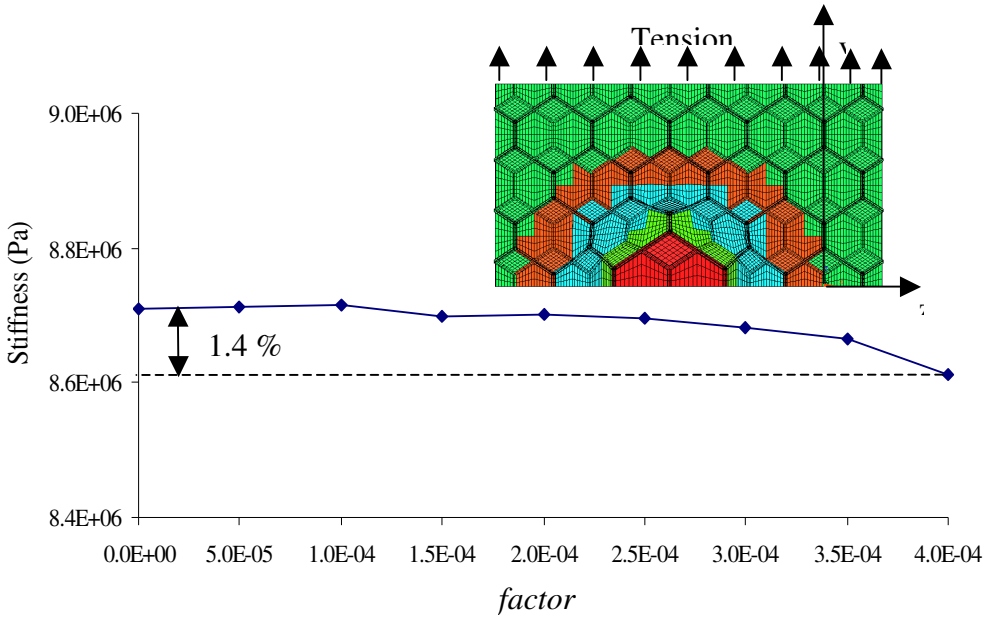

Figure 4.15 Variation of stiffness along the *factor*

Figure 4.16 shows where the effective stiffness from the distorted array model lies in comparison to the experimental results [4]. When foam is manufactured, layers of foam material are sprayed on top of each other (the direction perpendicular to the layers is called the rising direction because the foam material expands in this direction). This causes a line defect known as knots to be formed at the interface between the different layers. These defects along with the fact that the foam material is anisotropic (due to the rising) results in different foam properties in different directions. It is seen that that effective properties obtained from the distorted array model lies in between the experimental values obtained from specimens loaded in the rising direction and those loaded perpendicular to the rising direction.

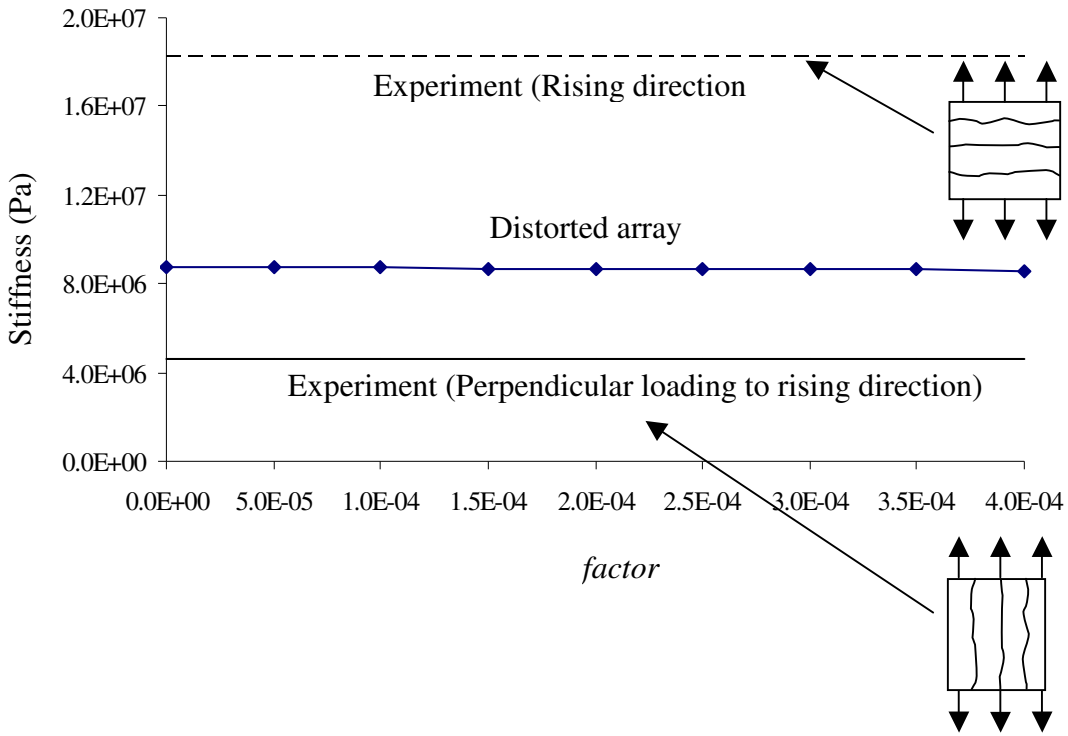

Figure 4.16 Comparison of stiffness from experiment and distorted array model

Although it is seen that the effective stiffness does not vary with the *factor* parameter, its effect on the maximum Von Mises stresses is significant. The maximum Von Mises stresses can be considered to give an indication of the strength of the foam material in the linear regime. Figure 4.17 shows that the maximum Von Mises stresse increases by upto 36.7% from that of the regular array model when the *factor* parameter is increased upto 0.0004.

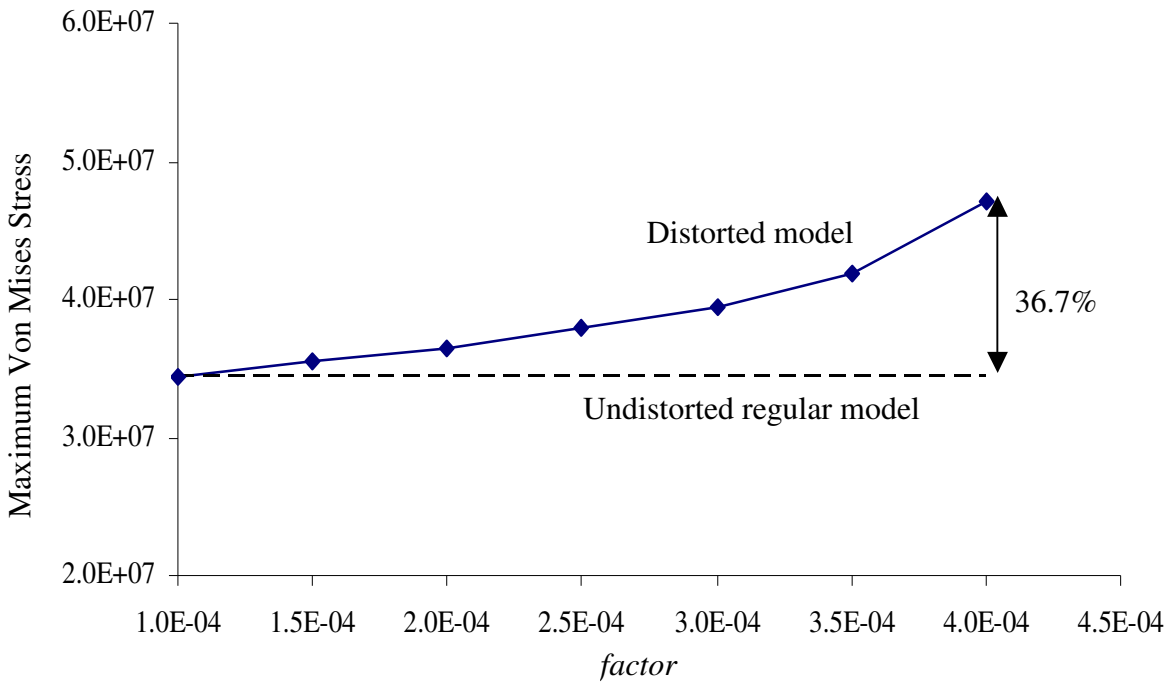

Figure 4.17 Maximum Von Mises stress versus *factor*

In order to find the effect of the defect size on the stress concentrations, we define Von Mises stress concentration as

= (Maximum Von Mises Stress) / volume averaged Von Mises stress

Figure 4.18 shows the effect of the factor parameter on the Von Mises stress concentration. It is seen that the stress concentration also increase by 36.7 % from that of the regular array model when the *factor* parameter is increased up to 0.0004.

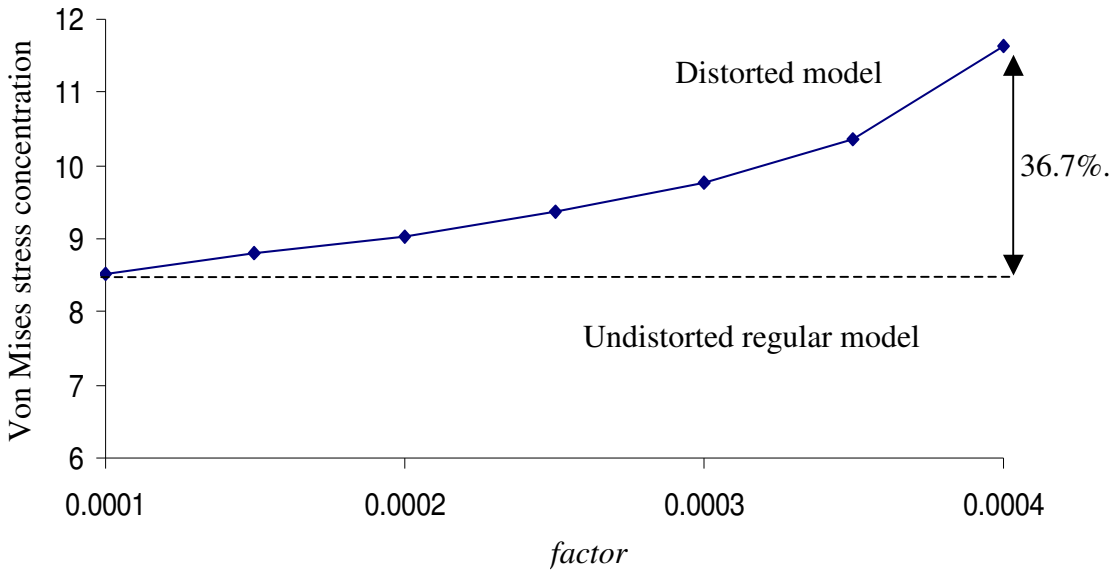

Figure 4.18 Von Mises stress concentration along *factor* for distorted array model

These results were then compared with an analysis using homogenized properties. A model using 3D solid elements was generated which had a spherical void denoting the defect (see Figure 4.19). The diameter of the defect was taken as the circumsphere of the corresponding unit cell denoting the defect in distorted multicell model.

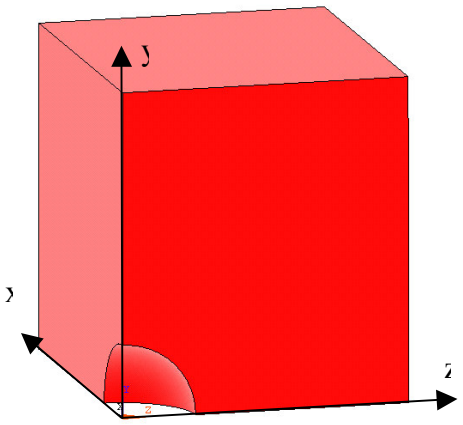

Figure 4.19 Typical homogenous model with defect

It was seen that when the factor was increased from 0.0001 to 0.0004, the Von Mises stress concentrations decreased by only 1.2%. Figure 4.20 shows the contours of the Von Mises stresses for the two cases. The position of the maximum Von Mises stress does not change when the *factor* parameter increases, whereas it is seen that when the discretized model is used, the position of the maximum Von Mises stress does change.

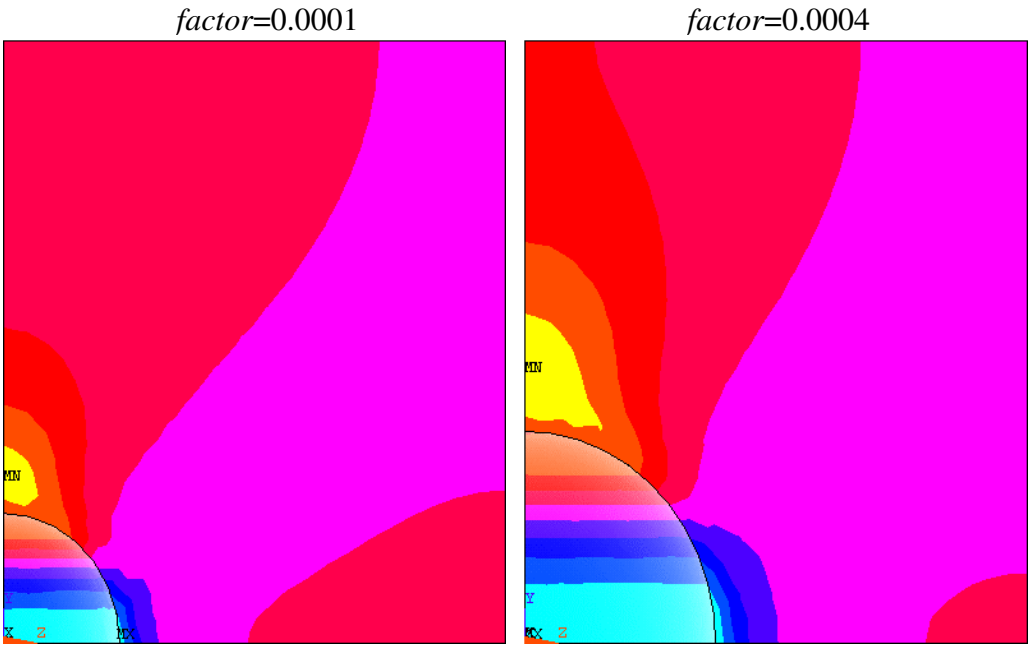

Figure 4.20 Comparison of Von Mises stress contour for different values of *factor*

Figure 4.21 gives the effect of the *factor* parameter on the Von Mises stress concentrations when using a homogenized model with a hole defect. It is seen that the stress concentrations remain almost constant for entire range of the *factor* parameter considered.

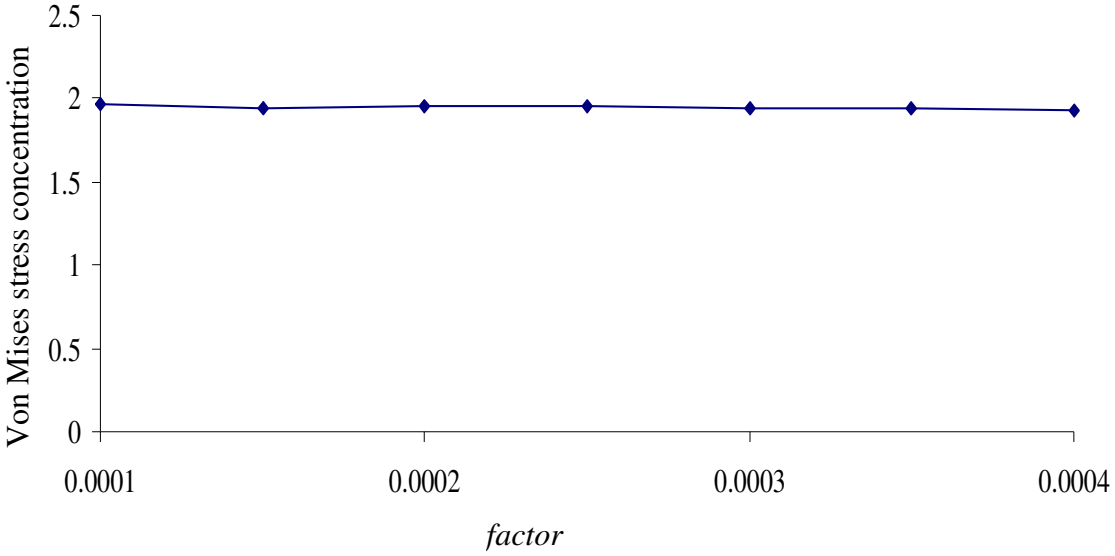

Figure 4.21 Von Mises stress concentration along *factor* for homogeneous model

Now we look at the position of the maximum Von Mises stress as obtained from the distorted multicell model. Figure 4.22 shows that for a *factor* = 0.00005, the maximum Von Mises stress occurs on the interior surface of the void as indicated by the arrows. As the factor parameter is increased to 0.0001, we see that the position now changes to the cells on the layer outside void. As shown in Figures 4.22 and 4.23, we see that this position stays in the same region as the factor parameter is increased to 0.0003. When the factor is further increased to 0.00035 and 0.0004, the position stays in the same layer of cells outside the void but moves to a different region as indicated by the arrows in figure 4.24 and 4.25. This kind of variation in the position is affected by the combined effect of the change in face thickness and edge thickness.

(a) *factor*=0.00005

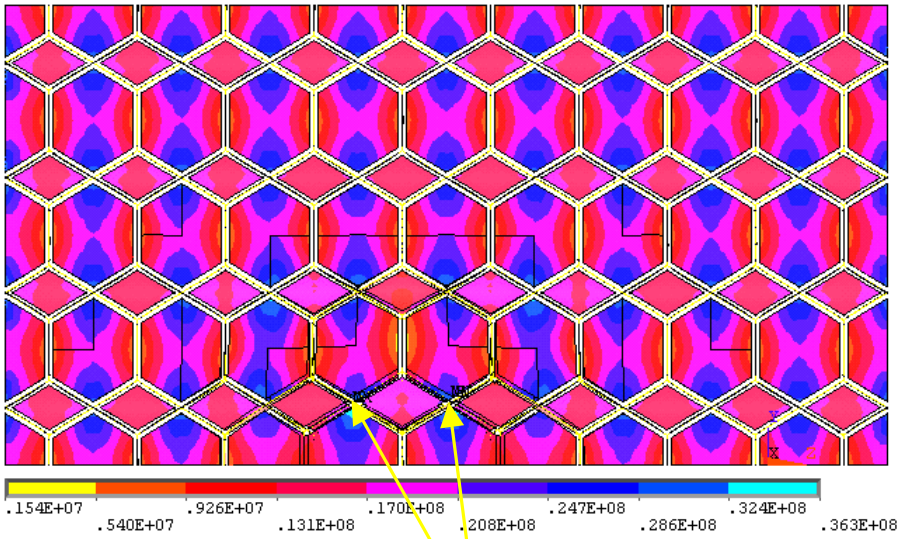

(b) *factor* =0.0001

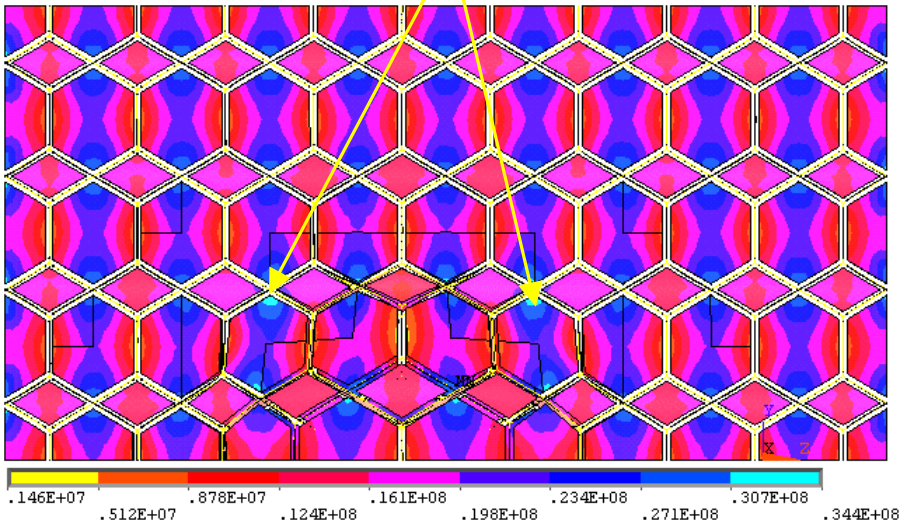

Figure 4.22 Position of maximum Von Mises stress
((a) *factor* =0.00005, (b) *factor* =0.0001)

(a) *factor* =0.00015

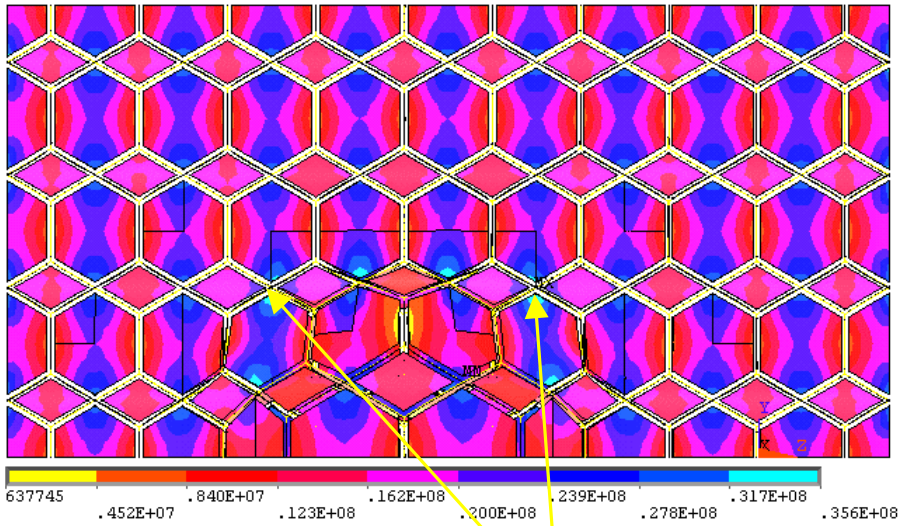

Maximum Von Mises stress

(b) *factor* =0.0002

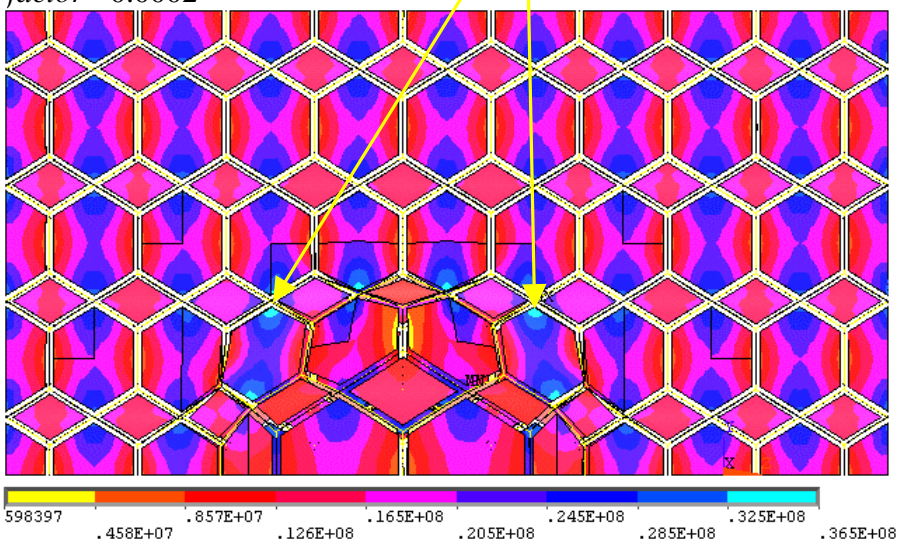

Figure 4.23 Position of maximum Von Mises stress
((a) *factor* =0.00015, (b) *factor* =0.0002)

(a) *factor* =0.00025

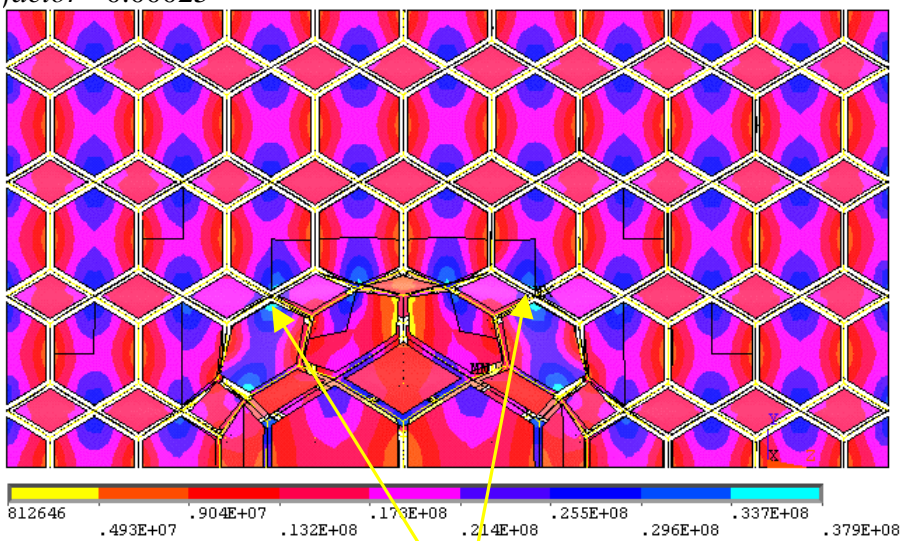

Maximum Von Mises stress

(b) *factor* =0.0003

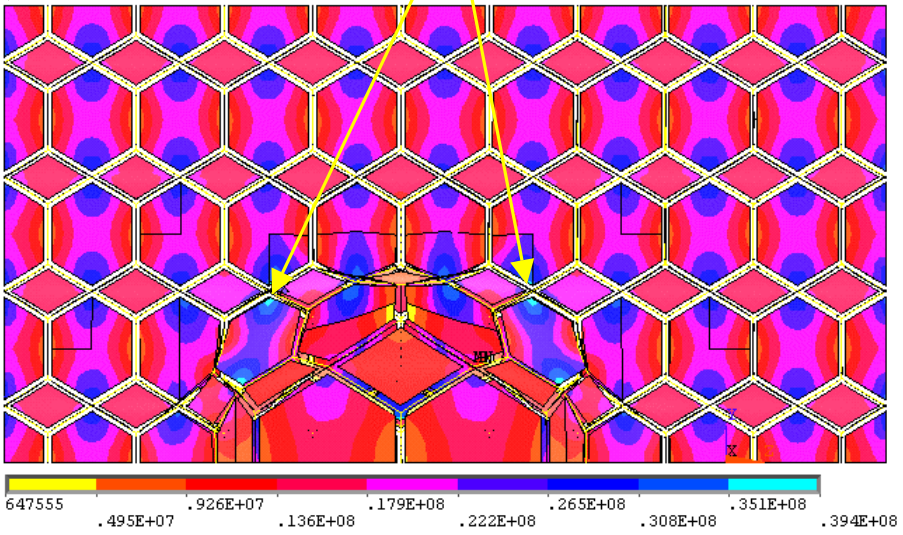

Figure 4.24 Position of maximum Von Mises stress
((a) *factor* =0.00025, (b) *factor* =0.0003)

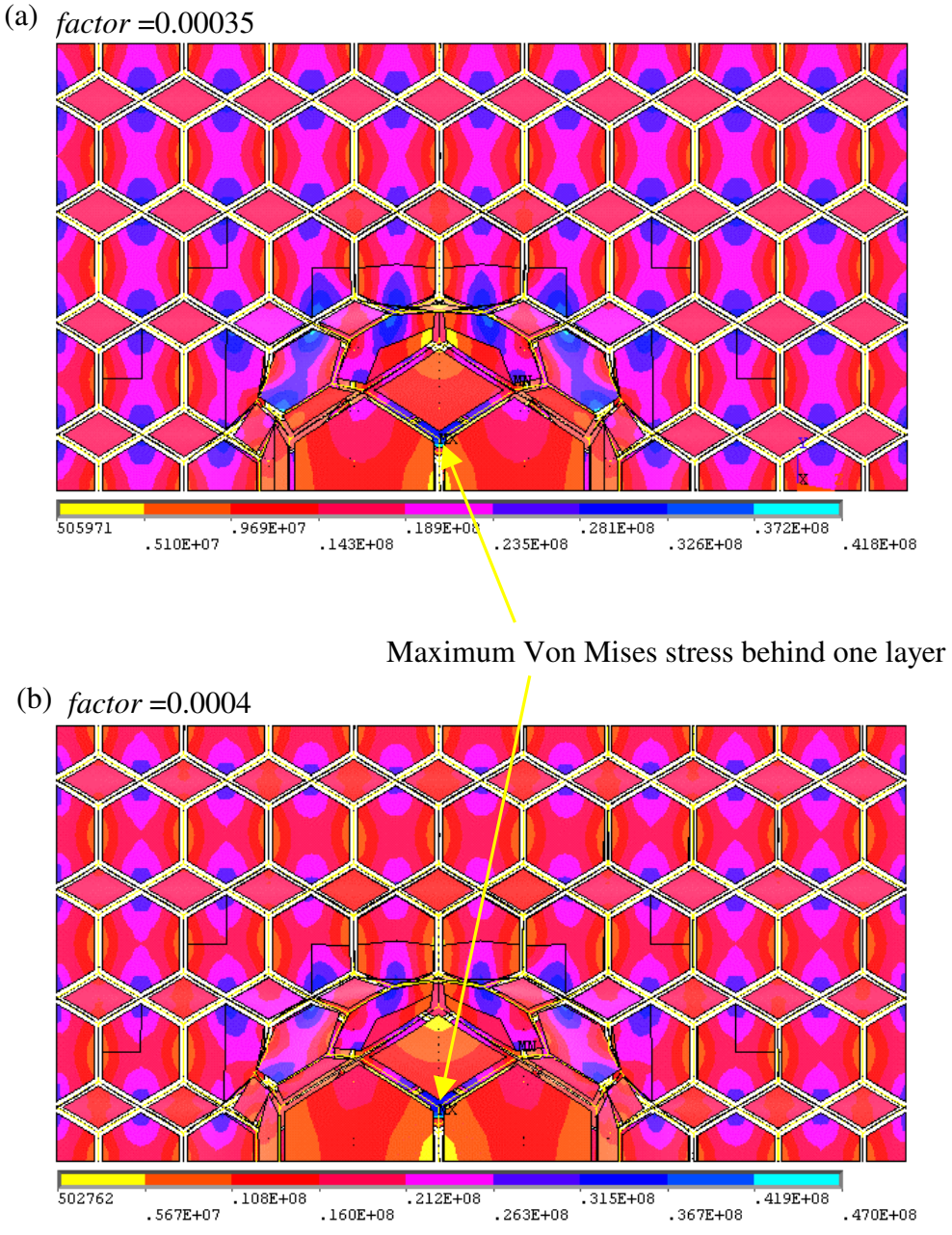

Figure 4.25 Position of maximum Von Mises stress
((a) *factor* =0.00035, (b) *factor* =0.0004)

4. 5. 3 Effect of defect density on the strength and effective stiffness of the foam

The defect density, which is a measure of the distance between two defects, is another parameter which is considered in this study. To examine the effect of defect density on the strength and effective stiffness of the foam, models of different lengths were generated and analyzed, all with one defect of the same size in the center. Figure 4.26 shows a typical distorted multicell model with a length of five unit cells whereas the other two dimensions are kept at a size of two unit cells. By varying the number of unit cells in the z-direction with the same defect size, the defect density can be varied. The models are loaded in tension in the y-direction.

Figure 4.27 compares the Von Mises stress contours for different cases where the length of the model is varied from 3 unit cells to 9 unit cells. It is seen that for all the cases, the effect of the void is restricted to a very small region surrounding the void. The value and position of the maximum Von Mises stresses is found to be roughly the same for all the cases. This indicates that the defect density has a limited effect on the strength of the foam material in the linear regime.

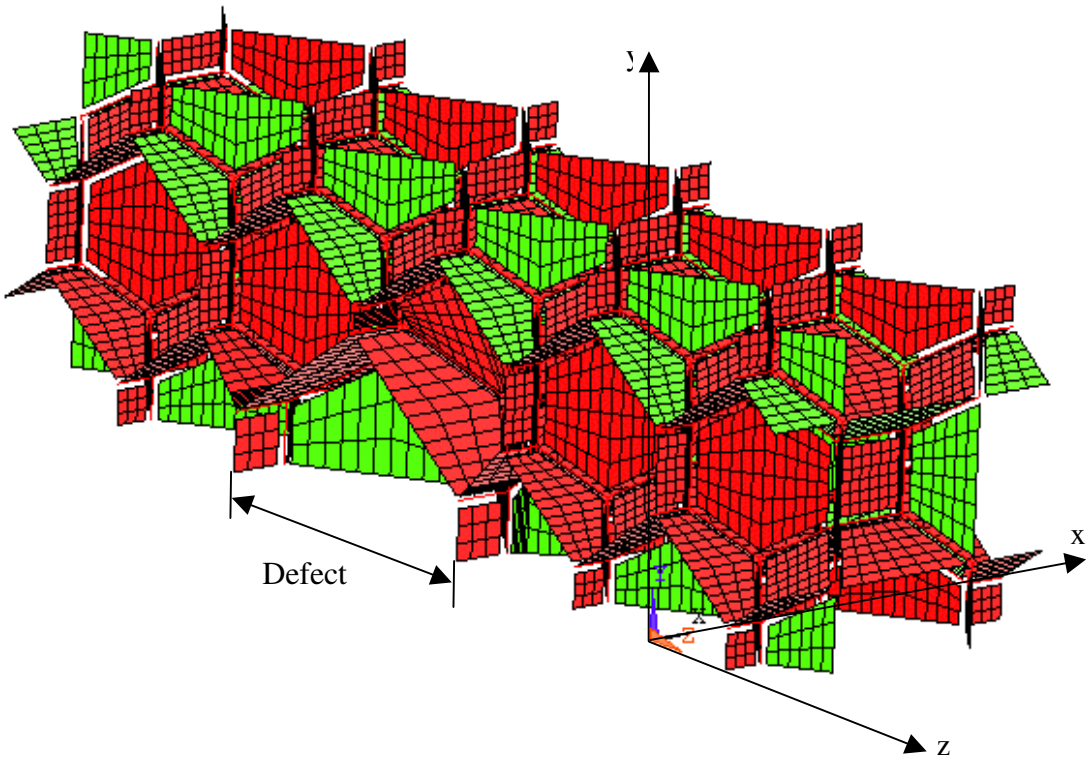

Figure 4.26 Distorted array model for the parametric study of defect density with five unit cells along z direction

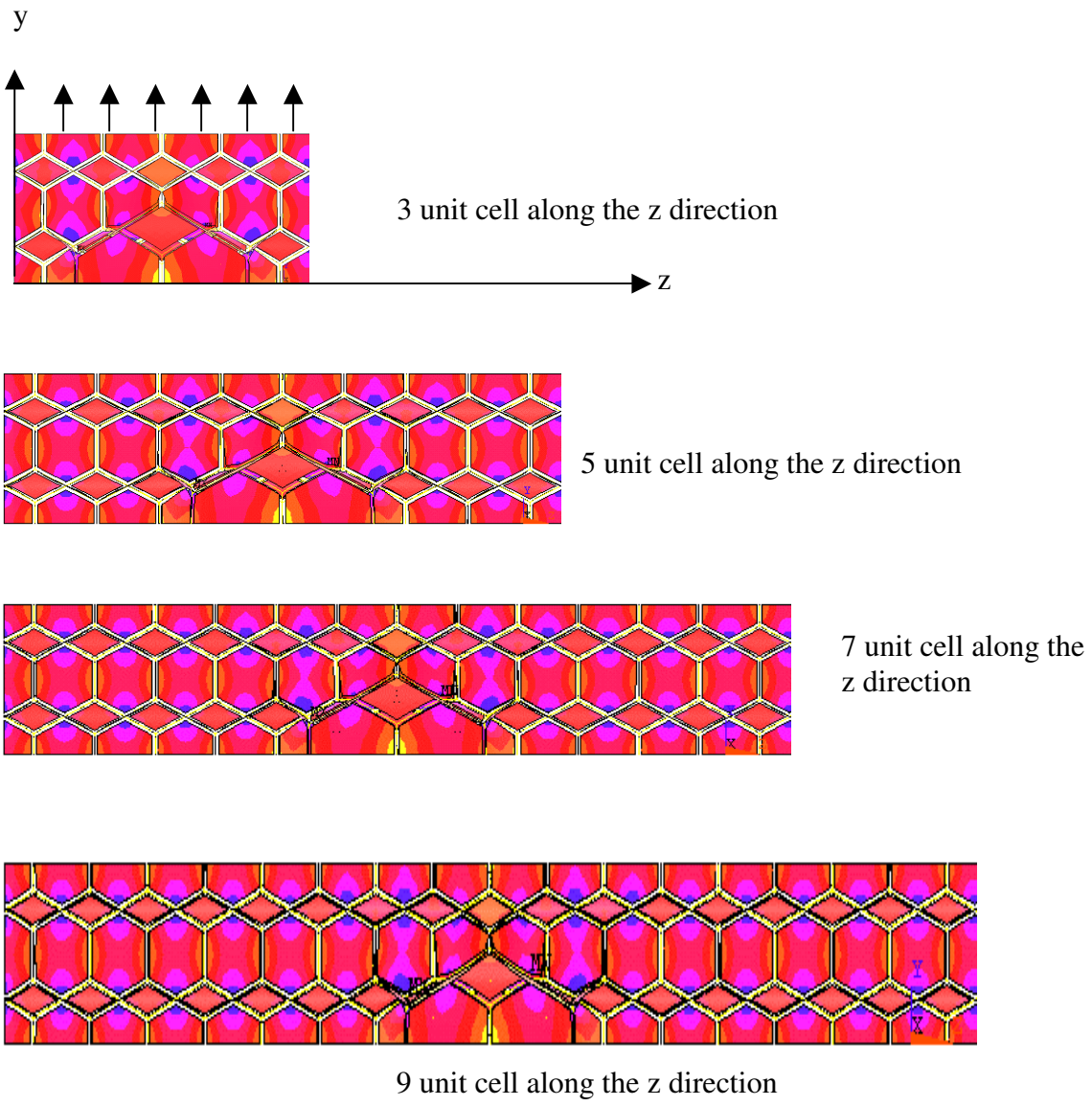

Figure 4.27 Von Mises stress contour for various length of distorted array model

To analyze the effect more quantitatively, the Von Mises stresses at particular points (numbered in Figure 4.28) in the model are determined and compared for the four cases shown in Figure 4.28. It is seen that there is only a 5.7% difference in maximum Von Mises stress at position 3 between the cases with 5 unit cell length and 9 unit cell length (Figure 4.29). This shows that the effect of defect density on the strength of the foam is minimal.

The effective stiffness of the foam was also found to be practically constant for all the four different cases. This means that the defect density does not affect the effective stiffness of the foam material.

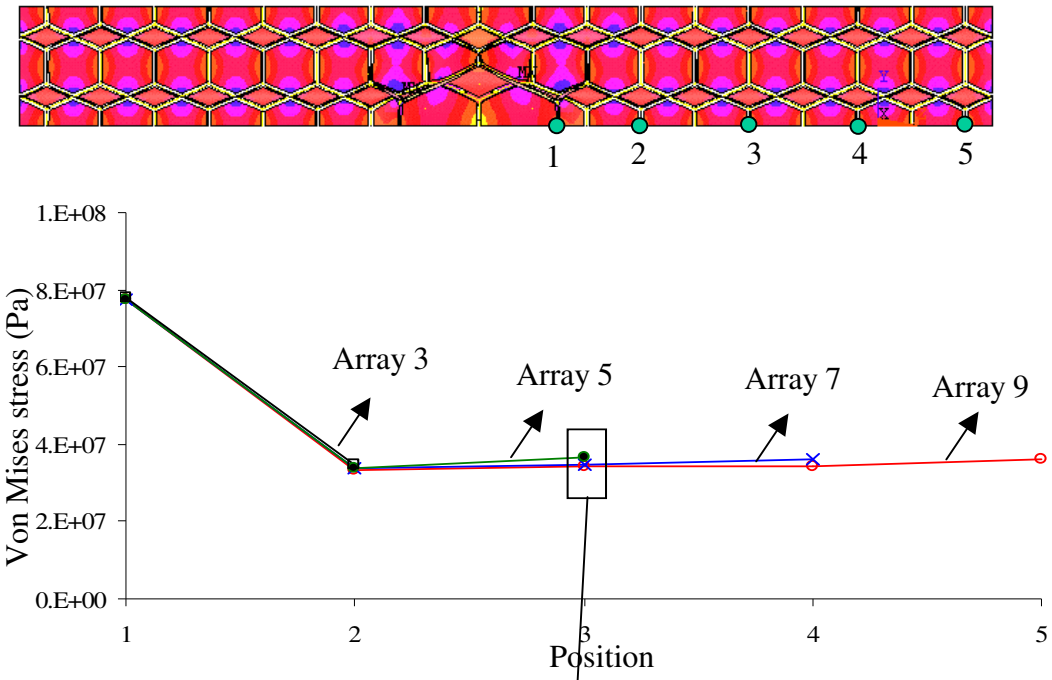

Figure 4.28 Maximum Von Mises stress along the certain position for various defect density models

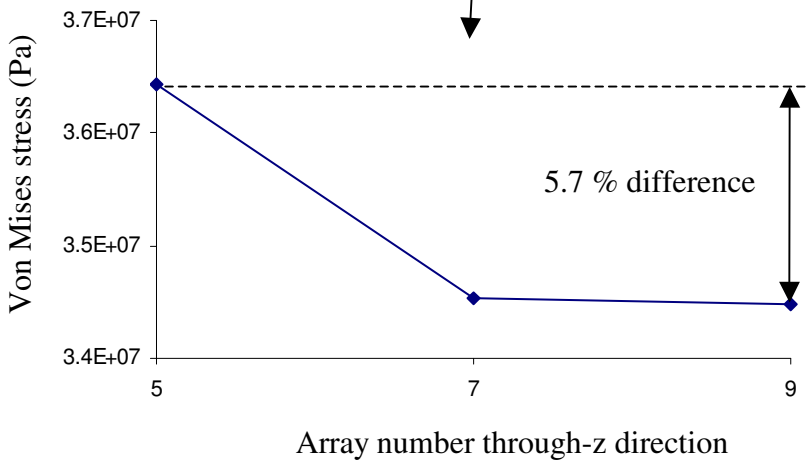

Figure 4.29 Difference of Von Mises stress for three different models with 3, 7 and cell length through z direction

CHAPTER V

SUMMARY AND CONCLUSIONS

A novel finite element model was developed for analyzing closed cell foam. This model consists of only beam and shell elements and is therefore much more computationally efficient than models using full 3D solid elements. The model agrees well with stiffness data from the literature. When beam and shell elements are used for a regular tetrakaidecahedral unit cells, certain problems arise. These problems are overcome by choosing a special RVE and by using rigid links in connecting the beam elements to the shell elements. The effect of material overlap was found to be significant in models that did not use rigid links, so the extra effort required to implement the rigid link model was justified. Parametric studies were performed to examine the effect of different properties such as relative density and edge fraction on the effective stiffness, Von Mises stress, and buckling stress. The thickness of the face plays an important role in the behavior of the foam material. The stiffness of the foam increases with face thickness. The maximum Von Mises stress also occurs at the face. The faces buckle before the edges, and therefore the linear buckling stress is also affected by the thickness of the face. The post-buckling behavior of the foam material was also studied and initial results show that the postbuckling response is not far from the linear response. This would permit one to model the homogenized region as a linear elastic material, thereby reducing the computational costs. More work is needed to validate this hypothesis.

A distorted multicell model is developed to analyze the effect of point defects on the foam behavior. The generation of this model is not a trivial task and various scripts had to be written in ANSYS to complete the task. In particular, the effect of defect size, defect density on the strength and the effective stiffness of the foam are studied. It was found that the defect size has an important effect on the strength of the foam but does not play a significant part in determining the effective stiffness. The distorted multicell model is found to be much more effective than the homogenous model in determining the strength of the foam material in the linear regime. It was found that the defect density does not affect the strength or the effective stiffness of the foam material.

CHAPTER VI

FUTURE WORK

The models that have been developed during the course of this research can be used to analyze multi scale models of closed cell foam materials. The beam and shell model is much less computationally intensive as compared to a full 3D solid element model. Therefore, this idealization can be used to model the regions that are reasonably far away from critical regions like that or a crack growth. One can think of performing crack propagation analysis efficiently on a material with such a complex microstructure if the framework for such a multiscale model is available.

In this work, only the modeling of point defects is discussed. Using the models described in this work, only small sized point defects can be modelled realistically. New models that can account for larger sized voids would also be an intersting research topic. Future work in this research area could be to incorporate surface defects into the models for the foam microstructure. One possible method to do this would be using the two directional distortion methods (Figure 4.3).

REFERENCES

[1] Poole, Eric L. and Rogers, Patrick R., 2005, "Structural Verification of the Redesigned Space Shuttle Sipod Foam Closeout" AIAA/ASME/ASCE/AHS/ASC/ Structure, Structural Dynamics & Materials Conf., AIAA, pp. 2005-2019.

[2] Columbia Accident Investigation Board Report, Volume 4, October 2003, Appendix F.5 Space Shuttle STS-107 Columbia Accident Investigation, External Tank Working Group Final Report – Volume 1, Washington, DC, pp. 239-395.

[3] Columbia Accident Investigation Board Report Volume 1, August 2003, Government Printing Office, ISBN 0-16-067904-4, Washington, DC.

[4] Ganpatye, A. S. and Kinra, V. K., 2006, "Fracture Toughness of Space Shuttle External Tank Insulation Foam," AIAA, pp. 2006-2020.

[5] Green, D. J., 1985, "Fabrication and Mechanical Properties of Lightweight Ceramics Produced by Sintering of Hollow Spheres," J. Am. Ceram. Soc., **68**, pp. 403.

[6] Silva, M.J., Hayes, W.C. and Gibson, L.J., 1995, "The Effects of Non-periodic Microstructure on the Elastic Properties of Two-dimensional Cellular Solids," Int. J. Mech. Sci., **11**, pp. 1161–1177.

[7] Chen, C., Lu, T.J. and Fleck, N.A., 1999, "Effect of Imperfections on the Yielding of Two Dimensional Foams," J. Mech. Phy. Solids, **47**, pp. 2235–2272.

[8] Lu, T.J. and Chen, C., 1999, "Thermal Transport and Fire Retardance Properties of Cellular Aluminium Alloys," Acta mater., **47**, pp. 1469–1485.

[9] Silva, M.J. and Gibson, L.J., 1997, "The Effect of Non-periodic Microstructure and Defects on the Compressive Strength of Two-dimensional Cellular Solids," Int. J. Mech. Sci., **39**, pp. 549–563.

[10] Gibson, L.J. and Ashby M. F., 1997, *Cellular Solids: Structure and Properties*, 2nd, Pergamon Press, Oxford

[11] L. Ya. Karas' and A. A. Tager, 1965, "Phase-equilibrea of Polystyrene Solutions," Polymer Science, U.S.S.R., **7** (5), pp. 983-991

[12] David R., Lee, S., 2002, *The Polyurethanes Book*, John Wiley & Sons, Hoboken,

pp. 137-150

[13] Thomson, W., Kelvin, Lord, 1887, "On the Division of Space with Minimum Partitional Area," Phil. Mag., **24**, pp. 503.

[14] Weaire, D. and Phelan, R., 1994, "A Counterexample to Kelvin's Conjecture on Minimal Surfaces," Phil. Mag. Lett., **69**, pp. 107-110.

[15] Zaslawsky, M., 1973, "Multiaxial Stress Studies on Rigid Polyurethane Foam," Exper. Mech., **2**, pp. 70.

[16] Gibson, L. J., Ashby, M. F., Zhang, J. and Triantaeillou, T. C., 1989, "Failure Surfaces for Cellular Materials: II Comparison of Models with Experiment," Int. J. Mech. Sci., **31**, pp. 635.

[17] Gibson, L. J. and Ashby, M. F., 1982, "The Mechanics of Two-Dimensional Cellular Materials," Proc. R. Soc. Lond., **382**, pp. 25-42

[18] Renz, R. and Ehrenstein, G. W., 1982, "Elastic Moduli of Model Random Three-dimensional Closed-cell Cellular Solids," Cellular Polymers, **1**, pp. 5.

[19] Kraynik, A.M., Neilsen, M.K., Reinelt, D.A., Warren, W.E., 1997, "Foam micromechanics," *Proceedings of the NATO Advanced Study Institute on Foams, Emulsions, and Cellular Materials*, Cargese, Corsica.

[20] Shulmeister, V., Van der Burg, M.W.D., Van der Giessen, E. and Marissen, R., 1998, "A Numerical Study of Large Deformations of Low-density Elastomeric Open-cell Foams," Mechanics Mat., **30,** pp. 125–140.

[21] Roberts, A.P. and Garboczi, E.J., 2001, "Elastic Moduli of Model Random Three-dimensional Closed-cell Cellular Solids," Acta mater., **49**, pp. 189–197.

[22] Simone, A. E. and Gibson, L. J., 1998, "The Effects of Cell Face Curvature and Corrugations on the Stiffness and Strength of Metallic Foams," Acta mater, **46**, pp. 2139.

[23] Grenestedt, J. L. and Tanaka, K., 1999, "Influence of Cell Shape Variations on Elastic Stiffness of Closed Cell Cellular Solids," Scripta mater., **40**, pp. 71.

[24] Grenestedt, J. L., 1999, "Effective Elastic Behavior of Some Models for 'Perfect' Cellular Solids," Int. J. Solids Struct., **36**, pp. 1471.

[25] Mills, N. J. and Zhu, H. X., J., 1999, "The High Strain Compression of Closed-cell Polymer Foams," Mech. Phys. Solids, **47**, pp. 669.

[26] Garboczi, E. J., 1989, "Effective-medium Theory of Percolation on Central-force Elastic Networks. II. Further results," Phys. Rev. B, **39**, pp. 2472.

[27] Grenestedt, J. L., 1998, "Influence of Wavy Imperfections in Cell Walls on Elastic Stiffness of Cellu-lar Solids," J. Mech. Phys. Solids, **46**, pp. 29.

[28] Zhu, H.X., Hobdell, J.R. and Windle, A.H., 2000, "Effects of Cell Irregularity on the Elastic Properties of Open-cell Foams," Acta Materialia, **48**, pp. 4893–4900.

[29] Patel, M. R. and Finnie, I., 1969, "The Deformation and Fracture of Rigid Cellular Plastics under Multiaxial Stress," Lawrence Livermore Laboratory Report UCRL-13420.

[30] Rusch, K. C., 1970, "Energy Absorbing Characteristics of Foamed Polymers," J. Appl. Polymer Sci., **14**, pp. 1263.

[31] Green, T. and Turner, A. B., 1992, "Ingestion Into the Upstream Wheelspace of an Axial Turbine Stage," ASME Paper No. 1992-GT-303.

[32] Morgan, J. S., Wood, J. L. and Bradt, R. C., 1981, "Cell Size Effects in the Strength of Foamed Glass," Mater. Sci. Engng, **47**, pp. 37.

[33] Ashby, M. F., 1983, "The Mechanical Properties of Cellular Solids," Metall. Trans., **14A**, pp. 1755.

[34] Mare, S. K., Gibson, L. J. and Ashby, M. F., 1984, "Deformation and Energy Absorption Diagrams for Cellular Materials," Acta Metall., **32**, pp. 1963.

[35] Mcintyre A. and Anderton G. E., 1979, "Fracture Properties of a Rigid Polyurethane Foam Over a Range of Densities," Polymer, **20**, pp. 247.

[36] Zwissler, J. G. and Adams M. A., 1983, "Fracture Mechanics of Cellular Glass," Fracture Mechanics of Ceramics, **6**, pp. 211.

.

[37] Maiti, S. K., Ashby, M. F. and Gibson, L. J., 1984, "Fracture Toughness of Brittle Cellular," Scripta Metall. **18**, pp. 213.

[38] Green, D. J., 1985, "Fabrication and Mechanical Properties of Lightweight Ceramics Produced by Sintering of Hollow Spheres," J. Am. Ceram. Soc., **68**, pp. 403.

[39] Shaw, M. C. and Sata, T., 1966, "The Plastic Behavior of Cellular Materials," Int. J. Mech. Sci., **8**, pp. 469.

[40] Triantafillou, T. C., Zhang, J., Shercliff, T. L., Gibson, L. J. and Ashby, M. F., 1989, "Failure Surfaces for Cellular Materials under Multiaxial Loads: I Modelling," Int. J. Mech. Sci., **31**, pp. 665.

[41] Choi, S. and Sankar, B.V., 2003, "Fracture Toughness of Carbon Foam," J. Composite Materials, **37**, 2101-2116.

[42] Zhu, H.X. and Windle, A.H., 2002, "Effects of Cell Irregularity on the High Strain Compression of Open-cell Foams," Acta Materialia, **50**, pp. 1041–1052.

[43] ANSYS Release 9.0 Documentation (15. 14), SAS IP, Inc.

[44] Roberts, A. P. and Knackstedt, M. A., 1995, "MA Mechanical and Transport Properties of Model Foamed Solids," J. Mater. Sci. Lett., **14**, pp. 1357.

[45] Garboczi, E. J. and Day, A. R., 1995, "An Algorithm for Computing the Effective Linear Elastic Properties of Heterogeneous Materials: 3-D Results for Composites with Equal Phase Poisson Ratios," J. Mech. Phys. Solids, **43**, pp. 1349.

[46] Stoyan, D., Kendall, W. S. and Mecke, J., 1995, "StochasticGeometry and its Applications," 2nd edn., Wiley, Chichester.

[47] Berk, N. F., 1987, "Scattering Properties of a Model Bicontinuous Structure with a Well Defined Length Scale," Phys. Rev. Lett., **58**, pp. 2718.

APPENDIX A

CALCULATION OF CORRECTION VOLUME

4 edges meet each other at the vertex with various angles. The angle is assumed as 90 degree. From this assumption, overlapped volume between two edges is calculated as Equation A.1 (Figure A.1). Total correct volume is Equation A.2.

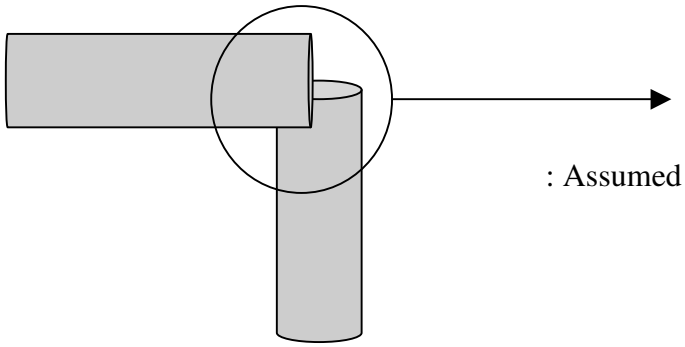

$$\frac{t_e}{2}\pi(\frac{t_e}{2})^2 \qquad A.1$$

: Assumed overlapped volume

Figure A.1 Schematic of overlapped volume between edges

Correction volume =

{number of vertices inside RVE (16) * (number of overlapped edge(4)-1)}*overlapped volume

$$correction\ factor = 16 \times 3 \times \frac{\pi(t_e)^3}{8} = 6\pi(t_e)^3 \qquad A.2$$

APPENDIX B

APDL CODE FOR DISTORTED MULTI CELL MODEL

```
/PREP7
! initial parameter
PI=2*ASIN(1)

!*  Geometry imformation
  factor=1e-3
  edget=3.59402E-05
  facet=4.04734E-06
  l=0.22e-3

  a=l*sqrt(2)
  b=l/sqrt(2)

  rdens=0.029166 !relative density
  efrac=0.7          !edge fraction
  ecorf=1            ! edge correction factor usually 3

!* for distortion
  rown=2
  column=2
  depthn=5           ! should be always odd number

   xwidth=rown*2*a
   ywidth=column*2*a
   zwidth=depthn*2*a


!---------- give the distortion parameters ----------!
kpstrain=0
! wn=x direction wave length always even
wn=1
lradi=3*b+b/2



!*  Mesh imformation
tsize=1
lsize=3

! Geometry model of Unit cell
k,1,l,l+2*l,b
k,2,2*l-l/2,3*l/2+2*l,0
```

```
k,3,l,l+2*l,-b
k,4,-3*l/2+2*l,l/2+2*l,0
!k,5 ,l,l+2*l,0

k,5,3*l,l+2*l,b
k,6,3*l/2+2*l,l/2+2*l,0
k,7,l+2*l,l+2*l,-b
k,8,l/2+2*l,3*l/2+2*l,0
!k,10,l,l,0

k,9,l+2*l,-l+2*l,b
k,10,l/2+2*l,-3*l/2+2*l,0
k,11,l+2*l,-l+2*l,-b
k,12,3*l/2+2*l,-l/2+2*l,0
!k,15,l+2*l,-l+2*l,0

k,13,-l+2*l,-l+2*l,b
k,14,-3*l/2+2*l,-l/2+2*l,0
k,15,-l+2*l,-l+2*l,-b
k,16,-l/2+2*l,-3*l/2+2*l,0
!k,20,-l+2*l,-l+2*l,0

k,17,l/2+2*l,l/2+2*l,a
k,18,-l/2+2*l,l/2+2*l,a
k,19,-l/2+2*l,-l/2+2*l,a
k,20,l/2+2*l,-l/2+2*l,a
k,21,2*l,+2*l,a
k,22,l/2+2*l,+2*l,a
k,23,2*l,l/2+2*l,a
k,24,-l/2+2*l,+2*l,a
k,25,2*l,-l/2+2*l,a

k,26,2*l,l+2*l,b
k,27,-l+2*l,0+2*l,b
k,28,2*l,-l+2*l,b
k,29,l+2*l,0+2*l,b
k,30,2*l,3*l/2+2*l,0
k,31,-3*l/2+2*l,0+2*l,0
k,32,2*l,-3*l/2+2*l,0
k,33,3*l/2+2*l,0+2*l,0
k,34,2*l,l+2*l,-b
k,35,-l+2*l,0+2*l,-b
k,36,2*l,-l+2*l,-b
k,37,l+2*l,0+2*l,-b

k,38,-l+2*l,l+2*l,a+b
k,39,-3*l/2+2*l,3*l/2+2*l,a
k,40,-l+2*l,-l+2*l,a+b
k,41,-3*l/2+2*l,-3*l/2+2*l,a
k,42,l+2*l,-l+2*l,a+b
k,43,3*l/2+2*l,-3*l/2+2*l,a
k,44,l+2*l,l+2*l,a+b
k,45,3*l/2+2*l,3*l/2+2*l,a
```

```
k,46,2*l+2*l,2*l+2*l,a
k,47,3*l/2+2*l,2*l+2*l,a
k,48,l+2*l,2*l+2*l,b
k,49,l/2+2*l,2*l+2*l,0
k,50,2*l,2*l+2*l,0
k,51,-l/2+2*l,2*l+2*l,0
k,52,-l+2*l,2*l+2*l,b
k,53,-3*l/2+2*l,2*l+2*l,a
k,54,-2*l+2*l,2*l+2*l,a

k,55,0,3*l/2+2*l,a
k,56,0,l+2*l,b
k,57,0,l/2+2*l,0
k,58,0,0+2*l,0
k,59,0,-l/2+2*l,0
k,60,0,-l+2*l,b
k,61,0,-3*l/2+2*l,a
k,62,0,-2*l+2*l,a

k,63,-3*l/2+2*l,-2*l+2*l,a
k,64,-l+2*l,-2*l+2*l,b
k,65,-l/2+2*l,-2*l+2*l,0
k,66,2*l,-2*l+2*l,0
k,67,l/2+2*l,-2*l+2*l,0
k,68,l+2*l,-2*l+2*l,b
k,69,3*l/2+2*l,-2*l+2*l,a
k,70,2*l+2*l,-2*l+2*l,a

k,71,4*l,-3*l/2+2*l,a
k,72,4*l,-l+2*l,b
k,73,4*l,-l/2+2*l,0
k,74,4*l,0+2*l,0
k,75,4*l,l/2+2*l,0
k,76,4*l,l+2*l,b
k,77,4*l,3*l/2+2*l,a

k,78,l+2*l,2*l+2*l,-b
k,79,-l+2*l,2*l+2*l,-b
k,80,-2*l+2*l,l+2*l,-b
k,81,-2*l+2*l,-l+2*l,-b
k,82,-l+2*l,-2*l+2*l,-b
k,83,l+2*l,-2*l+2*l,-b
k,84,2*l+2*l,-l+2*l,-b
k,85,2*l+2*l,l+2*l,-b

k,86,2*l+2*l,l+2*l,a+b
k,87,l+2*l,2*l+2*l,a+b
k,88,-l+2*l,2*l+2*l,a+b
k,89,-2*l+2*l,l+2*l,a+b
k,90,-2*l+2*l,-l+2*l,a+b
k,91,-l+2*l,-2*l+2*l,a+b
k,92,l+2*l,-2*l+2*l,a+b
```

```
k,93,2*l+2*l,-l+2*l,a+b

k,94,l+2*l,0+2*l,b+a
k,95,+2*l,l+2*l,b+a
k,96,-l+2*l,0+2*l,b+a
k,97,+2*l,-l+2*l,b+a

!! square
a,1,2,3,4
a,5,6,7,8
a,9,10,11,12
a,13,14,15,16
a,17,23,21,22
a,18,24,21,23
a,19,25,21,24
a,20,22,21,25

a,18,1,39,38
a,19,13,41,40
a,20,9,43,42
a,17,5,45,44

a,45,77,46,47
a,39,53,54,55
a,41,61,62,63
a,43,69,70,71

a,8,49,50,30
a,2,30,50,51
a,4,57,58,31
a,14,31,58,59
a,16,65,66,32
a,10,32,66,67
a,12,73,74,33
a,6,33,74,75

!! hexagonal
a,8,30,26,5
a,2,1,26,30
a,18,23,26,1
a,17,5,26,23

a,18,1,27,24
a,4,31,27,1
a,14,13,27,31
a,19,24,27,13

a,20,25,28,9
a,19,13,28,25
a,16,32,28,13
a,10,9,28,32

a,6,5,29,33
```

```
a,17,22,29,5
a,20,9,29,22
a,12,33,29,9

! back hexagonal
a,4,31,35,3
a,14,15,35,31
a,16,32,36,15
a,10,11,36,32
a,12,33,37,11
a,6,7,37,33
a,8,30,34,7
a,2,3,34,30

!front hexagonal
a,45,44,86,77
a,45,47,87,44
a,39,38,88,53
a,39,55,89,38
a,41,40,90,61
a,41,63,91,40
a,43,42,92,69
a,43,71,93,42

a,17,22,94,44
a,17,44,95,23
a,18,23,95,38
a,18,38,96,24
a,19,24,96,40
a,19,40,97,25
a,20,25,97,42
a,20,42,94,22

!sencond back hexagonal
a,45,47,48,5
a,8,5,48,49
a,2,51,52,1
a,39,1,52,53
a,39,55,56,1
a,4,1,56,57
a,14,59,60,13
a,41,13,60,61
a,41,63,64,13
a,16,13,64,65
a,10,67,68,9
a,43,9,68,69
a,43,71,72,9
a,12,9,72,73
a,6,75,76,5
a,45,5,76,77

!last back hexagonal
a,8,7,78,49
```

```
a,2,51,79,3
a,4,3,80,57
a,14,59,81,15
a,16,15,82,65
a,10,67,83,11
a,12,11,84,73
a,6,75,85,7

adele,all

k,100,3*l/2+edget/2+2*l,3*l/2+edget/2+2*l,a
k,101,l/2-edget/2+2*l,3*l/2+edget/2+2*l,0
k,102,l/2-edget/2+2*l,l/2-edget/2+2*l,a
k,103,3*l/2+edget/2+2*l,l/2-edget/2+2*l,0

k,104,l+2*l,l+2*l,a-edget/sqrt(2)+b
k,105,l+2*l,l+2*l,edget/sqrt(2)+b
k,106,l+2*l,l+2*l,-edget/sqrt(2)+b
k,107,l+2*l,l+2*l,-2*b+edget/sqrt(2)+b

k,108,3*l/2-edget/2+2*l,3*l/2-edget/2+2*l,a
k,109,l/2+edget/2+2*l,3*l/2-edget/2+2*l,0
k,110,l/2+edget/2+2*l,l/2+edget/2+2*l,a
k,111,3*l/2-edget/2+2*l,l/2+edget/2+2*l,0

k,156,2*l+2*l,3*l/2+edget/2+2*l,a
k,157,3*l/2+edget/2+2*l,2*l+2*l,a
k,158,l/2-edget/2+2*l,2*l+2*l,
k,159,0+2*l,3*l/2+edget/2+2*l,
k,160,0+2*l,l/2-edget/2+2*l, 2*b
k,161,l/2-edget/2+2*l,0+2*l, 2*b
k,162,3*l/2+edget/2+2*l,0+2*l,
k,163,2*l+2*l,l/2-edget/2+2*l,

cskp,20,,26,5,30
csys,20
k,112,0,-l*sqrt(3)/2+edget/2
k,113,l/2-edget/(2*sqrt(3)),-l*sqrt(3)/2+edget/2
k,114,l-edget/(sqrt(3)),
k,115,l/2-edget/(2*sqrt(3)),l*sqrt(3)/2-edget/2
k,116,0,l*sqrt(3)/2-edget/2
csys

cskp,21,,29,5,22
csys,21
k,117,0,-l*sqrt(3)/2+edget/2
k,118,l/2-edget/(2*sqrt(3)),-l*sqrt(3)/2+edget/2
k,119,l-edget/(sqrt(3)),
k,120,l/2-edget/(2*sqrt(3)),l*sqrt(3)/2-edget/2
k,121,0,l*sqrt(3)/2-edget/2
csys

cskp,22,,76,5,75
```

```
csys,22
k,122,0,-l*sqrt(3)/2+edget/2
k,123,l/2-edget/(2*sqrt(3)),-l*sqrt(3)/2+edget/2
k,124,l-edget/(sqrt(3)),
k,125,l/2-edget/(2*sqrt(3)),l*sqrt(3)/2-edget/2
k,126,0,l*sqrt(3)/2-edget/2
csys

cskp,23,,48,5,49
csys,23
k,127,0,-l*sqrt(3)/2+edget/2
k,128,l/2-edget/(2*sqrt(3)),-l*sqrt(3)/2+edget/2
k,129,l-edget/(sqrt(3)),
k,130,l/2-edget/(2*sqrt(3)),l*sqrt(3)/2-edget/2
k,131,0,l*sqrt(3)/2-edget/2
csys

cskp,24,,95,44,23
csys,24
k,132,l-edget/(sqrt(3)),
k,133,l/2-edget/(2*sqrt(3)),l*sqrt(3)/2-edget/2
k,134,0,l*sqrt(3)/2-edget/2
csys

cskp,25,,94,44,22
csys,25
k,135,l-edget/(sqrt(3)),
k,136,l/2-edget/(2*sqrt(3)),l*sqrt(3)/2-edget/2
k,137,0,l*sqrt(3)/2-edget/2
csys

cskp,26,,86,44,77
csys,26
k,138,l-edget/(sqrt(3)),
k,139,l/2-edget/(2*sqrt(3)),l*sqrt(3)/2-edget/2
k,140,0,l*sqrt(3)/2-edget/2
csys

cskp,27,,87,44,47
csys,27
k,141,l-edget/(sqrt(3)),
k,142,l/2-edget/(2*sqrt(3)),l*sqrt(3)/2-edget/2
k,143,0,l*sqrt(3)/2-edget/2
csys

cskp,28,,85,7,75
csys,28
k,144,l-edget/(sqrt(3)),
k,145,l/2-edget/(2*sqrt(3)),l*sqrt(3)/2-edget/2
k,146,0,l*sqrt(3)/2-edget/2
csys

cskp,29,,78,7,49
```

```
csys,29
k,147,l-edget/(sqrt(3)),
k,148,l/2-edget/(2*sqrt(3)),l*sqrt(3)/2-edget/2
k,149,0,l*sqrt(3)/2-edget/2
csys

cskp,30,,34,7,30
csys,30
k,150,l-edget/(sqrt(3)),
k,151,l/2-edget/(2*sqrt(3)),l*sqrt(3)/2-edget/2
k,152,0,l*sqrt(3)/2-edget/2
csys

cskp,31,,37,7,33
csys,31
k,153,l-edget/(sqrt(3)),
k,154,l/2-edget/(2*sqrt(3)),l*sqrt(3)/2-edget/2
k,155,0,l*sqrt(3)/2-edget/2
csys

! square area
a,108,105,110,104
a,109,106,111,107
a,100,156,46,157
a,101,158,50,159
a,102,160,21,161
a,103,162,74,163

! hexa area
a,115,116,26,114
a,113,114,26,112
a,118,119,29,117
a,120,121,29,119
a,123,124,76,122
a,125,126,76,124
a,130,129,48,131
a,128,127,48,129
a,133,132,95,134
a,136,137,94,135
a,139,140,86,138
a,142,143,87,141
a,145,146,85,144
a,148,149,78,147
a,151,152,34,150
a,154,155,37,153

clocal,11,,2*l,2*l,b
ARSYM,X,all, , , ,0,0
ARSYM,y,all, , , ,0,0
aglue,all
csys

btol,0.1E-6
```

```
lovlap,all
lsel,s,length,,edget/2
lsel,a,length,,edget/sqrt(3)
ldele,all,,,1
allsel,all
btol

asel,s,area,,all,,,1
lsel,inve
lsel,r,loc,x,0
ldel,all,,,1
allsel,all

asel,s,area,,all,,,1
lsel,inve
lsel,r,loc,x,4*l
ldel,all,,,1
allsel,all

asel,s,area,,all,,,1
lsel,inve
lsel,r,loc,y,4*l
ldel,all,,,1
allsel,all

asel,s,area,,all,,,1
lsel,inve
lsel,r,loc,y,0
ldel,all,,,1
allsel,all

asel,s,area,,all,,,1
lsel,inve
lsel,r,loc,z,-1*b
ldel,all,,,1
allsel,all

asel,s,area,,all,,,1
lsel,inve
lsel,r,loc,z,3*b
ldel,all,,,1
allsel,all

asel,s,area,,all,,,1
lsel,inve
lsel,r,length,,l-edget/(sqrt(3))
ldel,all,,,1
allsel,all

lsel,s,line,,462,463
lsel,a,line,,467,470,3
lsel,a,line,,518,564,46
```

```
lsel,a,line,,609,633,24
lsel,a,line,,685,689,4
ldele,all,,,1

asel,s,area,,all,,,1
lsel,inve
cm,beaml,line
allsel,all

!---> finish the unit model



! start to make multi cell model
agen,rown,all,,,4*l
agen,column,all,,,,4*l
agen,depthn,all,,,,,-4*b
aglue,all
allsel,all

asel,s,area,,all,,,1
cm,areal,line
allsel,all

cmsel,s,beaml,line
lgen,rown,all,,,4*l
lgen,column,all,,,,4*l
lgen,depthn,all,,,,,-4*b
lglue,all
allsel,all

asel,s,area,,all,,,1
lsel,inve
cm,tbeaml,line
allsel,all

lsel,s,length,,l/2
lsel,a,length,,l/2-edget/2
lesize,all,,,lsize
allsel,all

lsel,s,length,,l-edget/sqrt(3)
lsel,r,tan1,x,1
lesize,all,,,lsize
allsel,all

lsel,s,length,,l-edget/sqrt(3)
lsel,r,tan1,x,-1
lesize,all,,,lsize
allsel,all

lsel,s,length,,l-edget/sqrt(3)
lsel,r,tan1,y,-1
```

```
lesize,all,,,lsize
allsel,all

lsel,s,length,,l-edget/sqrt(3)
lsel,r,tan1,y,1
lesize,all,,,lsize
allsel,all

lsel,s,length,,l
lsel,a,length,,l-edget
lesize,all,,,lsize*2
allsel,all

lsel,s,length,,l-edget/sqrt(3)
lsel,a,length,,l*sqrt(3)/2-edget/2
lesize,all,,,lsize*2
allsel,all

lsel,s,length,,distkp(127,128)
lesize,all,,,lsize
allsel,all

!!!!!----------------------------------------------------------!!!!!
!!!!!    make table for geometry information of surface    !!!!!
!!!!!----------------------------------------------------------!!!!!
!       table format                          !
!-------------------------------------------------------------------!
! face   !face  !kp    !line          !
! type    !area !number   !number         !
!-------------------------------------------------------------------!
!face type: front square (1), inclined square (2), hexagonal(3)  !
!face area: full(1), half(2), quater(3)         !
!-------------------------------------------------------------------!
inumber1=2*depthn*(2*column+1)*(2*rown+1)+2*depthn*(2*column)*(2*rown)
inumber2=16*(depthn+1)*(column+1)*(rown+1)
inumber=inumber1+inumber2
*dim,surfi,,inumber,50
*dim,sqkpi,,8,2
*dim,sqkpo,,8,2
*dim,centil,,8,2
*dim,centol,,8,2

!! for out side upright square area
sqkpi(1,1)=l/2-edget/2
sqkpi(1,2)=0
sqkpi(2,1)=l/2-edget/2
sqkpi(2,2)=l/2-edget/2
sqkpi(3,1)=0
sqkpi(3,2)=l/2-edget/2
sqkpi(4,1)=-(l/2-edget/2)
sqkpi(4,2)=l/2-edget/2
sqkpi(5,1)=-(l/2-edget/2)
sqkpi(5,2)=0
```

```
sqkpi(6,1)=-(l/2-edget/2)
sqkpi(6,2)=-(l/2-edget/2)
sqkpi(7,1)=0
sqkpi(7,2)=-(l/2-edget/2)
sqkpi(8,1)=(l/2-edget/2)
sqkpi(8,2)=-(l/2-edget/2)
sqkpo(1,1)=l/2
sqkpo(1,2)=0
sqkpo(2,1)=l/2
sqkpo(2,2)=l/2
sqkpo(3,1)=0
sqkpo(3,2)=l/2
sqkpo(4,1)=-l/2
sqkpo(4,2)=l/2
sqkpo(5,1)=-l/2
sqkpo(5,2)=0
sqkpo(6,1)=-l/2
sqkpo(6,2)=-l/2
sqkpo(7,1)=0
sqkpo(7,2)=-l/2
sqkpo(8,1)=l/2
sqkpo(8,2)=-l/2

*do,i,1,7
  centil(i,1)=(sqkpi(i,1)+sqkpi(i+1,1))/2
  centil(i,2)=(sqkpi(i,2)+sqkpi(i+1,2))/2
  centol(i,1)=(sqkpo(i,1)+sqkpo(i+1,1))/2
  centol(i,2)=(sqkpo(i,2)+sqkpo(i+1,2))/2
*enddo
  centil(8,1)=(sqkpi(8,1)+sqkpi(1,1))/2
  centil(8,2)=(sqkpi(8,2)+sqkpi(1,2))/2
  centol(8,1)=(sqkpo(8,1)+sqkpo(1,1))/2
  centol(8,2)=(sqkpo(8,2)+sqkpo(1,2))/2
cskp,11,,332,333,331
csys,11
icount=1
*do,i,1,2*depthn
  *do,j,1,2*column+1
   *do,k,1,2*rown+1
    csys,11
    clocal, 12, ,2*l*(k-1),2*l*(j-1),-2*b*(i-1)
    csys,12
    ksel,s,loc,x,0
    ksel,r,loc,y,0
    ksel,r,loc,z,0
    *get,origkp,kp,0,count
    *if,origkp,lt,1,then
    *else
     surfi(icount,1)=1
     surfi(icount,3)=kp(0,0,0)
     *do,ii,1,8
      ksel,s,loc,x,sqkpi(ii,1)
      ksel,r,loc,y,sqkpi(ii,2)
```

```
      ksel,r,loc,z,0
      *get,testkp,kp,0,count
      allsel,all
      *if,testkp,lt,1,then
       surfi(icount,3+ii)=0
       surfi(icount,3+8+ii)=0
      *else
       surfi(icount,ii+3)=kp(sqkpi(ii,1),sqkpi(ii,2),0)
       surfi(icount,ii+3+8)=kp(sqkpo(ii,1),sqkpo(ii,2),0)
      *endif
      lsel,s,loc,x,centil(ii,1)
      lsel,r,loc,y,centil(ii,2)
      lsel,r,loc,z,0
      *get,testline,line,0,count
      *get,lnumi,line,0,num,min
      lsel,s,loc,x,centol(ii,1)
      lsel,r,loc,y,centol(ii,2)
      lsel,r,loc,z,0
      *get,lnumo,line,0,num,min
      allsel,all
      *if,testline,lt,1,then
       surfi(icount,19+ii)=0
       surfi(icount,27+ii)=0
      *else
       surfi(icount,ii+19)=lnumi
       surfi(icount,ii+27)=lnumo
      *endif
     *enddo
     icount=icount+1
    *endif
   *enddo
  *enddo
*enddo
allsel,all
csys

!! for insize declined square area
sqkpi(1,1)= edget/2
sqkpi(1,2)= edget/2
sqkpi(2,1)= l-edget/2
sqkpi(2,2)= edget/2
sqkpi(3,1)= l-edget/2
sqkpi(3,2)= l-edget/2
sqkpi(4,1)= edget/2
sqkpi(4,2)= l-edget/2
sqkpo(1,1)= 0
sqkpo(1,2)= 0
sqkpo(2,1)= l
sqkpo(2,2)= 0
sqkpo(3,1)= l
sqkpo(3,2)= l
sqkpo(4,1)= 0
sqkpo(4,2)= l
```

```
*do,i,1,3
  centil(i,1)=(sqkpi(i,1)+sqkpi(i+1,1))/2
  centil(i,2)=(sqkpi(i,2)+sqkpi(i+1,2))/2
  centol(i,1)=(sqkpo(i,1)+sqkpo(i+1,1))/2
  centol(i,2)=(sqkpo(i,2)+sqkpo(i+1,2))/2
*enddo
  centil(4,1)=(sqkpi(4,1)+sqkpi(1,1))/2
  centil(4,2)=(sqkpi(4,2)+sqkpi(1,2))/2
  centol(4,1)=(sqkpo(4,1)+sqkpo(1,1))/2
  centol(4,2)=(sqkpo(4,2)+sqkpo(1,2))/2

cskp,11,,40,19,41
cskp,12,,42,43,20
cskp,13,,16,13,15
cskp,14,,10,11,9
cskp,15,,4,1,3
cskp,16,,6,7,5
cskp,17,,18,1,38
cskp,18,,44,45,17

*do,i,1,depthn
  *do,j,1,column
   *do,k,1,rown
    *do,jj,1,8
      csys,jj+10
      *get,cdsysx,cdsys,jj+10,loc,x
      *get,cdsysy,cdsys,jj+10,loc,y
      *get,cdsysz,cdsys,jj+10,loc,z
      *get,cdsysxy,cdsys,jj+10,ang,xy
      *get,cdsysyz,cdsys,jj+10,ang,yz
      *get,cdsyszx,cdsys,jj+10,ang,zx
      local, 19, ,cdsysx+4*l*(k-1),cdsysy+4*l*(j-1),cdsysz-4*b*(i-1),cdsysxy,cdsysyz,cdsyszx
      csys,19
      surfi(icount,1)=2
      surfi(icount,3)=kp(0,0,0)
      lsel,s,loc,x,centil(ii,1)
      lsel,r,loc,y,centil(ii,2)
      lsel,r,loc,z,0
      *get,lnumi,line,0,num,min
      lsel,s,loc,x,centol(ii,1)
      lsel,r,loc,y,centol(ii,2)
      lsel,r,loc,z,0
      *get,lnumo,line,0,num,min
      *do,ii,1,4
        surfi(icount,ii+3)=kp(sqkpi(ii,1),sqkpi(ii,2),0)
        surfi(icount,ii+3+8)=kp(sqkpo(ii,1),sqkpo(ii,2),0)
        surfi(icount,ii+19)=lnumi
        surfi(icount,ii+27)=lnumo
        surfi(icount,7+ii)=0
        surfi(icount,15+ii)=0
        surfi(icount,23+ii)=0
        surfi(icount,31+ii)=0
      *enddo
```

```
      icount=icount+1
    *enddo
   *enddo
  *enddo
*enddo
allsel,all

!! for hexagonal area
sqkpi(1,1)=l*sqrt(3)/2-edget/2
sqkpi(1,2)=0
sqkpi(2,1)=l*sqrt(3)/2-edget/2
sqkpi(2,2)=l/2-edget/(2*sqrt(3))
sqkpi(3,1)=0
sqkpi(3,2)=l-edget/(sqrt(3))
sqkpi(4,1)=-l*sqrt(3)/2+edget/2
sqkpi(4,2)=l/2-edget/(2*sqrt(3))
sqkpi(5,1)=-l*sqrt(3)/2+edget/2
sqkpi(5,2)=0
sqkpi(6,1)=-l*sqrt(3)/2+edget/2
sqkpi(6,2)=-l/2+edget/(2*sqrt(3))
sqkpi(7,1)=0
sqkpi(7,2)=-l+edget/(sqrt(3))
sqkpi(8,1)=l*sqrt(3)/2-edget/2
sqkpi(8,2)=-l/2+edget/(2*sqrt(3))
sqkpo(1,1)=l*sqrt(3)/2
sqkpo(1,2)=0
sqkpo(2,1)=l*sqrt(3)/2
sqkpo(2,2)=l/2
sqkpo(3,1)=0
sqkpo(3,2)=l
sqkpo(4,1)=-l*sqrt(3)/2
sqkpo(4,2)=l/2
sqkpo(5,1)=-l*sqrt(3)/2
sqkpo(5,2)=0
sqkpo(6,1)=-l*sqrt(3)/2
sqkpo(6,2)=-l/2
sqkpo(7,1)=0
sqkpo(7,2)=-l
sqkpo(8,1)=l*sqrt(3)/2
sqkpo(8,2)=-l/2
*do,i,1,7
  centil(i,1)=(sqkpi(i,1)+sqkpi(i+1,1))/2
  centil(i,2)=(sqkpi(i,2)+sqkpi(i+1,2))/2
  centol(i,1)=(sqkpo(i,1)+sqkpo(i+1,1))/2
  centol(i,2)=(sqkpo(i,2)+sqkpo(i+1,2))/2
*enddo
  centil(8,1)=(sqkpi(8,1)+sqkpi(1,1))/2
  centil(8,2)=(sqkpi(8,2)+sqkpi(1,2))/2
  centol(8,1)=(sqkpo(8,1)+sqkpo(1,1))/2
  centol(8,2)=(sqkpo(8,2)+sqkpo(1,2))/2

! hexagonal area coordinate sys and iteration table
*dim,coordtab,,6,8
```

```
cskp,19,,366,367,365
cskp,20,,286,289,285
cskp,21,,384,383,385
cskp,22,,304,303,305
cskp,23,,220,219,221
cskp,24,,380,379,381
cskp,25,,360,361,359
cskp,26,,200,203,199
cskp,27,,216,215,217
cskp,28,,94,137,135
cskp,29,,292,293,371
cskp,30,,95,134,211
cskp,31,,194,197,193
cskp,32,,268,271,349
cskp,33,,29,117,119
cskp,34,,26,116,189

*VFILL,coordtab(1,1),DATA,2   ,2   ,2   ,2   ,4   ,4
*VFILL,coordtab(1,2),DATA,19  ,21   ,23   ,25   ,27   ,31
*VFILL,coordtab(1,3),DATA,20  ,22   ,24   ,26   ,28   ,32
*VFILL,coordtab(1,4),DATA,0   ,0   ,0   ,0   ,29   ,33
*VFILL,coordtab(1,5),DATA,0   ,0   ,0   ,0   ,30   ,34
*VFILL,coordtab(1,6),DATA,rown   ,rown   ,rown+1  ,rown+1  ,rown  ,rown
*VFILL,coordtab(1,7),DATA,column+1  ,column+1  ,column ,column ,column ,column
*VFILL,coordtab(1,8),DATA,depthn  ,depthn+1 ,depthn+1 ,depthn  ,depthn+1 ,depthn
*do,kk,1,6
  *do,i,1,coordtab(kk,8)
  *do,j,1,coordtab(kk,7)
   *do,k,1,coordtab(kk,6)
    *do,jj,1,coordtab(kk,1)
     csys,coordtab(kk,1+jj)
      *get,cdsysx,cdsys,coordtab(kk,1+jj),loc,x
      *get,cdsysy,cdsys,coordtab(kk,1+jj),loc,y
      *get,cdsysz,cdsys,coordtab(kk,1+jj),loc,z
      *get,cdsysxy,cdsys,coordtab(kk,1+jj),ang,xy
      *get,cdsysyz,cdsys,coordtab(kk,1+jj),ang,yz
      *get,cdsyszx,cdsys,coordtab(kk,1+jj),ang,zx
      local, 12, ,cdsysx+4*l*(k-1),cdsysy+4*l*(j-1),cdsysz-4*b*(i-1),cdsysxy,cdsysyz,cdsyszx
      csys,12
       surfi(icount,1)=3
       surfi(icount,3)=kp(0,0,0)
       *do,ii,1,8
        ksel,s,loc,x,sqkpi(ii,1)
        ksel,r,loc,y,sqkpi(ii,2)
        ksel,r,loc,z,0
        *get,testkp,kp,0,count
        allsel,all
        *if,testkp,lt,1,then
         surfi(icount,3+ii)=0
         surfi(icount,3+8+ii)=0
        *else
         surfi(icount,ii+3)=kp(sqkpi(ii,1),sqkpi(ii,2),0)
         surfi(icount,ii+3+8)=kp(sqkpo(ii,1),sqkpo(ii,2),0)
```

```
          *endif
          lsel,s,loc,x,centil(ii,1)
          lsel,r,loc,y,centil(ii,2)
          lsel,r,loc,z,0
          *get,testline,line,0,count
          *get,lnumi,line,0,num,min
          lsel,s,loc,x,centol(ii,1)
          lsel,r,loc,y,centol(ii,2)
          lsel,r,loc,z,0
          *get,lnumo,line,0,num,min
          allsel,all
          *if,testline,lt,1,then
           surfi(icount,19+ii)=0
           surfi(icount,27+ii)=0
          *else
           surfi(icount,ii+19)=lnumi
           surfi(icount,ii+27)=lnumo
          *endif
         *enddo
         icount=icount+1
      *enddo
    *enddo
   *enddo
  *enddo
*enddo
allsel,all
csys

!!-------------------------------------------------------------!!
!!                                                             !!
!!                  Give the distortion                       !!
!!                                                             !!
!!-------------------------------------------------------------!!
/NERR, 0,
*dim,distd,,17,3
*dim,lsquare,,3,3
*dim,ilsquare,,3,3
*dim,flsquare,,3,1
*dim,rcoef,,3,1
*dim,tdefkp,,4,4
*dim,midkp,,4,5
*dim,conjkp,,8,2
*dim,testck,,9,1
eerr=0.0000001

midkp(1,1)=1
midkp(1,2)=2
midkp(1,3)=3
midkp(1,4)=7
midkp(1,5)=8
midkp(2,1)=3
midkp(2,2)=1
midkp(2,3)=2
```

```
midkp(2,4)=4
midkp(2,5)=5
midkp(3,1)=5
midkp(3,2)=3
midkp(3,3)=4
midkp(3,4)=6
midkp(3,5)=7
midkp(4,1)=7
midkp(4,2)=1
midkp(4,3)=5
midkp(4,4)=6
midkp(4,5)=8

conjkp(1,1)=5
conjkp(1,2)=0
conjkp(2,1)=8
conjkp(2,2)=4
conjkp(3,1)=7
conjkp(3,2)=0
conjkp(4,1)=2
conjkp(4,2)=6
conjkp(5,1)=1
conjkp(5,2)=0
conjkp(6,1)=4
conjkp(6,2)=8
conjkp(7,1)=3
conjkp(7,2)=0
conjkp(8,1)=2
conjkp(8,2)=6

!--- find center of array model ---!
xwidth=rown*4*l
ywidth=column*4*l
zwidth=depthn*4*b
centerx=0
centery=0
centerz=-((depthn-1)/2)*4*b

!--- search the the domain radius which to calculate the edge and face thickness ---!
*dim,radkp,,depthn-1
radkp(1)=kp(l/2,3*l/2,centerz)
*do,i,1,depthn-2
  *if,mod(i,2),eq,0,then
  j=1
  *else
     j=0
  *endif
  radkp(i+1)=kp(3*l/2*(1-j),0,centerz-2*b*(i+1))
*enddo

!-----------------------------------------!
!              edge distortion            !
!-----------------------------------------!
```

```
asel,s,area,,all,,,1
lsel,inve
*get,lnum,line,,count
*dim,distl,,lnum,3
allsel,all
asel,s,area,,all,,,1
ksel,inve
*get,knum,kp,,count
*get,minkp,kp,,num,min
ii=1
*do,i,1,knum
  xpo=kx(minkp)
  ypo=ky(minkp)
  zpo=kz(minkp)
  delx=xpo-centerx
  dely=ypo-centery
  delz=zpo-centerz
  sradi=sqrt(delx*delx+dely*dely+delz*delz)
  *if,sradi,lt,lradi,then
   primr=kpstrain*cos(wn*pi*sradi/(2*lradi))
    pdelx=primr*delx/sradi
    pdely=primr*dely/sradi
    pdelz=primr*delz/sradi
    allsel,all
    testx=kx(minkp)
    testy=ky(minkp)
    *if,testx,eq,0,or,testy,eq,0,then
     asel,s,area,,all,,,1
    lsel,inve
    *get,minl,line,,num,min
     *do,j,1,lnum
      allsel,all
     *get,flinen,line,minl,kp,1
     *get,slinen,line,minl,kp,2
     *if,flinen,eq,minkp,or,slinen,eq,minkp,then
      distl(ii,1)=minl
      distl(ii,2)=minkp
      *if,flinen,eq,minkp,then
       distl(ii,3)=slinen
      *else
       distl(ii,3)=flinen
      *endif
      ii=ii+1
     *endif
     asel,s,area,,all,,,1
     lsel,inve
     *get,minl,line,minl,NXTH
   *enddo
  *endif
  allsel,all
   kmodif,minkp,xpo+pdelx,ypo+pdely,zpo+pdelz
 *ENDIF
 asel,s,area,,all,,,1
```

```
  ksel,inve
  minkp=KPNEXT(minkp)
*enddo
allsel,all
*do,i,1,ii-1
  *if,kx(distl(i,2)),eq,0,then
  imagkx=-1*kx(distl(i,3))
  imagky=ky(distl(i,3))
  imagkz=kz(distl(i,3))
  *else
  imagkx=kx(distl(i,3))
  imagky=-1*ky(distl(i,3))
  imagkz=kz(distl(i,3))
  *endif
  kmodif,distl(i,2),(imagkx+kx(distl(i,3)))/2,(imagky+ky(distl(i,3)))/2,(imagkz+kz(distl(i,3)))/2
*enddo
allsel,all

adele,all
!-----------------------------------------!
!                face distortion          !
!-----------------------------------------!
*do,i,1,icount-1
!i=15
  kpcount=0
  checkd=0
  *do,j,1,8
   *if,surfi(i,j+3),ne,0,then
    kpcount=kpcount+1
    xpo=kx(surfi(i,j+3))
    ypo=ky(surfi(i,j+3))
    zpo=kz(surfi(i,j+3))
    delx=xpo-centerx
    dely=ypo-centery
    delz=zpo-centerz
    sradi=sqrt(delx*delx+dely*dely+delz*delz)
    *if,sradi,lt,lradi,then
     checkd=checkd+1
    *ENDIF
   *endif
  *enddo
  *if,checkd,gt,0,then
   *if,kpcount,eq,4,then
    rpnum=4      ! inclined square face
    *do,j,1,4
     distd(j,1)=kx(surfi(i,j+3))
     distd(j,2)=ky(surfi(i,j+3))
     distd(j,3)=kz(surfi(i,j+3))-centerz
     distd(j+4,1)=kx(surfi(i,j+11))
     distd(j+4,2)=ky(surfi(i,j+11))
     distd(j+4,3)=kz(surfi(i,j+11))-centerz
    *enddo
   *else
```

```
rpnum=9      ! other all square face
*if,kpcount,eq,3,then
 distd(1,1)=kx(surfi(i,3))
 distd(1,2)=ky(surfi(i,3))
 distd(1,3)=kz(surfi(i,3))-centerz
 *do,j,1,3
  distd(j+1,1)=kx(surfi(i,j+3))
  distd(j+1,2)=ky(surfi(i,j+3))
  distd(j+1,3)=kz(surfi(i,j+3))-centerz
  distd(j+9,1)=kx(surfi(i,j+11))
  distd(j+9,2)=ky(surfi(i,j+11))
  distd(j+9,3)=kz(surfi(i,j+11))-centerz
 *enddo
 *do,j,1,2
  distd(5+8*(j-1),1)=-1*kx(surfi(i,5+8*(j-1)))
  distd(5+8*(j-1),2)=ky(surfi(i,5+8*(j-1)))
  distd(5+8*(j-1),3)=kz(surfi(i,5+8*(j-1)))-centerz
  distd(6+8*(j-1),1)=-1*kx(surfi(i,4+8*(j-1)))
  distd(6+8*(j-1),2)=ky(surfi(i,4+8*(j-1)))
  distd(6+8*(j-1),3)=kz(surfi(i,4+8*(j-1)))-centerz
  distd(7+8*(j-1),1)=-1*kx(surfi(i,5+8*(j-1)))
  distd(7+8*(j-1),2)=-1*ky(surfi(i,5+8*(j-1)))
  distd(7+8*(j-1),3)=kz(surfi(i,5+8*(j-1)))-centerz
  distd(8+8*(j-1),1)=kx(surfi(i,6+8*(j-1)))
  distd(8+8*(j-1),2)=-1*ky(surfi(i,6+8*(j-1)))
  distd(8+8*(j-1),3)=kz(surfi(i,6+8*(j-1)))-centerz
  distd(9+8*(j-1),1)=kx(surfi(i,5+8*(j-1)))
  distd(9+8*(j-1),2)=-1*ky(surfi(i,5+8*(j-1)))
  distd(9+8*(j-1),3)=kz(surfi(i,5+8*(j-1)))-centerz
 *enddo
*elseif,kpcount,eq,8,then
 distd(1,1)=kx(surfi(i,3))
 distd(1,2)=ky(surfi(i,3))
 distd(1,3)=kz(surfi(i,3))-centerz
 *do,j,1,8
  distd(j+1,1)=kx(surfi(i,j+3))
  distd(j+1,2)=ky(surfi(i,j+3))
  distd(j+1,3)=kz(surfi(i,j+3))-centerz
  distd(j+9,1)=kx(surfi(i,j+11))
  distd(j+9,2)=ky(surfi(i,j+11))
  distd(j+9,3)=kz(surfi(i,j+11))-centerz
 *enddo
*else
 distd(1,1)=kx(surfi(i,3))
 distd(1,2)=ky(surfi(i,3))
 distd(1,3)=kz(surfi(i,3))-centerz
 *do,j,1,8
  *if,surfi(i,j+3),ne,0,then
   distd(j+1,1)=kx(surfi(i,j+3))
   distd(j+1,2)=ky(surfi(i,j+3))
   distd(j+1,3)=kz(surfi(i,j+3))-centerz
   distd(j+9,1)=kx(surfi(i,j+11))
   distd(j+9,2)=ky(surfi(i,j+11))
```

```
      distd(j+9,3)=kz(surfi(i,j+11))-centerz
      !testck(j,1)=surfi(i,j+2)
     *else
      *if,surfi(i,conjkp(j,1)+3),ne,0,then
       tfs=1
      *else
       tfs=2
      *endif
      *if,kx(surfi(i,3)),eq,0,then
       distd(j+1,1)=-1*kx(surfi(i,conjkp(j,tfs)+3))
         distd(j+1,2)=ky(surfi(i,conjkp(j,tfs)+3))
           distd(j+1,3)=kz(surfi(i,conjkp(j,tfs)+3))-centerz
           distd(j+9,1)=-1*kx(surfi(i,conjkp(j,tfs)+11))
         distd(j+9,2)=ky(surfi(i,conjkp(j,tfs)+11))
           distd(j+9,3)=kz(surfi(i,conjkp(j,tfs)+11))-centerz
           !testck(j,1)=surfi(i,conjkp(j,tfs)+3)
         *else
           distd(j+1,1)=kx(surfi(i,conjkp(j,tfs)+3))
         distd(j+1,2)=-1*ky(surfi(i,conjkp(j,tfs)+3))
           distd(j+1,3)=kz(surfi(i,conjkp(j,tfs)+3))-centerz
           distd(j+9,1)=kx(surfi(i,conjkp(j,tfs)+11))
         distd(j+9,2)=-1*ky(surfi(i,conjkp(j,tfs)+11))
           distd(j+9,3)=kz(surfi(i,conjkp(j,tfs)+11))-centerz
           !testck(j,1)=surfi(i,conjkp(j,tfs)+3)
         *endif
     *endif
    *enddo
   *endif
  *endif

! k=1
  *do,j,1,rpnum
   xpo=distd(j,1)
   ypo=distd(j,2)
   zpo=distd(j,3)
   delx=xpo-centerx
   dely=ypo-centery
   delz=zpo
   sradi=sqrt(delx*delx+dely*dely+delz*delz)
   *if,sradi,lt,lradi,then
    primr=kpstrain*cos(wn*pi*sradi/(2*lradi))
    pdelx=primr*delx/sradi
    pdely=primr*dely/sradi
    pdelz=primr*delz/sradi
    distd(j,1)=xpo+pdelx
    distd(j,2)=ypo+pdely
    distd(j,3)=zpo+pdelz
    checkd=checkd+1
   *ENDIF
  *enddo
  *do,k,1,3
   flsquare(k,1)=0
   *do,ii,1,3
```

```
  lsquare(k,ii)=0
 *enddo
*enddo
*if,kpcount,eq,4,then
 rpnum=4      ! inclined square face
 gapp=4
*else
 rpnum=8      ! other all square face
 gapp=9
*endif
*do,k,1,rpnum
 lsquare(1,1)=lsquare(1,1)+distd(k+gapp,1)*distd(k+gapp,1)
 lsquare(1,2)=lsquare(1,2)+distd(k+gapp,1)*distd(k+gapp,2)
 lsquare(1,3)=lsquare(1,3)+distd(k+gapp,1)*distd(k+gapp,3)
 lsquare(2,2)=lsquare(2,2)+distd(k+gapp,2)*distd(k+gapp,2)
 lsquare(2,3)=lsquare(2,3)+distd(k+gapp,3)*distd(k+gapp,2)
 lsquare(3,3)=lsquare(3,3)+distd(k+gapp,3)*distd(k+gapp,3)
 flsquare(1,1)=flsquare(1,1)+distd(k+gapp,1)
 flsquare(2,1)=flsquare(2,1)+distd(k+gapp,2)
 flsquare(3,1)=flsquare(3,1)+distd(k+gapp,3)
*enddo
lsquare(2,1)=lsquare(1,2)
lsquare(3,1)=lsquare(1,3)
lsquare(3,2)=lsquare(2,3)
d1=lsquare(1,1)*(lsquare(2,2)*lsquare(3,3)-lsquare(3,2)*lsquare(2,3))
d2=lsquare(1,2)*(lsquare(2,3)*lsquare(3,1)-lsquare(3,3)*lsquare(2,1))
d3=lsquare(1,3)*(lsquare(2,1)*lsquare(3,2)-lsquare(3,1)*lsquare(2,2))
detam=d1+d2+d3
*if,rpnum,eq,4,then
 tkp=3
*else
 tkp=2
*endif
*if,kpcount,eq,4,then
 rpnum=4      ! inclined square face
*else
 rpnum=9      ! other all square face
*endif
*if,detam,ne,0,then
 *moper,ilsquare(1,1),lsquare(1,1),invert
 *moper,rcoef(1),ilsquare(1,1),mult,flsquare(1,1)
 aa=rcoef(1,1)
 bb=rcoef(2,1)
 cc=rcoef(3,1)
 *do,ii,1,rpnum
  !*if,surfi(i,ii+tkp),ne,0,then
   h=abs(aa*distd(ii,1)+bb*distd(ii,2)+cc*distd(ii,3)-1)/sqrt(aa*aa+bb*bb+cc*cc)
   normal=sqrt(aa*aa+bb*bb+cc*cc)
   tx=distd(ii,1)-h*aa/normal
   ty=distd(ii,2)-h*bb/normal
   tz=distd(ii,3)-h*cc/normal
   tonp=abs(aa*tx+bb*ty+cc*tz-1)
   *if,tonp,lt,eerr,then
```

```
     fpm=-1
    *else
     fpm=1
    *endif
    distd(ii,1)=distd(ii,1)+fpm*h*aa/normal
    distd(ii,2)=distd(ii,2)+fpm*h*bb/normal
    distd(ii,3)=distd(ii,3)+fpm*h*cc/normal+centerz
   !*endif
  *enddo
*else
  *do,ii,1,rpnum
   distd(ii,3)=distd(ii,3)+centerz
  *enddo
*endif


! ------- give distortion and mid point control -------- !
*do,ii,1,rpnum
  *if,rpnum,eq,4,then
   kmodif,surfi(i,ii+tkp),distd(ii,1),distd(ii,2),distd(ii,3)
  *elseif,surfi(i,1),eq,3,then
   *if,ii,eq,2,or,ii,eq,6,then
    *if,ii,eq,2,then
     prepx=distd(3,1)
     propx=distd(9,1)
     prepy=distd(3,2)
     propy=distd(9,2)
     prepz=distd(3,3)
     propz=distd(9,3)
    *else
     prepx=distd(ii-1,1)
     propx=distd(ii+1,1)
     prepy=distd(ii-1,2)
     propy=distd(ii+1,2)
     prepz=distd(ii-1,3)
     propz=distd(ii+1,3)
    *endif
    distd(ii,1)=(prepx+propx)/2
    distd(ii,2)=(prepy+propy)/2
    distd(ii,3)=(prepz+propz)/2
    *if,surfi(i,ii+tkp),ne,0,then
     kmodif,surfi(i,ii+tkp),(prepx+propx)/2,(prepy+propy)/2,(prepz+propz)/2
    *endif
   *else
    *if,surfi(i,ii+tkp),ne,0,then
     kmodif,surfi(i,ii+tkp),distd(ii,1),distd(ii,2),distd(ii,3)
    *endif
   *endif
  *elseif,surfi(i,1),eq,1,then
   *if,mod(ii,2),eq,0,then
    *if,ii,eq,2,then
     prepx=distd(3,1)
     propx=distd(9,1)
```

```
        prepy=distd(3,2)
        propy=distd(9,2)
        prepz=distd(3,3)
        propz=distd(9,3)
       *else
        prepx=distd(ii-1,1)
        propx=distd(ii+1,1)
        prepy=distd(ii-1,2)
        propy=distd(ii+1,2)
        prepz=distd(ii-1,3)
        propz=distd(ii+1,3)
       *endif
       distd(ii,1)=(prepx+propx)/2
       distd(ii,2)=(prepy+propy)/2
       distd(ii,3)=(prepz+propz)/2
       *if,surfi(i,ii+tkp),ne,0,then
        kmodif,surfi(i,ii+tkp),(prepx+propx)/2,(prepy+propy)/2,(prepz+propz)/2
       *endif
      *else
       *if,surfi(i,ii+tkp),ne,0,then
        kmodif,surfi(i,ii+tkp),distd(ii,1),distd(ii,2),distd(ii,3)
       *endif
      *endif
     *endif
    *enddo
    ! ---- center point contral ---- !
    *if,surfi(i,1),eq,3,or,surfi(i,1),eq,1,then
     prepx=distd(4,1)
       propx=distd(8,1)
       prepy=distd(4,2)
       propy=distd(8,2)
       prepz=distd(4,3)
       propz=distd(8,3)
       kmodif,surfi(i,3),(prepx+propx)/2,(prepy+propy)/2,(prepz+propz)/2
    *endif
    *endif
  *enddo

!!!------------ make areas again ---------------!!!

  *do,i,1,icount-1
    *if,surfi(i,1),eq,2,then
    a,surfi(i,4),surfi(i,5),surfi(i,6),surfi(i,7),surfi(i,4)
    *else
    *do,j,1,3
     checkz=0
     *do,k,1,3
      *if,surfi(i,2*j+1+k),eq,0,then
       checkz=1
      *endif
     *enddo
     *if,checkz,eq,0,then
      a,surfi(i,2*j+2),surfi(i,2*j+3),surfi(i,2*j+4),surfi(i,3),surfi(i,2*j+2)
```

```
    *endif
   *enddo
   checkz=0
   *if,surfi(i,10),eq,0,or,surfi(i,11),eq,0,then
    checkz=1
   *else
    *if,surfi(i,4),eq,0,then
     checkz=1
    *endif
   *endif
   *if,checkz,eq,0,then
    a,surfi(i,10),surfi(i,11),surfi(i,4),surfi(i,3),surfi(i,10)
   *endif
  *endif
*enddo


!!----------------------!!
!!      Meshing    !!
!!----------------------!!

ET,1,shell63
!KEYOPT,1,1,1

ET,2,BEAM188

ET,3,mass21
ET,4,mpc184

*do,i,1,depthn
  MP,EX,i,1.6E9,
  MP,nuXY,i,0.3,
*enddo

!!-------------------------------------------------!!
!!                          find vertice                    !!
!!-------------------------------------------------!!

allsel,all
asel,s,area,,all,,,1
lsel,inve
*get,lnum,line,,count
*dim,edgel,,lnum+1
*get,minl,line,,num,min
edgel(1)=lnum
*do,i,1,lnum
  edgel(i+1)=minl
  asel,s,area,,all,,,1
  lsel,inve
  *get,minl,line,minl,NXTH
*enddo

allsel,all
```

```
asel,s,area,,all,,,1
ksel,inve
*get,knum,kp,,count
*dim,vcount,,knum+1
ii=1
*get,mink,kp,,num,min
*do,i,1,knum
  *if,kx(mink),eq,0,or,ky(mink),eq,0,then
  *else
   checkc=0
   *do,j,1,edgel(1)
    *get,flinen,line,edgel(j+1),kp,1
    *get,slinen,line,edgel(j+1),kp,2
    *if,flinen,eq,mink,or,slinen,eq,mink,then
     checkc=checkc+1
    *endif
   *enddo
   *if,checkc,eq,4,then
    vcount(ii+1)=mink
    ii=ii+1
   *endif
  *endif
  asel,s,area,,all,,,1
  ksel,inve
  *get,mink,kp,mink,NXTH
*enddo
vcount(1)=ii-1

!!-------------------------------------------------------------!!
!   Calculate edge thickness and face thickness   !!
!!-------------------------------------------------------------!!
allsel,all
*get,anum,area,,count
*dim,sarea,,depthn,anum
*dim,sline,,depthn,lnum
*dim,vertn,,depthn
*dim,thickn,,depthn,2
! thickn(i,1) => face thickness
! thickn(i,2) => edge thickness

allsel,all
*do,j,1,depthn
  farea=0
  elength=0
  *if,j,eq,1,then
   iradd=0
   xpo=kX(radkp(1))
   ypo=ky(radkp(1))
   zpo=kz(radkp(1))
   delx=xpo-centerx
   dely=ypo-centery
   delz=zpo-centerz
   oradd=sqrt(delx*delx+dely*dely+delz*delz)
```

```
tvolum=pi*(oradd**3)/3
*elseif,j,eq,2,then
iradd=ky(radkp(1))
oradd=abs(kz(radkp(2))-centerz)
tvolum=pi*(oradd**3-iradd**3)/3
*elseif,j,eq,depthn,then
iradd=abs(kz(radkp(j-1))-centerz)
oradd=100
tvolum=(xwidth*ywidth*zwidth-(pi*iradd**3)/3)
*else
iradd=abs(kz(radkp(j-1))-centerz)
oradd=abs(kz(radkp(j))-centerz)
tvolum=pi*(oradd**3-iradd**3)/3
*endif

! to count face area number within given region
k=1
asel,s,area,,all
*get,mina,area,,num,min
*do,i,1,anum
!i=1
asel,s,area,,mina
asum
*GET, xpo, AREA, , CENT, X,
*GET, ypo, AREA, , CENT, y,
*GET, zpo, AREA, , CENT, z,
delx=xpo-centerx
dely=ypo-centery
delz=zpo-centerz
sradi=sqrt(delx*delx+dely*dely+delz*delz)
*if,sradi,le,oradd,and,sradi,gt,iradd,then
 sarea(j,k+1)=mina
 k=k+1
 *get,tempa,area,mina,area
 farea=farea+tempa
*ENDIF
asel,s,area,,all
*get,mina,area,mina,NXTH
*enddo
sarea(j,1)=k-1

! to count edge line number within given region
k=1
asel,s,area,,all,,,1
lsel,inve
*get,minl,line,,num,min
*do,i,1,lnum
!i=1
lsel,s,line,,minl
lsum
*GET, xpo, line, , CENT, X,
*GET, ypo, line, , CENT, y,
*GET, zpo, line, , CENT, z,
```

```
delx=xpo-centerx
dely=ypo-centery
delz=zpo-centerz
sradi=sqrt(delx*delx+dely*dely+delz*delz)
*if,sradi,le,oradd,and,sradi,gt,iradd,then
 sline(j,k+1)=minl
 k=k+1
 *get,templ,line,minl,leng
 elength=elength+templ
*ENDIF
asel,s,area,,all,,,1
lsel,inve
*get,minl,line,minl,NXTH
*enddo
sline(j,1)=k-1

! to count vertice number within given region
k=1
*do,i,1,vcount(1)
xpo=kX(vcount(i+1))
ypo=ky(vcount(i+1))
zpo=kz(vcount(i+1))
delx=xpo-centerx
dely=ypo-centery
delz=zpo-centerz
sradi=sqrt(delx*delx+dely*dely+delz*delz)
*if,sradi,le,oradd,and,sradi,gt,iradd,then
 k=k+1
*ENDIF
*enddo
vertn(j)=k-1
thickn(j,1)=(1-efrac)*tvolum*rdens/farea
alpha=efrac*farea*thickn(j,1)/(1-efrac)
thickn(j,2)=sqrt(alpha/(elength*pi/4-vertn(j)*ecorf*pi*thickn(j,1)/8))

R,j,thickn(j,1),thickn(j,1),thickn(j,1),thickn(j,1), ,
sectype,9+j,beam,csolid
!R = Radius
!N = Number of divisions around the circumference.
!T = Number of divisions through the radius
secdata,thickn(j,2)/2,4,2

!! area meshing !!
asel,s,area,,sarea(j,2)
*do,i,1,sarea(j,1)
asel,a,area,,sarea(j,i+1)
*enddo
type,1
real,j
mat,j
amesh,all
allsel,all
```

```
  !! edge meshing !!
  lsel,s,line,,sline(j,2)
  *do,i,2,sline(j,1)
  lsel,a,line,,sline(j,i+1)
  *enddo
  Type,2
  mat,j
  secnum,9+j
  lmesh,all
  allse,all
*enddo

allsel,all
r,2*depthn+1,1,1,1,1,1,1

!!* dummy node mesh
*get,maxkp,kp,0,num,maxd
k,maxkp+1,(rown+1)*4*l,(column+1)*4*l,(depthn+2)*4*b
type,3
mat,1
real,2*depthn+1
kmesh,maxkp+1
dummyn=node(kx(maxkp+1),ky(maxkp+1),kz(maxkp+1))

!!!-----------------------------------------------------!!
!!!       Periodic boundary condition       !!
!!!-----------------------------------------------------!!
!symetry condition
nsel,s,loc,x,0
d,all,ux,0
d,all,rotz,0
d,all,roty,0
nsel,s,loc,y,0
d,all,uy,0
d,all,rotz,0
d,all,rotx,0
allsel,all

!* bottom to top constraint
*dim,kotv,,20
*dim,notv,,12*depthn*rown
kotv(1)=253,255,287,289,303,311,333,335,367,369,383,391
count1=1
*do,i,1,depthn
  *do,j,1,rown
  *do,k,1,12
   notv(count1)=node(kx(kotv(k))+4*l*(j-1),4*l*column,kz(kotv(k))-4*b*(i-1))
   count1=count1+1
  *enddo
  *enddo
*enddo

nsel,s,loc,y,4*l*column
```

```
*get,ncount,node,,count
*get,smaln,node,,num,min
*do,i,1,ncount
 leftn=smaln
 checkid=0
 *do,j,1,12*depthn*rown
  *if,notv(j),eq,leftn,then
   checkid=1
  *endif
 *enddo
*if,checkid,eq,1,then
*else
  !ce,i,0,leftn,ux,1,dummyn,rotx,-4*l*column
  ce,i+ncount,0,leftn,uy,1,dummyn,uy,-4*l*column
  !ce,i+2*ncount,0,leftn,uz,1,dummyn,rotz,-4*l*column
 *endif
 *get,nsmaln,node,leftn,nxth
 smaln=nsmaln
*enddo
allsel,all


!* left to right constraint
*dim,nolv,,12*depthn*column
kotv(1)=171,219,201,379,361,331,203,227,185,345,363,387
count1=1
*do,i,1,depthn
  *do,j,1,column
   *do,k,1,12
    nolv(count1)=node(4*l*rown,ky(kotv(k))+4*l*(j-1),kz(kotv(k))-4*b*(i-1))
    count1=count1+1
   *enddo
  *enddo
*enddo
nsel,s,loc,x,4*l*rown
*get,ncount1,node,,count
*get,smaln,node,,num,min
*do,i,1,ncount1
 leftn=smaln
 checkid=0
 *do,j,1,12*depthn*column
  *if,nolv(j),eq,leftn,then
   checkid=1
  *endif
 *enddo
*if,checkid,eq,1,then
*else
  ce,i+3*ncount,0,leftn,ux,1,dummyn,ux,-4*l*rown
  !ce,i+3*ncount+ncount1,0,leftn,uy,1,dummyn,rotx,-4*l*rown
  !ce,i+3*ncount+2*ncount1,0,leftn,uz,1,dummyn,roty,-4*l*rown
 *endif
 *get,nsmaln,node,leftn,nxth
 smaln=nsmaln
```

```
*enddo
!d,dummyn,ux,0
!d,dummyn,rotz,0
allsel,all


!* back to front constraint
*dim,nofv,,20*rown*column

kotv(1)=104,141,138,132,135,225,165,211,217,221,245,297,291,301,305,377,381,385
kotv(19)=325
kotv(20)=371

count1=1
*do,i,1,column
  *do,j,1,rown
  *do,k,1,20
   nofv(count1)=node(kx(kotv(k))+4*l*(j-1),ky(kotv(k))+4*l*(i-1),3*b-4*b*depthn)
   count1=count1+1
  *enddo
  *enddo
*enddo

nsel,s,node,,nofv(1)
*do,i,1,count1-2
nsel,a,node,,nofv(i)
*enddo

nsel,s,loc,z,3*b-4*b*depthn
*get,ncount2,node,,count
*get,smaln,node,,num,min
*do,i,1,ncount2
 leftn=smaln
 *get,xlocn,node,smaln,loc,x
 *get,ylocn,node,smaln,loc,y
 allsel,all
 checkid=0
 *do,j,1,20*rown*column
  *if,nofv(j),eq,leftn,then
  checkid=1
  *endif
 *enddo
rightn=node(xlocn,ylocn,3*b)
 *if,checkid,eq,1,then
*elseif,ny(leftn),eq,4*l*column
  ce,i+3*ncount1+3*ncount,0,rightn,ux,1,leftn,ux,-1,dummyn,roty,-4*b*depthn
  ce,i+3*ncount1+3*ncount+2*ncount2,0,rightn,uz,1,leftn,uz,-1,dummyn,uz,-4*b*depthn
 *elseif,nx(leftn),eq,4*l*rown
  ce,i+3*ncount1+3*ncount+ncount2,0,rightn,uy,1,leftn,uy,-1,dummyn,rotz,-4*b*depthn
  ce,i+3*ncount1+3*ncount+2*ncount2,0,rightn,uz,1,leftn,uz,-1,dummyn,uz,-4*b*depthn
 *else
  ce,i+3*ncount1+3*ncount,0,rightn,ux,1,leftn,ux,-1,dummyn,roty,-4*b*depthn
  ce,i+3*ncount1+3*ncount+ncount2,0,rightn,uy,1,leftn,uy,-1,dummyn,rotz,-4*b*depthn
```

```
  ce,i+3*ncount1+3*ncount+2*ncount2,0,rightn,uz,1,leftn,uz,-1,dummyn,uz,-4*b*depthn
 *endif
 nsel,s,loc,z,3*b-4*b*depthn
 *get,nsmaln,node,leftn,nxth
 smaln=nsmaln
*enddo
allsel,all

!!-----------------------------------------------------!!
!!   APPLY rigid link by element mpc184    !!
!!-----------------------------------------------------!!
*do,i,1,icount-1
  *if,surfi(i,1),eq,2,then
  *do,j,1,3
   *do,k,1,lsize*2
    ikx=kx(surfi(i,3+j))+kx(surfi(i,4+j))*(k-1)/(lsize*2)-kx(surfi(i,3+j))*(k-1)/(lsize*2)
    iky=ky(surfi(i,3+j))+ky(surfi(i,4+j))*(k-1)/(lsize*2)-ky(surfi(i,3+j))*(k-1)/(lsize*2)
    ikz=kz(surfi(i,3+j))+kz(surfi(i,4+j))*(k-1)/(lsize*2)-kz(surfi(i,3+j))*(k-1)/(lsize*2)
    okx=kx(surfi(i,11+j))+kx(surfi(i,12+j))*(k-1)/(lsize*2)-kx(surfi(i,11+j))*(k-1)/(lsize*2)
    oky=ky(surfi(i,11+j))+ky(surfi(i,12+j))*(k-1)/(lsize*2)-ky(surfi(i,11+j))*(k-1)/(lsize*2)
    okz=kz(surfi(i,11+j))+kz(surfi(i,12+j))*(k-1)/(lsize*2)-kz(surfi(i,11+j))*(k-1)/(lsize*2)
    snode1=node(ikx,iky,ikz)
    mnode1=node(okx,oky,okz)
    type,4
    !e,mnode1,snode1
    cerig,mnode1,snode1,all
    !cerig,snode1,mnode1,all
   *enddo
  *enddo
  !segli=DISTKP(surfi(i,7),surfi(i,4))
  !seglo=DISTKP(surfi(i,15),surfi(i,12))
  *do,k,1,lsize*2
   ikx=kx(surfi(i,7))+ kx(surfi(i,4))*(k-1)/(lsize*2)- kx(surfi(i,7))*(k-1)/(lsize*2)
   iky=ky(surfi(i,7))+ ky(surfi(i,4))*(k-1)/(lsize*2)- ky(surfi(i,7))*(k-1)/(lsize*2)
   ikz=kz(surfi(i,7))+ kz(surfi(i,4))*(k-1)/(lsize*2)- kz(surfi(i,7))*(k-1)/(lsize*2)
   okx=kx(surfi(i,15))+kx(surfi(i,12))*(k-1)/(lsize*2)-kx(surfi(i,15))*(k-1)/(lsize*2)
   oky=ky(surfi(i,15))+ky(surfi(i,12))*(k-1)/(lsize*2)-ky(surfi(i,15))*(k-1)/(lsize*2)
   okz=kz(surfi(i,15))+kz(surfi(i,12))*(k-1)/(lsize*2)-kz(surfi(i,15))*(k-1)/(lsize*2)
   snode1=node(ikx,iky,ikz)
   mnode1=node(okx,oky,okz)
   type,4
   !e,mnode1,snode1
   cerig,mnode1,snode1,all
   !cerig,snode1,mnode1,all
  *enddo
  *else
  checkc=0
  comparl=0
  *do,j,1,8
   *if,surfi(i,19+j),ne,0,then
   checkc=checkc+1
   *endif
  *enddo
```

```
*do,j,1,8
 *if,surfi(i,19+j),ne,0,then
  comparl=comparl+1
  *if,comparl,eq,checkc,then
   lastl=j
  *endif
 *endif
*enddo
*do,j,1,8
 *if,surfi(i,19+j),eq,0,then
 *else
  *if,surfi(i,1),eq,1,then
     linen2=lsize
    *if,j,eq,lastl,and,checkc,ne,8,then
     linen1=lsize+1
     *if,checkc,eq,4,and,surfi(i,22),eq,0,then
      *if,surfi(i,25),eq,0,and,j,eq,8,then
        linen1=lsize
      *endif
     *endif
    *else
     linen1=lsize
     *if,checkc,eq,4,and,surfi(i,22),eq,0,then
      *if,surfi(i,25),eq,0,and,j,eq,2,then
        linen1=lsize+1
      *endif
     *endif
    *endif
   *else
   doublet=0
   *if,j,eq,1,or,j,eq,4,then
    doublet=1
   *elseif,j,eq,5,or,j,eq,8,then
      doublet=1
   *endif
   *if,doublet,eq,1,then
    linen2=lsize
    *if,j,eq,lastl,and,checkc,ne,8,then
     linen1=lsize+1
     *if,checkc,eq,4,and,surfi(i,22),eq,0,then
     *if,surfi(i,25),eq,0,and,j,eq,8,then
       linen1=lsize
     *endif
    *endif
    *else
     linen1=lsize
     *if,checkc,eq,4,and,surfi(i,22),eq,0,then
      *if,surfi(i,25),eq,0,and,j,eq,2,then
        linen1=lsize+1
      *endif
     *endif
    *endif
   *else
```

```
          linen2=lsize*2
          *if,j,eq,lastl,and,checkc,ne,8,then
           linen1=2*lsize+1
           *if,checkc,eq,4,and,surfi(i,22),eq,0,then
           *if,surfi(i,25),eq,0,and,j,eq,8,then
             linen1=2*lsize
           *endif
          *endif
          *else
           linen1=2*lsize
           *if,checkc,eq,4,and,surfi(i,22),eq,0,then
            *if,surfi(i,25),eq,0,and,j,eq,2,then
              linen1=2*lsize+1
            *endif
           *endif
          *endif
         *endif
         *endif
        *if,j,eq,8,then
         *do,k,1,linen1
          ikx=kx(surfi(i,11))+ kx(surfi(i,4))*(k-1)/linen2- kx(surfi(i,11))*(k-1)/linen2
          iky=ky(surfi(i,11))+ ky(surfi(i,4))*(k-1)/linen2- ky(surfi(i,11))*(k-1)/linen2
          ikz=kz(surfi(i,11))+ kz(surfi(i,4))*(k-1)/linen2- kz(surfi(i,11))*(k-1)/linen2
          okx=kx(surfi(i,19))+kx(surfi(i,12))*(k-1)/linen2-kx(surfi(i,19))*(k-1)/linen2
          oky=ky(surfi(i,19))+ky(surfi(i,12))*(k-1)/linen2-ky(surfi(i,19))*(k-1)/linen2
          okz=kz(surfi(i,19))+kz(surfi(i,12))*(k-1)/linen2-kz(surfi(i,19))*(k-1)/linen2
          snode1=node(ikx,iky,ikz)
          mnode1=node(okx,oky,okz)
          type,4
          !e,mnode1,snode1
          cerig,mnode1,snode1,all
          !cerig,snode1,mnode1,all
         *enddo
        *else
         *do,k,1,linen1
          ikx=kx(surfi(i,3+j))+kx(surfi(i,4+j))*(k-1)/linen2-kx(surfi(i,3+j))*(k-1)/linen2
          iky=ky(surfi(i,3+j))+ky(surfi(i,4+j))*(k-1)/linen2-ky(surfi(i,3+j))*(k-1)/linen2
          ikz=kz(surfi(i,3+j))+kz(surfi(i,4+j))*(k-1)/linen2-kz(surfi(i,3+j))*(k-1)/linen2
          okx=kx(surfi(i,11+j))+kx(surfi(i,12+j))*(k-1)/linen2-kx(surfi(i,11+j))*(k-1)/linen2
          oky=ky(surfi(i,11+j))+ky(surfi(i,12+j))*(k-1)/linen2-ky(surfi(i,11+j))*(k-1)/linen2
          okz=kz(surfi(i,11+j))+kz(surfi(i,12+j))*(k-1)/linen2-kz(surfi(i,11+j))*(k-1)/linen2
          snode1=node(ikx,iky,ikz)
          mnode1=node(okx,oky,okz)
          type,4
          !e,mnode1,snode1
          cerig,mnode1,snode1,all
          !cerig,snode1,mnode1,all
         *enddo
        *endif
       *endif
      *enddo
     *endif
    *endif
*enddo
```

```
allsel,all
csys

/solu
ANTYPE,STATIC          ! STATIC ANALYSIS
PSTRES,off

allsel,all
f,dummyn,fy,-1e-3
allsel,all
SOLVE
FINISH

esel,u,type,,3
```

VITA

JI WOONG SUE received his Bachelor of E ngineering degree in mechanical engineering from Hanyoung University in Korea in 1996. He received a Master's degree in mechanical design from Hanyang University in Korea in 1 998. After g raduation, he worked as a researcher for the BK 21 project at Hanyang University in Korea. A year later, in 1999, he moved to Texas to attend Texas A&M University working toward Ph.D. in mechanical engineering. After three years, he changed to the material science and engineering department receiving his Ph.D. in December 2006. After completion of his Ph.D., the author plans to work for Samsung Semi Conductor, Inc. in Korea.

To contact the author, Please send email to: jiwoong@hotmail.com or write

Address: Dr. John D. Whitcomb.

Texas A&M University

Department of Aerospace Engineering

H.R. Bright Building, Rm. 724, Ross Street - TAMU 3141

College Station TX 77843-3141